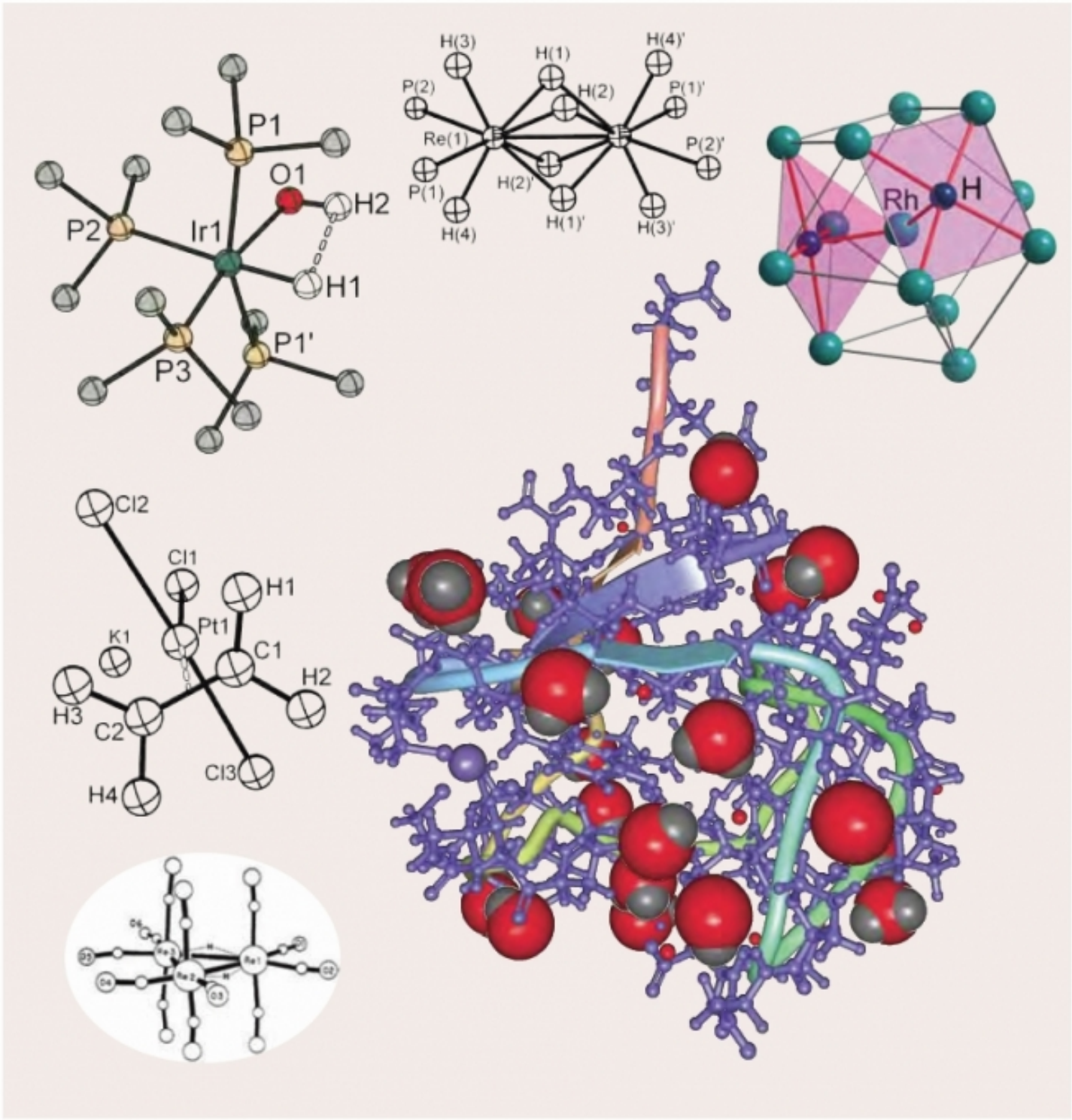


***ACA 2010***

***Transactions Symposium***

***The First Element***




**TRANSACTIONS OF THE SYMPOSIUM HELD AT THE 2010 AMERICAN CRYSTALLOGRAPHIC ASSOCIATION ANNUAL MEETING, Chicago, IL July 24 - 29 2010**

## The First Element: In Memory of Bob Bau

**A symposium to honor the memory of Bob Bau, chemist, diffractionist, neutron scattering expert and promoter and will focus on research achievements and future of studies involving hydrogen, which featured prominently in Bob's path-breaking research. Organizing Committee: Christina Hoffman, Larry Falvello,Thomas Proffen, Nibuo Niimura**

**Session Chairs: Arthur Schultz, Thomas Koetzle**

## Table of Contents (Click on the title to download the paper)

C. H. Schwalbe, M. Ramirez, B. R. Conway, C. J. Bache, S. J. Coles and P. Timmins

NEUTRON DIFFRACTION STUDIES OF METAL-HYDRIDES: INVESTIGATIONS OF OXIDATIVE ADDITION OF DIHYRDOGEN TO A METAL CENTER AND HYDRIDES IN METAL CLUSTERS

Muhammed Yousufuddin

# BOB BAU AND TOPAZ

Arthur J. Schultz
*X-Ray Science Division, Argonne National Laboratory, Argonne, IL 60439*

One of Bob Bau's great aspirations was to witness the development of instrumentation that would permit the collection of single crystal neutron diffraction data on "X-ray size" crystals. To advance that goal, Bob became an active leader and participant in the development of the TOPAZ single crystal diffractometer at the Spallation Neutron Source (SNS) at Oak Ridge National Laboratory.

On a cold, snowy day on March 1, 2002, the "SNS Single-Crystal Diffractometer Workshop" met at the Intense Pulsed Neutron Source (IPNS) at Argonne National Laboratory. Bob had helped to organize and chair the workshop of about two dozen scientists, who decided to form an Instrument Development Team (IDT) for an SNS single crystal diffractometer, later to be named TOPAZ. The group unanimously elected Bob as Chair of the IDT.

**Figure 1**. Bob Bau with his wife, Margaret Churchill, at the 2005 TOPAZ IDT meeting at the SNS. Bob had injured his foot, so Margaret came along to help him get around.

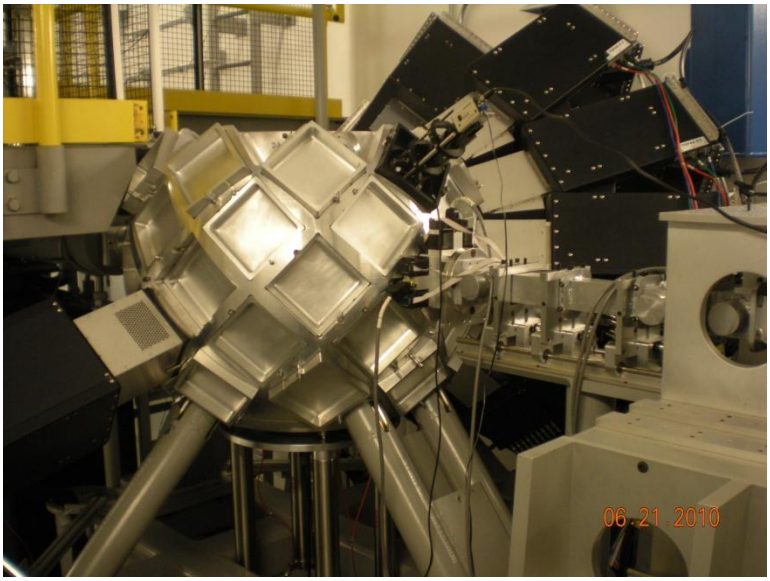


**Figure 2**. The SNS TOPAZ diffractometer in June, 2010, with 14 position-sensitive area detectors mounted on the detector array tank (DAT). The neutrons emerge from the right and samples are mounted from the bottom or the top of the DAT.

Thus began a busy six years of proposal writing, meetings, workshops, phone and video conferences, ACA breakout sessions and brain-storming. Christina Hoffmann, the TOPAZ instrument scientist at the SNS, along with Tom Koetzle, Paula Piccoli and myself at the IPNS, and many others, worked with Bob planning, designing and discussing the instrument development. It also didn't hurt that the IPNS Division Director, Ray Teller, was a former Bau student and strongly supported our efforts at the IPNS on behalf of the SNS TOPAZ project. As shown

in Figure 1, with the help of his wife Margaret, Bob led the 2005 IDT meeting at the SNS even with a broken foot. It was largely because of Bob's efforts that Knoxville was selected as the site of the 2008 ACA meeting, enabling the participants to tour the SNS. The TOPAZ instrument (Figure 2), currently in its commissioning phase, is becoming a reality. Unfortunately, Bob did not live long enough to actually use the instrument, but his efforts to advance neutron crystallography for the next generation of scientists is greatly appreciated, especially by those of us who had the honor to know him and to work with him.

# BEYOND SINGLE-CRYSTAL STRUCTURE DETERMINATION INTERPRETATION OF 3D DISORDER DIFFUSE SCATTERING

**Hans Beat Bürgi**
*Univ. of Zurich, Zurich and Univ. of Bern, Bern, Switzerland*

**Jürg Hauser**
*Univ. of Bern, Bern, Switzerland*

**Vickie Lynch**
*Oak Ridge National Laboratory, Oak Ridge, TN, USA*

The interpretation of diffuse scattering is far from routine. Sometimes the important information can be obtained from qualitative, ad hoc arguments and some simple modeling calculations, sometimes significant computational resources are required to perform elaborate Monte Carlo modeling. Both types of interpretation are illustrated with examples. The collaborative effort between groups at Oak Ridge National Laboratory, Federal Institute of Technology and the University of Zürich to construct a general tool for the interpretation of diffuse scattering is sketched.

## 1. INTRODUCTION

Single crystal structure determination from Bragg diffraction has become a largely routine operation: experiments and data interpretation are automated to a large extent, as is the validation of results. This situation is the result of continuous progress in the theoretical understanding of the X-ray and neutron diffraction processes and of continuous technological advances in radiation sources, detectors, software to interpret the experimental data and computational power. However, there have always been some crystal structures that were difficult or impossible to solve. In the early days structure determination was restricted to very simple, highly symmetric crystal structures [1]. With the advent in the 1930s of the heavy atom (Patterson) method [2], a first systematic way to estimate phases, the scope of X-ray diffraction became broader. In the 1950s phase estimation by direct methods opened the possibility of studying complex equal-atom structures, organic molecules in particular, in a more or less routine way [3]. Before the time of computers and automated four-circle diffractometers, triclinic structures were very tedious to determine and thus relatively underrepresented. The general availability of computers also led to least-squares refinement procedures, graphics programs and eventually to the full armory of tools which enable today's service labs dedicated to chemical crystallography to determine crystal structures in a matter of hours. Synchrotrons boosted the study of much more complex structure determinations, proteins, nucleic acids and viruses in particular. The mathematical tools derived from crystallography in higher dimensions eventually opened up the field of incommensurately modulated and quasi-crystals [4].

In view of a continuing success story that has already lasted nearly 100 years, one might ask in which field of structure determination - if any - there are still major problems waiting to be tackled. Here we discuss one such field: diffuse scattering. A general diffuse background scattering due to atomic motion was predicted almost immediately after the discovery of single crystal X-ray diffraction [5], a more detailed theory suggested a concentration of these features in

the neighborhood of the sharp Bragg reflections [6]. Using the 20th-century area detectors, i.e. photographic film, diffuse features were eventually confirmed, not only near Bragg reflections, but sometimes also between them as diffuse lines, planes or 3D clouds [7]. Although the theory of diffuse scattering has been continuously developed since the late 1940s, the interpretation of diffuse scattering is associated with several difficulties: signals are weak, data sets are large and tailor-made software for data interpretation is largely lacking. This has discouraged many crystallographers from systematically studying diffuse scattering. So far the data for only a limited number of compounds has been interpreted in terms of elaborate, often *ad hoc* structural models which are tested and optimized with the help of Monte-Carlo simulations, genetic algorithms and numerical least-squares calculations [8,9].

In this paper a very elementary introduction into diffuse scattering phenomena will be given. Scattering patterns will be presented for several materials, their diffuse features systematized and their investigation justified in terms of materials properties. Finally the application of genetic algorithms to the interpretation of linear diffuse scattering from a molecular material will be summarized and our present efforts towards new software sketched. Since the theoretical, technical and computational prerequisites for developing general and accessible methods of measuring, processing and interpreting diffuse scattering data are now available, the knowledge of crystallographers would seem to be a promising resource for advancing in the near future the interpretation of such data and making the information available to the materials-science community.

## 2. A MINI-INTRODUCTION INTO DIFFUSE SCATTERING

In the context of X-ray or neutron crystallography and taken literally, the terms ‘crystal structure determination’ implies locating every single atom in the crystal under investigation. However, the discontinuous, discrete distribution of Bragg reflections implies a perfectly 3D-periodic distribution of scattering matter with all crystal faults, i.e. deviations from periodicity, neatly filtered out. Our ‘crystal structures’ merely represent a time- and space-average over the entire sample projected into a single, representative unit cell. Such ‘crystal structures’ often show un-chemical features such as partial atoms (occupancy $< 1$) and un-physically anisotropic Atomic Displacement Parameters (ADPs highly oblate or prolate). Partial occupation can only mean that a given site is occupied by one atom type in some unit cells, but by others (including vacancies) in other unit cells. Highly anisotropic ADPs usually indicate that a given atom occupies slightly different positions in different unit cells, the distance between these positions (projected into the representative cell) being smaller than the resolution limit of the Bragg data. These phenomena are known as occupational and positional disorder.

To illustrate such disorder we consider two highly simplified examples: a 1D structure with a unit cell containing a single (disordered) atom. In the first example this atom may be either a strong or a weak scatterer (filled or empty circle: see Figure 1). The sequence of these atoms is not periodic, although there is a certain tendency towards alternation. The 1D scattering pattern shows sharp Bragg reflections at integral values of the reciprocal space coordinate h and broad features in-between. Their location at half integral values of h reflects the local doubling of the translation distance (short-range order). Their width reflects the finite and variable lengths of locally ordered domains. The structure derived from the Bragg reflections alone would show occupational disorder, e.g. half a strong and half a weak scatterer. In the second example the atom may take two positions, one slightly displaced from the centre of the cell to the left, one slightly to the right. The corresponding scattering patterns shows again the sharp Bragg reflections, this time

superimposed on broad features. Their position indicates no essential deviation from the overall periodicity indicated by the Bragg reflections, their width and intensity are related to the degree of atomic displacement. This example is representative of two situations: first, of the random atomic displacements caused by thermal motion and thus of the so-called thermal diffuse scattering, the details of which depend on temperature; second, it is representative of positional disorder as described above; and thus of temperature-independent static diffuse scattering. In the following sections we concentrate on the latter. Note that the total amount of scattering depends only on the composition of a given sample, the fraction that appears as Bragg scattering reflects the degree of order in the sample, the fraction that appears as diffuse scattering reflects the degree of disorder.

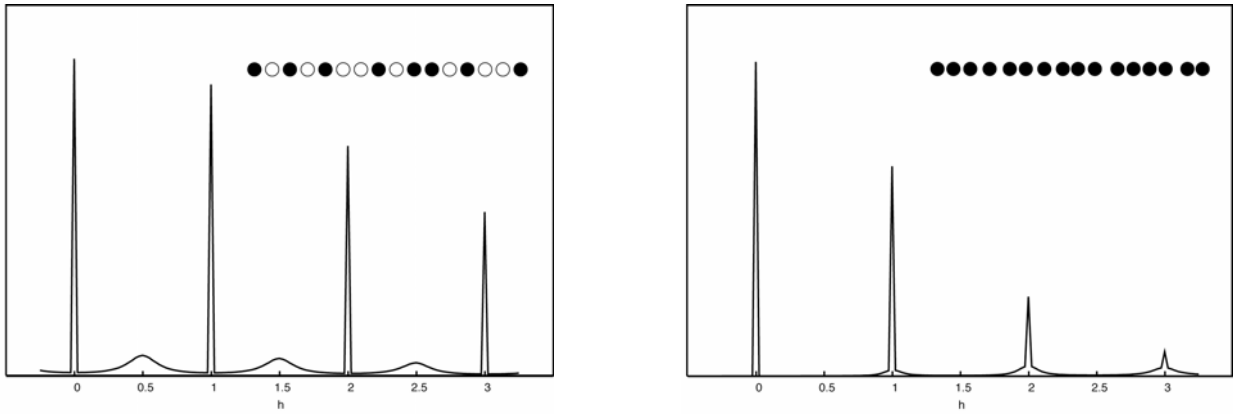


Figure 1. Left: an example of occupational disorder between a strong and a weak scatterer (filled and empty circles, respectively). Note the sharp Bragg reflections at integral h and the broad, diffuse features at half integral h. – Right: an example of displacive disorder. Note the sharp Bragg reflections at integral h superimposed on diffuse features. (Courtesy of Dr. T. Weber, ETHZ)

## 3. SOME REAL-WORLD EXAMPLES

In the real world things are more complicated as will be illustrated by several examples from our research over the last few years:

3.1 The first example concerns so called 'pigment red 170', based on an organic molecule and used with spray paints in the automotive industry. A partial structure of the α-polymorph of this material has been determined from the powder diffraction pattern of an isotypic compound in combination with packing-energy calculations [10]. With some effort a sample looking like a single crystal could be obtained. Reciprocal space reconstructions of diffraction data taken with a MAR-area detector at the Swiss Norwegian Beam Lines BM01A (European Synchrotron Radiation Facility, Grenoble, France) showed extensive linear diffuse scattering as illustrated by the h3l-layer shown on the left [11]. Interpretation of these data is underway and will hopefully provide a structural basis for understanding some of the properties of this material.

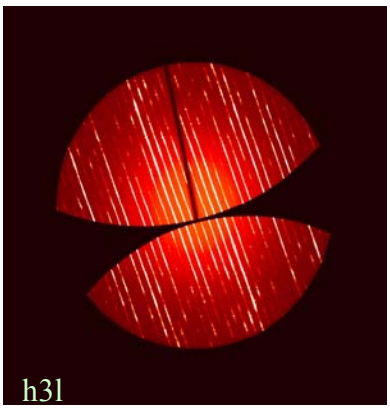


3.2 The second example has to do with rare earth-doped $NaLnF_4$, a member of a family of highly efficient light up-conversion materials. Our investigation [12] was initiated by a discrepancy

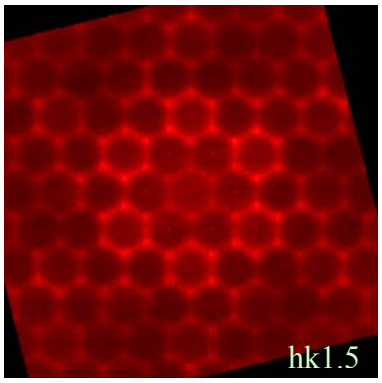


between UV/VIS spectroscopy and a single-crystal structure analysis. The former indicated two active metal sites, one with trivial ($C_1$) and one with threefold symmetry ($C_3$), the crystal structure analysis which was of high quality (R1 = 0.01) indicated two sites with threefold symmetry, but showed occupational disorder on one of the two sites (Na/2+Ln/2). The scattering showed diffuse layers parallel to the ($a^*b^*$)-plane at half integral values of l; layer h k 3/2 is shown as an example. The honey-comb pattern which shows clear intensity modulations, is sharp in the $c^*$-direction (perpendicular to the plane of the picture), as sharp as found for the Bragg reflections. The pattern has been interpreted in terms of ordered columns with Na and Ln ions strictly alternating along $c$; these columns show a trigonal packing in which the atoms at z = 0 are sometimes Ln and sometimes Na. The resulting disordered structure has been interpreted as frustrated due to coulomb interactions. Details are described in Ref. 12.

3.3 The third example is a purely organic host-guest compound which shows second-harmonic generation. The chiral, tri-cyclic perhydrotriphenylene host molecules ($C_{18}H_{30}$) which are present in the crystal as a racemate are arranged in stacks which form a honey-comb pattern of channels. The channels contain the *p*-nitrophenylpiperazine host molecules [ 13 ]. Given the racemic mixture of host molecules it was of some interest to look for the origin of polarity in this material. The diffraction pattern obtained from the orthorhombic crystals came as a complete surprise [14].

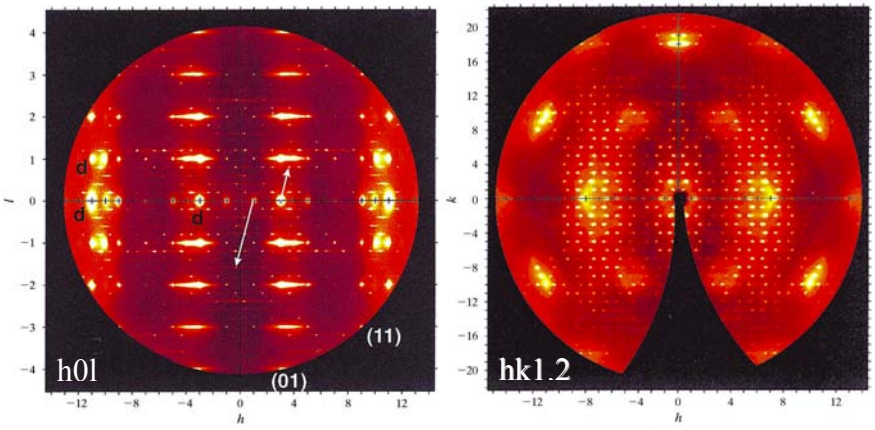


The h0l layer showed cloud-like features at large values of h and a system of horizontal lines that turned out to be oblate features of finite extension in the planes 1kl, 2kl, etc.. The layer h k 1.2 revealed a rich pattern of diffuse scattering on top of incommensurate satellite reflections. Although the patterns appear very complex it was possible to assign the main features to the main disorder-types found in the average structure. The oblate patches in the nkl-layers are associated with the perhydrotriphenylene sites which are occupied with molecules of opposite chirality in a 1:1 ratio. The (incomplete) hexagonal pattern in the h k 1.2 layer is also due to the host molecules whereas the moon-like and central features (including the incommensurate satellites) originate from the guest molecules. A quantitative analysis of the occupational disorder between R- and S-host molecules showed homochiral stacks with average length ~14 molecules [15,16]. The remaining features await interpretation.

3.4 The fourth example is $Mn_3[Mn(CN)_6]_2(H_2O)_6.xH_2O$. So far it is the only member of the large family of Prussian blue compounds for which (small) single crystals could be grown. The crystal structure is closely related to the NaCl structure with the $[Mn(CN)_6]^{3-}$ anions occupying Cl-position and the $Mn^{2+}$ cations occupying Na-positions. As the ratio of anions to cations is 2:3, the vacant anion positions are filled with $(H_2O)_6$ clusters thus implying occupational disorder of the

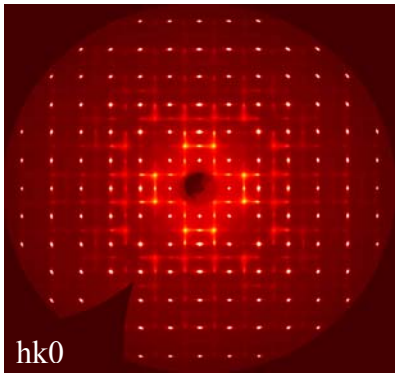


anion position. In addition there is 'zeolitic' water ($xH_2O$) in the cubes surrounded by four cations and four anions. The diffraction pattern shows a net of orthogonal diffuse lines superimposed on the Bragg reflections at h=2n, k=2n. The conspicuous lack of diffuse intensity in the neighborhood of the systematic absence (330) has been shown to be due to the occupational disorder between anions and $(H_2O)_6$ clusters [17,18]. A more detailed description of the anion distribution is of interest in view of the many physical properties of this family of compounds: mixed-valence, magnetic and photo-magnetic to mention but a few.

## 4. MOTIVATIONS FOR STUDYING DIFFUSE SCATTERING

Why do we want to study materials like the ones presented above? There are scientific and technical reasons. On the scientific side we note that many materials owe whatever interesting properties they have to disordered arrangements of atoms and molecules. Alloys, high-$T_c$ superconductors, giant-magneto-resistance, magnetic, dielectric and ferroelectric materials are among them. A better knowledge of their atomic scale structure provides a basis for modelling and understanding their physical properties. Whereas ordered crystal structures can be systematized crystallographically in terms of 230 space groups, no general scheme for classifying materials showing Bragg and diffuse scattering seems to exist. Developing such a scheme may well be a worthwhile undertaking.

To the technical side: some of the scattering patterns shown above show that disorder diffuse scattering is smeared out and structured over the whole of reciprocal space. As a consequence diffuse signals are often weak compared to Bragg reflections, thus requiring relatively long exposure times or very intense radiation sources to make them visible. With the new intense neutron beams now available at the Spallation Neutron Source (Oak Ridge National Laboratory) and with synchrotron radiation available world-wide diffuse scattering may be measured reliably. Fine-slicing of reciprocal space with noise-free detectors provides the required, high-quality, point-by-point mapping of the 1D, 2D or 3D modulations in reciprocal space. Such mappings lead to very large data sets, often orders of magnitude larger than the number of integrated Bragg intensities used in structure determination work. Their interpretation requires correspondingly large computational resources. With today's ever increasing computing power this should no longer present a major problem as will be illustrated below. However, and in contrast to single crystal structure determination, there is a lack of general, user-friendly software for interpreting such data.

## 5. A GENERAL STRATEGY AND AN EXAMPLE

### 5.1 Strategy

As became apparent from the examples shown in section three, we concentrate our efforts on materials which show a combination of diffuse scattering and clearly discernible Bragg diffraction. For such materials we have adopted the following strategy:

1) Do the best experiment possible, both with respect to diffuse scattering and Bragg diffraction, i.e. use a high intensity primary beam and a single-photon, low(no)-noise pixel detector (e.g. a Pilatus detector [19])

2) Find the best average structure and scrutinize it for features that contradict the principles of physics and chemistry, e.g. partial occupation of atomic sites, physically unreasonable atomic displacement parameters and geometrical parameters deviating to an unreasonable degree from the information stored in organic and inorganic data bases.
3) Look for diffuse scattering and attempt a qualitative interpretation with simple (analytical) models.
4) Develop a quantitative model of disorder and optimize its parameters by numerical methods, e.g. by a genetic algorithm or by (numerical) least-squares calculations.

5.2 An example

The hydrocarbon molecule $C_{18}H_{18}$ occurs in two modifications, a hexagonal and a monoclinic one. The scattering pattern of the former shows lines of signals, discrete Bragg reflections for –h+k=3n and continuous streaks for –h+k≠3n. Both polymorphs consist of two types of molecular layers (see figure below, the second type is the inversion-symmetric variant) alternating along *c*, in a disordered arrangement for the hexagonal polymorph and a (largely) ordered arrangement for the monoclinic polymorph [20]. The structure was solved from the larger reciprocal unit cell containing only the Bragg reflections (R1=0.03). The average structure shows molecules as given in the layer drawing, but also at the crosses between the molecules. Decreasing the *a**- and *b**-distances to include the diffuse streaks increases the unit cell constants *a* and *b* and thins the packing of the molecules as shown.

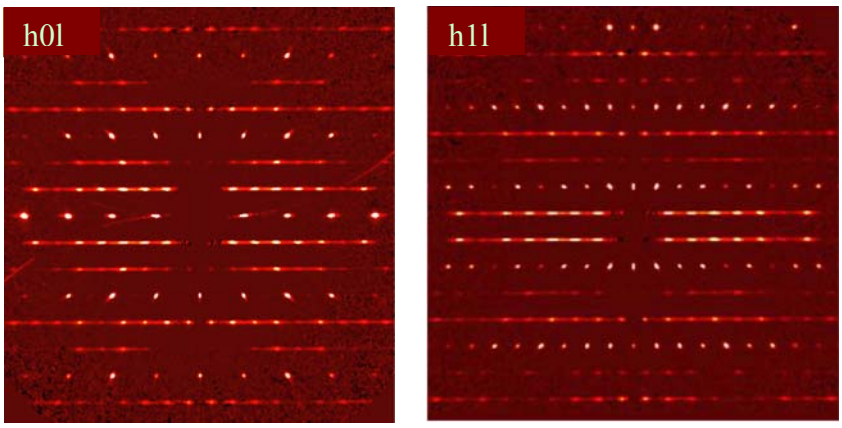


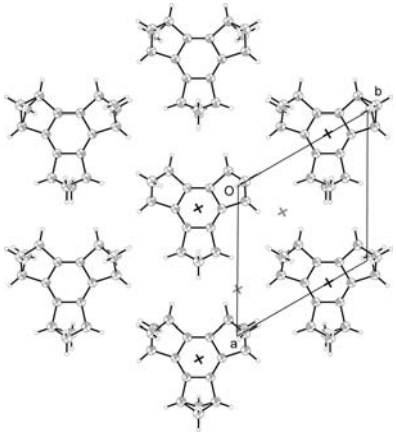


For discussing the stacking variants the layers of molecules are simplified into a single tri-star. Here we consider a growth model in which a new layer 'feels' the top three layers of the already formed crystal. These three layers, grey followed by black followed by green, come in two types, a 'bent' one (left) and an 'eclipsed' one. There are three possibilities for the fourth layer (red) to be placed on top of the bent arrangement. The respective probabilities obviously follow the condition $c+t+e_1=1$. There are three different attachment possibilities on an eclipsed crystal surface, an eclipsed and two bent ones (not shown) with probabilities $e_2$ and $(1-e_2)/2$. Using available theory the expression for the intensity along the streaks is

$$I(L)=|F(L)|^2 \cdot S(L|\ c,\ t,\ e_1,\ e_2)$$

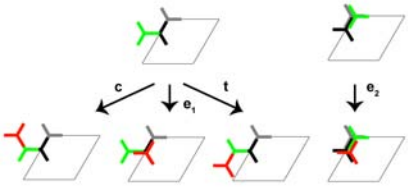


The first term derives from the Fourier transform of a single layer of molecules. The second term, the so called interference function, depends on the probabilities c, t, $e_1$ and $e_2$. This

approach has two limitations: first, F(L) is taken to be the same independently of the actual stacking sequence and does not allow layer deformations depending on the local environment. Second, the expression S(L) is very complicated, even for the present three layer interaction [21]. We have therefore chosen a numerical approach in which new layers are added to the growing crystal according to the probabilities c, t, $e_1$, $e_2$ and the molecules within the layers are allowed to undergo a concerted tilt (a feature suggested by the ordered monoclinic polymorph).

Numerical values of the parameters - probabilities and tilt angle - are chosen more or less randomly and crystals consisting of $10^5$ layers are built. These are subdivided into smaller lots which are Fourier transformed, squared, added and compared to the experimentally observed diffuse streaks. As we have no *a priori* knowledge of the parameters we have repeated the process with 40 different sets of parameters resulting in 40 calculated intensity patterns with different R-factors which we take as a measure of their fitness. Due to the probabilistic nature of our approach each calculated pattern belongs to a distribution of related patterns with slightly different fitness. We have therefore also calculated up to 40 clones from a given parameter set and the fitness of their average. In order to further optimize the parameters new parameter sets were obtained by recombination and a certain degree of mutation of the 40 sets of parameters, through a process called 'differential evolution' [15]. The process was repeated through up to 150 generations until the fitness of the 40 parameter sets differed insignificantly and didn't change from generation to generation.

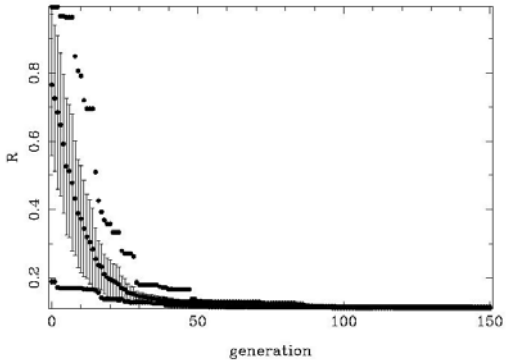


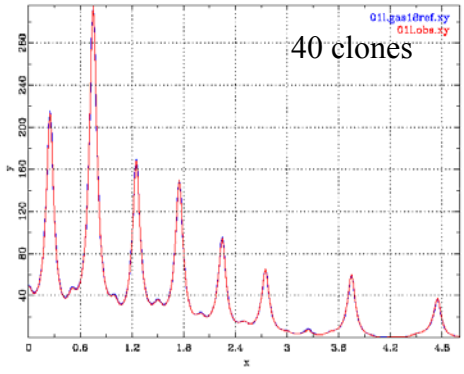


It is obvious from the preceding description that the computational effort for the interpretation of the diffuse streaks is substantial, but also that the problem lends itself to parallelization. Each clone of each individual can run on a separate processor. Computations were performed successfully on the TeraGrid (NSTG and Ranger) and Oak Ridge Institutional cluster (OIC) using up to 160 cores. Calculations of 150 generations took 6 hours to 3 days. The procedure was tested on a noise-free reference data set. Its performance for a single clone is remarkable, for 40 clones it is near perfect. The same approach will now be applied to experimental data.

## 6. CONCLUSION

The examples presented here show that interpretation of diffuse scattering is far from routine. Sometimes important information can be obtained from qualitative, *ad hoc* arguments and some simple modeling calculations. Sometimes significant computational resources are required to perform elaborate modeling.

The experience gained with the above examples has encouraged us to engage in a collaborative effort between groups at Oak Ridge National Laboratory, the Federal Institute of Technology and the University of Zürich to generalize the approach outlined in section 5 and to design and

develop multi-purpose software for analysing 1D, 2D and 3D diffuse scattering with simple or Monte-Carlo-type probabilistic models and for optimizing model parameters with differential evolution and least-squares algorithms [22].

---

REFERENCES


[1] W. L. Bragg, Proc. Roy. Soc. Lond. **A89** (1913), 248.
[2] A. L. Patterson, Z. Kristallogr. **90** (1935), 517.
[3] J. Karle and H. Hauptmann, Acta Crystallogr. **9** (1956), 635.
[4] A. Janner, T. Janssen, Phys. Rev. B **15** (1977), 643.
[5] P. Debye, Ann. Phys. **43** (1914), 49.
[6] I. Waller, Z. Phys. **51** (1928), 213.
[7] K. Lonsdale, Proc. Phys. Soc. **54** (1942), 314.
[8] T. R. Welberry, Diffuse X-ray Scattering and Models of Disorder (Oxford University Press, Oxford, 2004).
[9] R. B. Neder, T. Proffen, Diffuse scattering and defect structure simulations: a cook book using the program DISCUS (Oxford University Press, Oxford, 2008).
[10] M. U. Schmidt, D. W. M. Hofmann, C. Buchsbaum, H. J. Metz, Angew. Chem. Int. Ed. 45 (2006) 1313.
[11] P. P. Das, A. Linden, unpublished result (2009).
[12] A. Aebischer, M. Hostettler, J. Hauser, K. Krämer, T. Weber, H. U. Güdel, H.-B. Bürgi, Angew. Chem. Int. Ed. 45 (2006), 2802.
[13] O. König, H.-B. Bürgi, T. Armbruster, J. Hulliger, T. Weber, J. Am. Chem. Soc. **119** (1997), 10632.
[14] T. Weber, M. A. Estermann, H.-B. Bürgi, Acta Cryst. **B57** (2001), 579.
[15] T. Weber, H.-B. Bürgi, Acta Cryst. **A58** (2002), 526.
[16] H. B. Bürgi, J. Hauser. T. Weber, R. B. Neder, Crystal Growth and Design, **5** (2005), 2073.
[17] P. Franz, C. Ambrus, A. Hauser, D. Chernyshov, M. Hostettler,J. Hauser, L. Keller, K. Kämer, H. Stoeckli-Evans, P. Pattison, H.-B. Bürgi, S. Decurtins, J. Am. Chem. Soc. **126** (2004), 16472.
[18] D. Chernyshov, A. Bosak, Phase Transitions **83** (2010), 115.
[19] See: http://pilatus.web.psi.ch/pilatus.htm
[20] H. Birkedal, H.-B. Bürgi, K. Komatsu, D. Schwarzenbach, J. Mol. Struct. **647** (2003), 233.
[21] H.-B. Bürgi, M. Hostettler, H. Birkedal, D. Schwarzenbach, Z. Kristallogr. **220** (2005), 1066.
[22] See: http://www.oci.uzh.ch/diversa/SNFProject/index.php

# STRUCTURAL COORDINATION CHEMISTRY BEYOND ROUTINE DIFFRACTION: SINGLE CRYSTAL TRANSFORMATIONS, SHAPE CHANGES AND AMBIGUITIES, AND NEUTRON SCATTERING

Larry R. Falvello
*University of Zaragoza – C.S.I.C., Department of Inorganic Chemistry and Aragón Materials Science Institute, Pedro Cerbuna 12, E-50009 Zaragoza, Spain*

## ABSTRACT
Diffraction analyses outside the realm of routine structure determination have been used to explore chemical and physical phenomena that would be difficult to observe either in the synthetic laboratory or in rapid, albeit high quality, x-ray structural studies. Chemical reactions within single crystals have been observed to yield products that would not be expected at the benchtop. The 1-D coordination polymer in $\{Cs_2[Co_7(citr)_4(H_2O)_{13.5}]\}_2 \cdot 15H_2O$ [citr = citrate, $C_6H_4O_7^{(4-)}$] in the crystalline state undergoes a concerted reaction to give a 2-D polymer in $Cs_2[Co(H_2O)_6]\{[Co_{6.5}(citr)_4(H_2O)_9]\}_2 \cdot 3H_2O$, cross-linked by an unusual Co(II) center surrounded by seven O-coordinated ligands. Another study involves *trans*-$[Ni(cyan)_2(NH_3)_4]$ (cyan = cyanurate, $C_3H_2N_3O_3^-$), a simple paramagnet that forms molecular crystals with a continuous phase transformation that leads to a smooth molecular shape change as either pressure or temperature is varied. Diffraction data give contradictory indications regarding the choice of space group. A seemingly more routine structural phenomenon such as the planar aqua ligand in transition metal complexes is subject to new insights through a parametric study which characterizes structural changes as a function of temperature. The latter two studies have been aided by neutron analyses and would be further enhanced by high-throughput neutron diffraction facilities.

## INTRODUCTION
Diffraction analysis for structure determination became important in chemical research because of the clear pictures it provided of molecular geometry. The use of diffraction techniques by non-specialists from the chemical community at large began almost half a century ago, as it started to become clear not only that chemists could make important discoveries about molecules on the basis of structure analyses, but also that chemists could miss important discoveries without them.

Crystals themselves had been studied long before x-ray diffraction was discovered, but that crystallography was largely a study of naturally occurring crystals, which are usually non-molecular substances – minerals in the large part. The study of *molecular* crystals on a large scale only became important when diffraction made such crystals a vehicle for studying molecular shape. The molecular crystal itself was not the entity of prime importance. The structure of the molecule was the desired result, and the crystal was a periodic support from which diffraction could be obtained.

When researchers interested in chemical structure analysis adopted single crystal diffraction first as a complement and then as an alternative to spectrocscopy, magnetism and other less accurate

structure-determination techniques, it was inevitable that the terms "crystallography," "structure analysis," and "single crystal diffraction" would merge as synonyms within the context of chemical analysis and under the more general term "chemical crystallography." This was not the crystallography of pre-diffraction times, that of morphology and optical and physical properties of natural crystals. This "crystallography" of recent decades has usually carried the connotation of diffraction analysis, at least within the chemical world, and in large part this has meant analysis of molecular crystals.

A field of study dedicated to molecular crystallography *per se* – that is, the physical and chemical properties of molecular crystals, independent of diffraction, and analogous to the crystallography practiced by mineralogists for centuries – has not really emerged as a clearly demarked scientific discipline. A modest amount of study is devoted to molecular crystals – how to prepare them with specific aggregation patterns, how to predict their structures, the measurement of thermodynamic properties and magnetic and structural cooperativity. But there is still a great deal to be learned about the molecular crystalline state. And it is not surprising that diffraction, which is so widespread now in chemical research, has provided a first window into some of the more interesting properties of molecular crystals. Such insight can occur when a structure analysis deviates from the routine.

This symposium honors the memory of Bob Bau, whose work invariably had some novel or otherwise interesting twist to it. The drawings on the cover of last winter's ACA Reflexions newsletter emphasize the importance of hydrogen and the related importance of neutron diffraction in Bob's work. Bob always brought added value to his readers. It was through reading something that Bob had written, for example, that I first learned about an asymmetrically deuterated compound, Li α-deuteroglycollate, published by Johnson *et al.* in 1965 [1], which yields a centrosymmetric crystal structure analysis when studied with x-rays and a chiral structure when studied with neutrons. This sort of added interest was a characteristic of Bob's work. In honoring Bob's memory, I would like to present results that I think lie outside of the routine use of diffraction and perhaps provoke some thought on the fundamental processes that generated the results.

In the following I will summarize three sets of results that reveal phenomena that can be observed in molecular crystals, but for which it would be difficult to imagine their occurring in any other state. One is a concerted two-site chemical reaction that accompanies a crystallographic phase transition and in which a one-dimensional polymer is crosslinked to form a two-dimensional net. The second is a continuous (second-order) phase transition in which a simple six-coordinate nickel complex changes shape smoothly as the temperature is varied. The third section introduces a mirage that can occur if we treat the results of a crystal structure determination as a description of a static system.

## AN UNUSUAL CHEMICAL REACTION IN THE CRYSTALLINE STATE

Solid-state chemical reactions and phase transformations have been studied extensively in traditional crystallography – for elements, binary compounds and their solid solutions, for example [2] – but studies of such processes for molecular crystals have often been limited to their structural characteristics.

We tend to treat reactions in molecular solids as curiosities, but it would not be appropriate to refer to every chemical reaction that takes place in a molecular crystal as being unusual, since a few careful investigators have been demonstrating for some years not only that such reactions are possible but that they can be controlled with some degree of precision. A reaction in molecular crystals is expected to involve topotaxy, the various definitions of which refer to maintaining a particular spatial relationship between molecules before and after the reaction [3-6]. The most important differences between chemical reactions in mobile phases – gas, solution, or melts, for example – and those in molecular solids are that the reactants in the solid already have an established relationship between their orientations and that the reaction itself, if not destructive of the phase, will not produce a great deal of spatial reorganization.

My colleagues (mostly) and I (largely as an observer) have been experimenting with open-system, non-adiabatic chemical processes in molecular crystals. This work, which has taken on some importance in my laboratory in recent years, was instigated by our observation that deliberate, controlled dehydration of one of our molecular-crystalline systems yielded a concerted two-site chemical reaction among the non-solvent components of the crystal, which led to a product that chemical intuition tells us would be impossible to obtain in a mobile-phase reaction. (We are of course aware that chemical intuition is a fickle counselor.)

The structural aspects of the reactant and product crystals have been described elsewhere [7]. The process begins with a one-dimensional polymer, **1**, whose basic building blocks are a cubane unit formed by Co(II) and citrate, "$[Co_4(citr)_4]^{(8-)}$" and two crystallographically unique Co(II) centers that bridge adjacent cubanes to form the polymer (Fig. 1). There are, in addition, two terminal Co(II) centers, Co7 and Co8, whose ligand sets each include one carboxyl oxygen from a citrate ligand of the cubane and five aqua ligands. Co8 is half occupied, a fact originally established on the basis of displacement parameters and later proved by symmetry

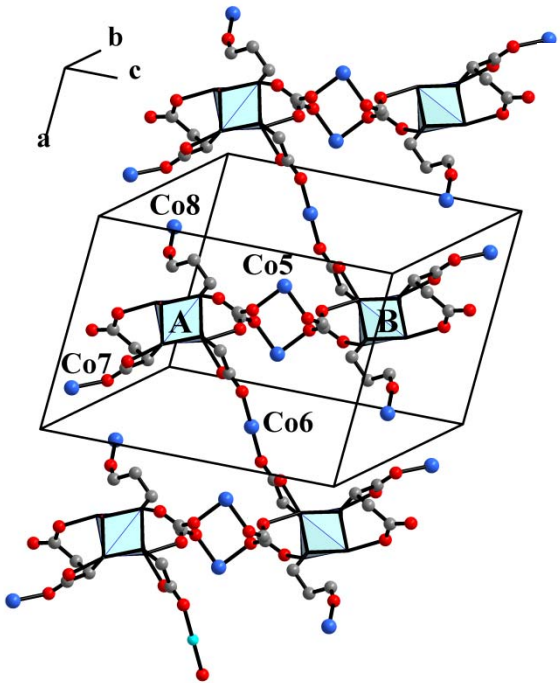


Figure 1. Zig-zag polymer of Co citrate cubanes in (**1**). Color codes blue: Co, red: O, gray: C.

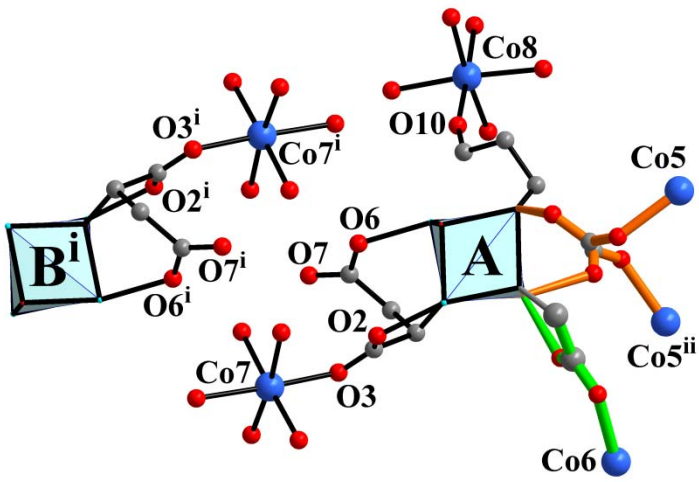


Figure 2. Reactive sites between adjacent polymers in crystals of (**1**). Symmetry codes (i: 1-x, -y, -z), (ii: 1-x, 1-y, 1-z). Unlabelled oxygen atoms attached to Co7, Co7$^{i}$ and Co8 are aqua ligands. Color codes blue: Co, red: O, gray: C.

considerations after the reaction (*vide infra*). Co8 and its aqua ligands, which are present half the time, share their zone with three partially populated unligated water molecules, which occupy that space the rest of the time. Figure 2 shows the space between cubane "A" and the symmetry relative of "B" from a neighboring chain. It is here and at Co8 that the chemical reactions occur.

When a crystal of **1** is dehydrated under mild conditions, its temperature raised above 278 K in a stream of nitrogen gas, a concerted chemical reaction occurs which produces **2**, a species represented in part in Figure 3. The cubane "A" and its symmetry relative "$B^{i}$" from a neighboring chain are now joined by a crosslink, doubly bridged by Co7 and $Co7^{i}$. And at what is an unrelated site, Co8 has separated from the chain and has become aquated, with rupture of the Co8---O10 bond, to give an independent $[Co(H_2O)_6]^{(2+)}$ unit which sits on a center of symmetry in the new unit cell. This position validates the stoichiometry derived for Co8 in the original structure. That this double process occurs at all was of sufficient interest to have been the main point of discussion in our original report on this system [7]. However, the chemistry that occurs at Co7 and Co8 merits further comment.

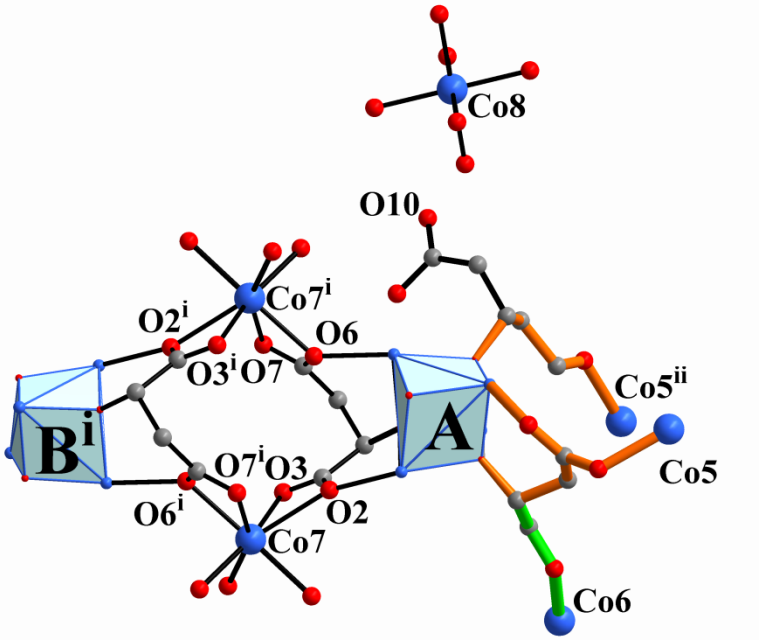


Figure 3. Polymer crosslink between cubanes "A" and "$B^{i}$" in which Co7 has become seven-coordinate. In the upper right is the hydrolyzed $[Co_8(H_2O)_6]^{(2+)}$ unit. Symmetry and color codes as in Figure 2.

Before the solid-state reaction, Co7 is a six-coordinate Co(II) center, whose observable features are unremarkable. However, upon mild dehydration of the crystal, two of the aqua ligands are substituted by three carboxylate oxygen atoms, with O2, $O7^{i}$ and $O6^{i}$ joining O3 in the coordination sphere of Co7 in the product **2**. The result is seven-coordinate Co(II), which has two four-membered chelates as part of a combined piano-stool / butterfly coordination. We are aware of some 26 reported crystal structures with Co surrounded by at least seven oxygen atoms – most of which involve macrocyclic ligands with four or five O-donor sites -- and there is one reported structure with eight-coordinate Co surrounded by four four-membered chelates [8]. Discarding one case in which a disordered ligand set gives the appearance of seven-coordinate Co with two four-membered chelates [9], I think this particular piano-stool / butterfly coordination geometry is new in compound **2**.

Substitution reactions at transition metal centers in solution are classified as dissociative if the leaving ligand exits before the entering ligand binds to the metal, and as associative if a new

ligand enters before the one being substituted leaves. The associative mechanism involves a transitory increase in the coordination number. In the crosslinking of **1** to form **2**, the fact that the reaction is initiated by mild dehydrating conditions and does not occur at 278 K, even in a stream of dry nitrogen, would imply that this reaction is dissociative. It is hard to imagine that the crystals of **1** would have formed in the first place at room temperature if attack at Co7 by the carboxylate ligands were a spontaneous process.

The simpler reaction at Co8 raises some interesting questions. After all, Co8 takes on one more aqua ligand under dehydrating conditions. Of the 40 ligated and unligated water molecules in the unit cell of **1**, 27 remain in **2**. The total of 27 Co-bound waters in **1** is reduced to 24 in **2**, and yet Co8 takes on one additional aqua ligand in the reaction. And while the carboxylate groups near Co7 form a well populated coordination shell involving two four-membered chelates, carboxylate oxygen atom O10 releases Co8, which takes on water. Moreover, since Co8 sits on a center of symmetry after the transformation, its stoichiometry relative to that of the cubane is clear. But it is curious that this stoichiometry existed in the original crystal, where no symmetry constraint requires it. Was the crystal of **1** really the first state formed in this sample, or did we just happen to catch it at that point?

This concerted reaction can be called topotactic, although the fact that the crystal loses mass in the process clouds the finer points of nomenclature. The extended structure of the crystal itself plays a role in stabilizing **1**, but it is robust enough to survive a crystallographic transformation that reduces its volume by 12%.

**A CONTINUOUS PHASE TRANSITION NEAR ITS END POINT: REFINEMENT USING AN "ALTERNATIVE" SPACE GROUP**

In a continuous, or second-order, phase transformation, the entropy and volume of the system are continuous functions of temperature (or pressure) through the course of the transformation. Such transitions have been known and studied for non-molecular systems [2] – that is, in traditional crystallography – but are less well characterized in molecular crystals.

A simple coordination complex of Ni(II) with cyanurate ligands, **3** (Figure 4), undergoes such a transition. This transition has been characterized structurally as a function of temperature [10].

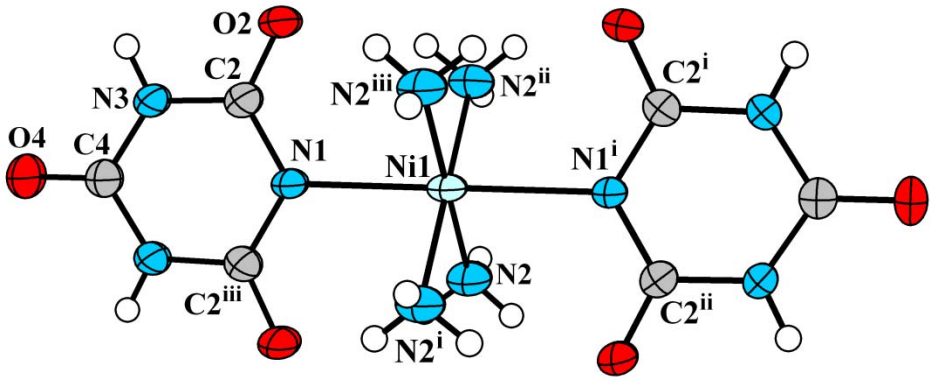


Figure 4. *trans*-[Ni(cyan)$_2$(NH$_3$)$_4$] at T = 298 K, space group *Fmmm,* with non-H atoms represented by 60% probability ellipsoids. Symmetry codes (i: x, -y, -z), (ii: -x, y, -z), (iii: -x, -y, z).

As often happens with interesting and out-of-the-ordinary phenomena in molecular crystals, the major crystallographic characterization of this system consisted of structural studies, although magnetic data and single-crystal polarized-light electronic spectroscopy were also used and proved to be informative.

Near room temperature an accurate but otherwise routine structure analysis gave space group *Fmmm,* with the molecule situated on a site of *mmm* symmetry. When the temperature is lowered to 223 K, the same crystal gives a very similar unit cell, but with space group *Cmcm* with the molecule on a site of *m2m* symmetry. At this temperature the cyanurate ligands are observed to have left their original positions on the no-longer-present mirror perpendicular to **b**, and to have tilted in the same direction [Figure 5(b)], with a dihedral angle of 21.61(4)º. What reveals the nature of this transition, however, is the fact that as the temperature is lowered, the distortion increases, as seen in the full set of drawings in Figure 5.

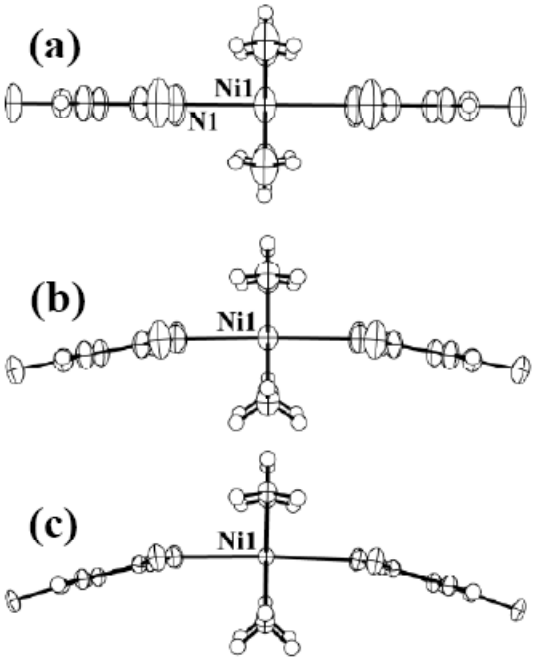


Figure 5. Evolution with temperature of molecular shape (Q = dihedral angle between the cyanurate ligands) and displacement parameters (60% ellipsoids) for *trans*-$[Ni(cyan)_2(NH_3)_4]$. (a) T = 298 K, *Fmmm,* Q = 0, symmetry code (i: x, -y, -z). (b) T = 223 K, *Cmcm,* Q = 21.61(4)º. (c) T = 139 K, *Cmcm,* Q = 32.14(5)º.

There is an interesting aspect of the refinement and reporting of the structure at 298 K, which has not been discussed in print. That is the subject of this section of the presentation.

A continuous structural transition of this type should obey a simple relationship between temperature and distortion [11]. Specifically, the square of a distortion parameter (generically, "Q") such as the dihedral angle between the cyanurate ligands should vary linearly with temperature – and it does. The relationship is given in Equation 1, in which $T_c$ is the "critical temperature," the temperature T at which the distortion Q has a value of zero.

$$Q^2 = Q_o^2 (1-T/T_c) \qquad (1)$$

$Q_o$ is the value that the distortion parameter would be observed to have at absolute zero temperature if the transition could be followed to that point.

As was indicated in the publication on this system [10], Equation 1 is obeyed; and depending on what structural feature one uses as the distortion parameter, the critical temperature – the temperature at which the distortion should be zero – is calculated to be in the vicinity of 310 K. It comes out to 314 K if we use the dihedral angle between the cyanurate ligands. However, our

attempts to measure diffraction data at this temperature failed, because the crystal ceased to give measurable diffraction when we raised the temperature above about 298 K.

This is a continuous transition in which the dihedral angle is diminished as the temperature is raised; and it should reach zero with a concomitant space group change from *Cmcm* to *Fmmm,* somewhere near 310 K. But the highest temperature at which we obtained diffraction data was 298 K, at which temperature the crystal and the experiment combine to give an interesting set of conflicting choices. (1) From our plot of Equation 1 using experimental diffraction data obtained at various temperatures, we are quite certain that the space group at T = 298 K is *Cmcm,* and that there is a very slight molecular distortion. (2) Our diffraction data at T = 298 K, collected using an in-house instrument with a conventional MoK$\alpha$ x-ray source, have the systematic absences for F-centering – not just those for C-centering. The reflections with $(h + \ell)$ odd and those with $(k + \ell)$ odd lose intensity continuously as the temperature is raised toward room temperature; and we simply could not measure them when we got to 298 K.

The experimental evidence leaves essentially no doubt about the facts of the case. The space group at T = 298 K is *Cmcm,* but the deviation of the arrangement of atoms in the cell from a pattern with *Fmmm* symmetry is so slight as to leave the diffraction pattern in an ambiguous state. An attempt to use space group *Cmcm* with the data at T = 298 K gave an unstable refinement. So with these data we had no choice but to refine the structure using the "nearby" space group *Fmmm.* This gives atomic coordinates that describe symmetry which, according to the analysis based on Equation 1, we are sure the structure does not possess rigorously. But we do have displacement parameters in the structural model; and faithful to their mission, as seen in Figure 5(a) they are prolate, elongated parallel to **b** to indicate the displacement whose origin we understand with certainty.

We can make a few observations about these results. First of all, we might benefit from taking the effort to measure diffraction data with a more brilliant radiation source. I am not sure that we would thus learn anything more about the system, but in general I am not inclined to argue against gathering data. At the same time, the available data do not leave much room for alternative interpretations of this system based on Bragg diffraction. We might well learn more from diffuse scattering. Secondly, and perhaps at odds with my first observation, I would like to quote from an abstract from the ACA Summer Meeting of 1971: "The amount of symmetry of an object ... [depends] on the nature of the properties measured, and on the sensitivities of the measuring devices." So although in structural crystallography our procedures treat symmetry as an "on/off" arrangement in which either there is symmetry or there is not, the idea of continuous symmetry measures is not new in chemistry [12,13] and would probably be useful in a case such as this.

## THE PLANAR WATER LIGAND IN COORDINATION CHEMISTRY

It is fair to say that the atomic coordinates derived from many thousands of crystal structure analyses have had a dominant role in the interpretation of much of what synthetic coordination chemistry has rendered in the last half century. The picture of the molecule, aggregate, polymer or whatever else emerges from the structure determination is what defines the result of the chemical reaction – even if it is the analysis of a low-yield, crystalline product of a reaction that produced other, non-crystalline products.

Looking a bit more closely at structural results, we sometimes encounter a picture that requires an explanation based on more than atomic coordinates. If we had seen only the room temperature structure of the nickel cyanurate complex of the previous section of this presentation, the observed displacement parameters would have called out for an explanation; and without the structures at the other temperatures, the explanation would not have been obvious. Another such structural curiosity is the planar water ligand in coordination chemistry.

The water, or aqua ligand is more often than not characterized in diffraction analyses as a pyramidal entity, in which the oxygen atom lies out of the plane formed by the metal and the two hydrogen atoms. But on occasion it is "observed" to be planar, if we consider the atomic coordinates to be the entirety of the observation. Figure 6 shows a molecule, *trans*-$[Co(sac)_2(H_2O)_4]$ (sac = saccharinate, $C_7H_4NO_3S^-$) [14] that has both planar (O1W) and pyramidal (O2W) aqua ligands. In this particular case, all four hydrogen atoms of the two unique aqua ligands were refined freely using data to 0.71 Å resolution; all are H-bond donors in O---H...O interactions with O...O in the range 2.7098(15) – 2.9564(16) Å and with the angle O---H...O in the range 164(2) – 170(3)º. Along with this appearance of high quality in the results, we note – as my colleagues and I have noted in every case of planar water that we have observed – that the displacement ellipsoid of the oxygen atom of the planar water, O1W, is elongated in the direction perpendicular to the plane of the ligand.

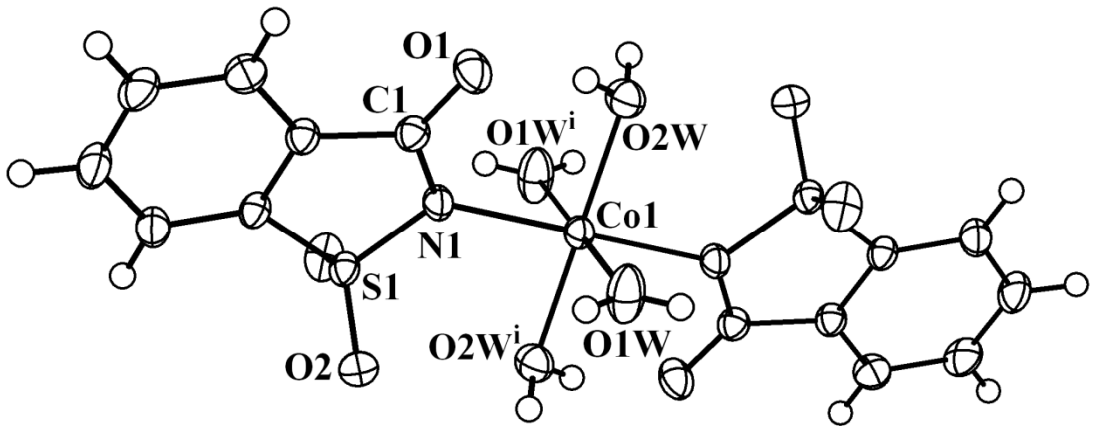


Figure 6. *trans*-$[Co(sac)_2(H_2O)_4]$ at T = 290 K, from the crystal structure of the dihydrate. Non-H atoms are represented by their 60% probability ellipsoids. Symmetry code (i: 1-x, 1-y, 1-z).

When we first looked at a high-quality refinement of a planar water some years ago, my colleague Milagros Tomás, an organometallic chemist by training, quickly invoked fluxionality between two pyramidal arrangements as the origin of this set of observations. Fluxionality is a common feature of organometallic chemistry, but the diffractionist – accustomed to disorder – does not often invoke it with such specificity. Much has been written about the importance of interpreting, as opposed to simply archiving or discarding, the atomic displacement parameters derived from diffraction analyses [15]. But it often happens that potentially interesting

phenomena observable in such parameters lie at the periphery of the objective of a structure determination.

In what remains of this presentation, I would like to describe what we think we know about planar water ligands, what my colleagues and I have measured in order to test the fluxionality hypothesis, and some preliminary results.

First of all, since planar aqua fragments involve hydrogen and are observed in atomic coordinates from diffraction analyses, could we dismiss them in advance on the basis of the unreliability of the hydrogen atom coordinates? (That would raise the question of why we are publishing coordinates that we do not trust, but that is not my topic at the moment.) Figure 7 plots the tetrahedral volumes of the M---$OH_2$ fragments found in the Cambridge Structural Database System [16], scaled on the basis of the M---O distance. A tetrahedral volume of zero, at the right end of the plot, indicates that the aqua ligand is planar. For all 14992 fragments found, there are more than 1200 planar cases. If we limit our consideration to structures which had $R \leq 0.05$, there are more than 700. And if we consider only those structures that gave $R \leq 0.03$, and which would have a better chance of producing well defined H-atom positions, there are still nearly 200 planar water ligands. If we further limit our consideration to neutron diffraction studies (not shown in the figure), for which the paucity of examples (27 structures / 41 fragments) breaks the smoothness of the tetrahedral volume frequency curve, we still find seven planar water fragments. In these cases it would be more difficult to question the veracity of the

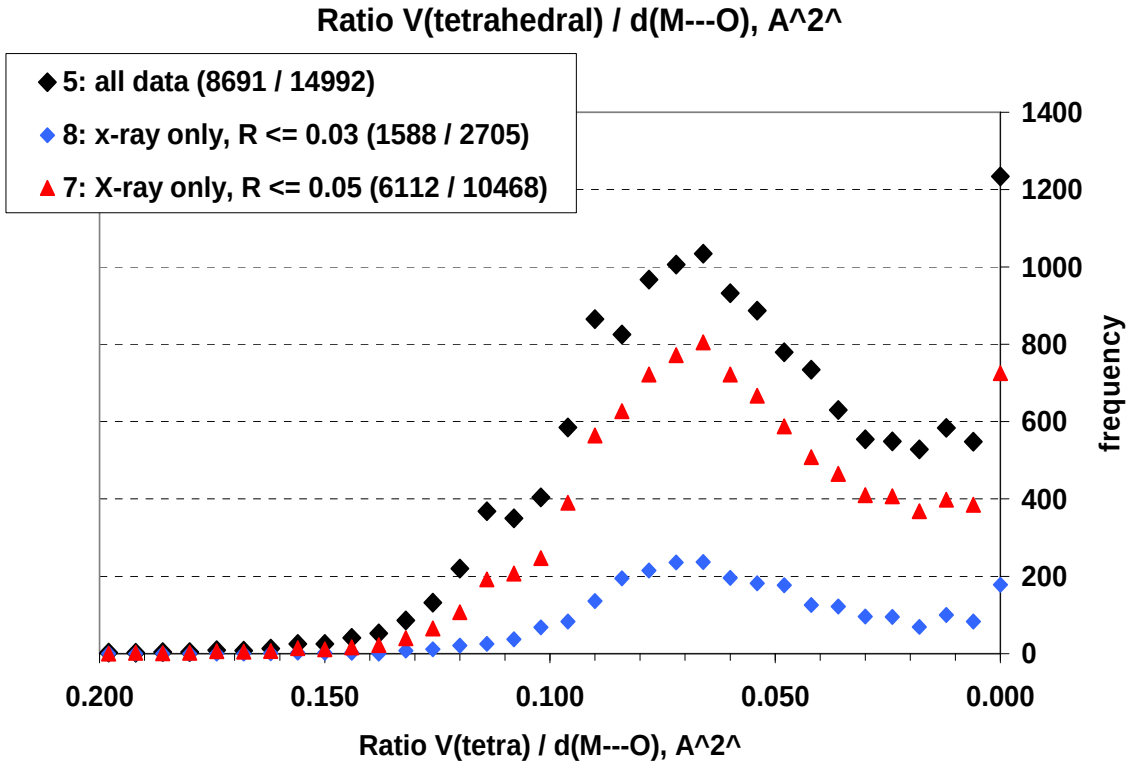


Figure 7. Tetrahedral volume ($Å^3$) of M—($OH_2$) fragments extracted from the Cambridge Structural Database System, scaled on the M---O distance. Black diamonds, all data (14992 fragments from 8691 structures); red triangles, 10468 fragments from 6112 structures with $R \leq 0.05$; blue diamonds, 2705 fragments from 1588 structures with $R \leq 0.03$.

hydrogen atom positions.

On the basis of the database results and our own observations of the displacement parameters of the oxygen atoms of planar water, we undertook to test the hypothesis that these groups are actually dynamic. A fluxional process, we expect, would have lower energy and greater amplitude than the well known factors that give atomic displacement parameters their magnitudes. So a parametric study of the axial displacement parameter of the O atom of the planar water should show it 'growing' faster than the displacement parameters elsewhere in the structure, as the temperature is raised. Our strategy for this study involves both x-ray and neutron diffraction, for several reasons. Neutron diffraction permits not only the reliable analysis of H atom positions, but also the refinement of their anisotropic displacement parameters. Neutron diffraction also effectively removes the lone-pair electron density of the water oxygen atom from the results. We want to use data gathered at as many temperatures as circumstances will allow, but logistical considerations oblige us to gather the majority of the data with in-house x-ray equipment. Neutron diffraction data at selected temperatures will be used not only for their own content, but also to ratify, if possible, the trends observed with the x-ray data.

We are studying three of the transition-metal saccharinates (Figure 6) – the Co complex, which I will describe here, and also the isostructural Ni and Zn complexes, which will be reported elsewhere. The Co complex presents an inherent weakness in the neutron diffraction analysis, because Co has a smaller coherent and a larger incoherent scattering length than the other atoms in the structure. In the actual event, problems refining the anisotropic displacement parameters of the Co center using neutron data detracted from the perceived reliability the neutron results for this compound.

We measured x-ray data in-house at five temperatures – 100, 123, 173, 223 and 290 K – with the aim of tracking the mean-square displacement of O1W (Figure 6) perpendicular to the plane of the aqua ligand, as a function of temperature. Our further and more important aim is to compare this to the trend of all of the displacement parameters of the structure in the same and in other directions. The critical question is, what is the best measure of the global increase in displacement, for the structure as a whole, with temperature, in a particular direction?

The thermal expansion tensor, which is second rank, is the relevant macroscopic property for this measurement. As has been expounded by others, this tensor is best calculated using *d*-spacings of a large number of reflections, rather than by using unit cell parameters [17]. That analysis is underway.

For now, I would like to show what we found for the Co complex, using more modest means of comparison. Figure 8 shows the mean-square displacement of O1W perpendicular to the direction of the plane of the ligand (top line), together with the mean-square displacement of O2W, the pyramidal aqua ligand, in the direction of its lone pair (middle line) – which coincides roughly with its largest-amplitude principal direction of displacement. Also plotted are the smallest principal displacements for these two atoms, which are almost identical to each other and vary identically over the temperature range studied. The most interesting features of this graph are (1) the almost perfect coincidence and evolution with temperature of the smallest principal displacements; (2) the identical slopes of the line for these two displacements and the

line for the largest principal displacement of the pyramidal O2W; and (3) the slope of the line for the largest (perpendicular) principal displacement for the planar water O1W, which is some two-thirds greater than the slopes of the other lines. These three features, taken together, are consistent with the temperature evolution of a soft displacement process for O1W. Fluxionality is such a process, and so is libration of the water ligand as a whole. I expect that the full analysis of all of the data, including the neutron diffraction data for the Ni and Zn complexes, will permit a clear distinction between these two possibilities, if indeed we find in all the data that an extra displacement is active at the planar water ligand.

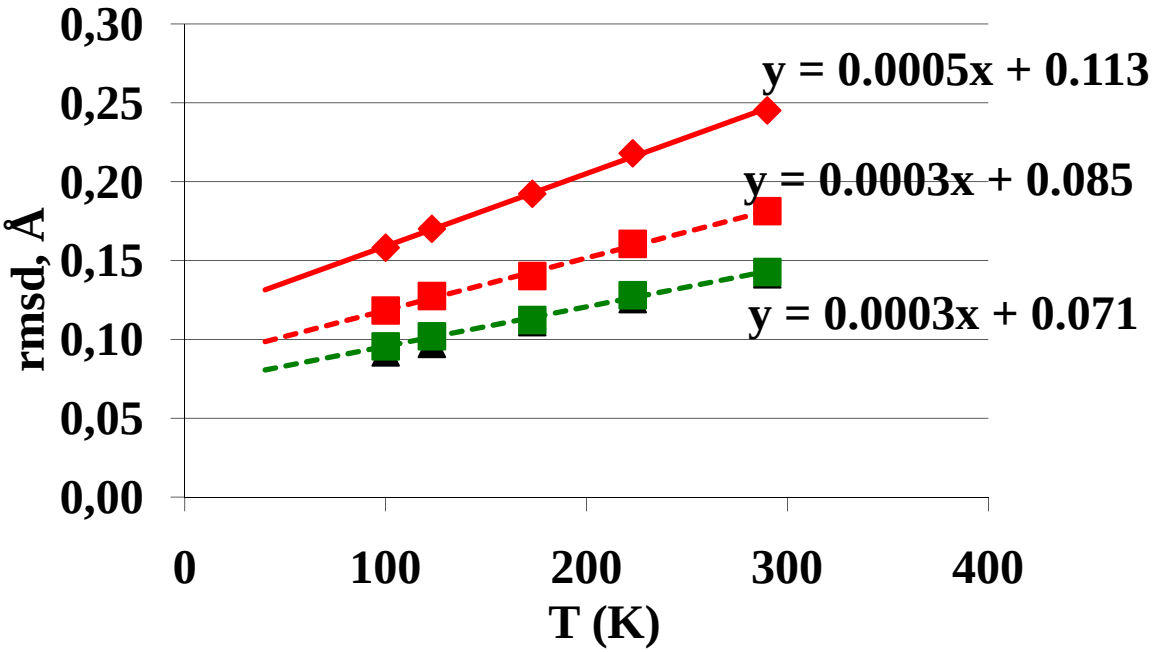


Figure 8. Root-mean-square displacements (Å) for the planar (O1W) and pyramidal (O2W) aqua ligands in *trans*-$[Co(sac)_2(H_2O)_4]$, determined at five temperatures by x-ray diffraction. Red diamonds (top), rmsd for O1W perpendicular to the plane of the ligand; red squares (middle), rmsd for O2W in the direction of the apex of the pyramid (lone pair direction); black triangles and green squares (bottom) smallest principal rmsd for O1W (triangles, obscured by squares) and for O2W (green squares).

## CLOSING COMMENTS

These three briefs illustrate some of the interesting phenomena that are to be found when exploring the molecular crystalline state. What I have presented is based on diffraction work, but this is not the only way to explore molecular crystals. For the planar water systems, we have undertaken neutron inelastic scattering measurements in collaboration with Alexander Kolesnikov. These should reveal the nature of any soft modes present. But even within the realm of diffraction work, there is plenty more that can be done. High-throughput neutron diffraction measurements will be a great aid in studying further systems with planar water. High-pressure diffraction analyses have been conducted on the antiferrodistortive transition in the nickel cyanurate. These are not published, as of this writing.

As most here know, Bob Bau was the chairman of the Instrument Development Team for the single crystal diffractometer at the Spallation Neutron Source. This instrument will be a great asset in studying systems like the ones that I have described; and as I say it is clear that there are many more to study. Although Bob himself will not be able to apply his special creative talents to the use of this instrument, his efforts on behalf of this project will be a benefit to all of its future users.

**ACKNOWLEDGMENTS**

Most of the work described in this presentation either is still in development or has suggested further study that is underway. The authors of Reference [7] are coworkers on the reactivity study in molecular crystals. Pressure measurements on the Ni cyanurate phase transition, as yet unpublished, were conducted by Art Schultz, Xiaoping Wang, and Rob Henning. The neutron diffraction measurements on the planar water systems were carried out by Art Schultz and Paula Piccoli. My university collaborators on the planar water study are Dr. Tatiana Soler and Ms. Carmen Cunchillos. Funding is provided by the Ministry of Science and Innovation (Spain), Grant MAT2008-04350 and CONSOLIDER-INGENIO in Molecular Nanoscience, ref. CSD 2007-00010. Additional funding is provided by the Regional Government of Aragón.

**REFERENCES**

[1] C. K. Johnson, E. J. Gabe, M. R. Taylor and I. A. Rose, J. Am. Chem. Soc. 87 (1965), 1802.
[2] D. McKie and C. McKie, Crystalline Solids, (Nelson, Surrey, UK, 1974), Chap. 13, 14.
[3] R. D. Shannon and D. C. Ross, Nature 202 (1964), 1000.
[4] F. K. Lotgering, J. Inorg. Nucl. Chem. 9 (1959), 113.
[5] A. L. Mackay, in: Reactivity of Solids, Proc. Fourth Intern. Symp. Reactivity of Solids 1960, eds. J. H. Boer *et al.* (Elsevier, Amsterdam 1960), p. 571.
[6] L. S. Dent Glasser, F. P. Glasser, H. F. W. Taylor, Quart. Rev. Chem. Soc. 16 (1962), 343.
[7] J. Campo, L. R. Falvello, I. Mayoral, F. Palacio, T. Soler and M. Tomás, J. Am. Chem. Soc. 130 (2008), 2932.
[8] J. G. Bergman and F. A. Cotton, Inorg. Chem. 5 (1966), 1208.
[9] L. Lisnard, F. Tuna, A. Candini, M. Affronte, R. E. P. Winpenny and E. J. L. McInnes, Angew. Chem., Int. Ed. 47 (2008), 9695.
[10] L. R. Falvello, M. A. Hitchman, F. Palacio, I. Pascual, A. J. Schultz, H. Stratemeier, M. Tomás, E. P. Urriolabeitia and D. M. Young, J. Am. Chem. Soc. 121 (1999), 2808.
[11] E. K. H. Salje, Acta Cryst., Section A A47 (1991), 453.
[12] H. Zabrodsky, S. Peleg and D. Avnir, J. Am. Chem. Soc. 114 (1992), 7843.
[13] H. Zabrodsky, S. Peleg and D. Avnir, J. Am. Chem. Soc. 115 (1993), 8278.
[14] S. Z. Haider, K. M. A. Malik, K. J. Ahmed, H. Hess, H. Riffel and M. B. Hursthouse, Inorg. Chim. Acta 72 (1983), 21.
[15] J. D. Dunitz, V. Schomaker and K. N. Trueblood, J. Phys. Chem 92 (1988), 856.
[16] F. H. Allen, Acta Cryst., Section B B58 (2002), 380.
[17] S. M. Jessen and H. Küppers, J. Appl. Cryst. 24 (1991), 239.

# ORGANIC-BASED MAGNETS: THE IMPORTANCE OF STRUCTURAL DETERMINATIONS FROM THE RIETVELD REFINEMENT OF THE POWDER X-RAY DATA

**Joel S. Miller**
*Department of Chemistry, University of Utah, Salt Lake City, UT 84112-0850, USA*

**Peter W. Stephens**
*Department of Physics and Astronomy, Stony Brook University, Stony Brook, NY 11794-3800, USA*

*Dedicated to Memory of Robert Bau*

## ABSTRACT
Magnets composed of molecular, and in particular organic, components that provide both electron spin(s) and spin coupling that can stabilize bulk magnetic ordering have been achieved. This was first reported for the ionic, electron transfer salt $[Fe(C_5Me_5)_2]^+[TCNE]^-$ (TCNE = tetracyanoethylene), which orders at $T_c$ = 4.8 K. After more than two decades of study, its structure has been recently established via the Rietveld refinement of the synchrotron powder X-ray diffraction data. This methodology has revealed the unexpected structures of $[Fe[TCNE](NCMe)_2][FeCl_4]$ ($T_c$ = 90 K) and $M^{II}[TCNE]_2$, M = Mn ($T_c$ = 75 K), Fe ($T_c$ = 100 K)], *e.g.*, $Fe[TCNE][C_4(CN)_8]_{1/2}\bullet zCH_2Cl_2$, and the unpredicted stoichiometry and structure of $Mn[TCNE]_{3/2}(I_3)_{1/2}\bullet THF/2$ ($T_c$ = 171 K).

## INTRODUCTION
Magnets have been limited to a few first-row transition metals (*i.e.*, Fe, Co, and Ni) and/or their oxides with the key component of all magnets, unpaired electron spins, solely residing in d-orbitals. Later magnets based upon rare earth metals with unpaired electron spins residing in f-orbitals were discovered. Magnets have evolved from being curiosities to being extremely technologically important with a plethora of applications that are common in our everyday life. As a consequence, improved magnets are an important goal of contemporary materials chemistry research [1].

Magnets based upon organic radicals were first alluded to in the mid-1960's from a conceptual point of view [2], but their experimental realization was not achieved until 1985 [3]. $[Fe(C_5Me_5)_2]^+[TCNE]^-$ (TCNE = tetracyanoethylene) with a magnetic ordering temperature, $T_c$, of 4.8 K was the first magnet that *i*) had electron spins in *p*-orbitals, *ii*) exhibited magnetic hysteresis, *iii*) did not require metallurgical preparative methods, *iv*) was soluble in conventional organic solvents, and *v*) lacked extended covalent network bonding in 1, 2, or 3 dimensions (*i.e.,* 0-D) [4]. Many examples of organic- and more broadly molecule-based magnets exhibiting magnetic ordering including ferromagnets, ferrimagnets, canted antiferromagnets/weak ferromagnets, metamagnets, and spin glasses have been established. These magnets range from

p-orbital-based organic nitroxides [5,6,7], d/p-orbital-based mixed organic, organometallic or inorganic coordination compounds [6,7,8,9], to the more common d-orbital-based inorganic coordination compounds {*e.g.,* mixed metal cyanides [6,10] and oxalates [6,11]}, with several families of the organic/metal-ion-containing materials possessing TCNE radical anions, $[TCNE]^{\bullet-}$, and related species, studied in our and other laboratories.

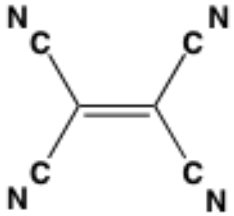

TCNE

Particularly in our laboratory, the structure of many organic and molecule-based magnets has to some extent suffered from a paucity of suitable single crystals to enable their single crystal structural determination. The structure is crucial both to understanding the properties of materials, and is essential to understanding the basis of magnetic interactions that lead to magnetic ordering. While it is commonly regarded that crystallography requires suitable single crystals, powder diffraction has been evolving into a method that can provide key structural information for many crystallographic problems. This is a consequence of developments in both instrumentation (*e.g.,* high resolution synchrotron, laboratory, and neutron diffractometers) and software. Except as noted, solutions and refinements presented here were performed using TOPAS Academic [12]. Typically, the obtained metric parameters from powder diffraction data have larger error bars than from single crystal refinements, but the ability to obtain a structure, even just the connectivity and relative orientation, of new materials via powder diffraction has permitted major advances in the understanding of magnetic materials etc. In our laboratory, these structural insights have shed new light on several problems.

Five families of TCNE-based molecule-based magnets have been reported, and they include, *i*) metallocene electron transfer salts of TCNE [13], $[M^{III}(C_5Me_5)_2]^+[TCNE]^{\bullet-}$ [4,14], several first-row transition metal ion salts of $[TCNE]^{\bullet-}$ [15], *ii*) $M[TCNE]_x$ (M = V, Mn, Fe, Co, Ni; x ~ 2), *iii*) $Mn(TCNE)_{3/2}I_{3/2}$, *iv*) $[Fe[TCNE](NCMe)_2][FeCl_4]$, and *v*) *meso*-tetraphenylporphinatomanganese(II) electron transfer salts of TCNE, $[Mn^{III}TPP]^+[TCNE]^{\bullet-}$ [15] typically as dichloromethane solvates. Of these, only $V[TCNE]_x$, a room temperature magnet [$T_c$ ~ 400 K (127 $^oC$)], has not been structurally characterized, due to its amorphous nature [16,17]. Nonetheless, based on several observed structures for *ii*-*iv*, aspects of the structure of $V[TCNE]_x$ can be surmised [17]. Herein, we review the chemistry, structure, and magnetic behavior of the first four of these families of magnets.

**$[Fe^{III}(C_5Me_5)_2]^+[TCNE]^{\bullet-}$**

The first organic-containing magnet, $[Fe^{III}(C_5Me_5)_2][TCNE]$, has been extensively studied and magnetically orders at $T_c$ = 4.8 K [17,18]. The material is prepared by crystallization from solvent, and the structure of the solvate was determined by single crystal techniques. However, the magnetic properties of the solvate differ from the unsolvated material. The determination of the structure has taken a score of years to solve, and required the solution from synchrotron powder X-ray diffraction data (PXRD). This is due to structural disorder in the as-grown sample

at ambient temperature, and the sample undergoing two structural phase transitions that destroy the single crystals before they reach the interesting magnetically ordered phase. The temperature dependent unit cell parameters, Figure 1, reflect the two phase transitions, and the structures at 12, 250, and 273 K were solved and refined [19].

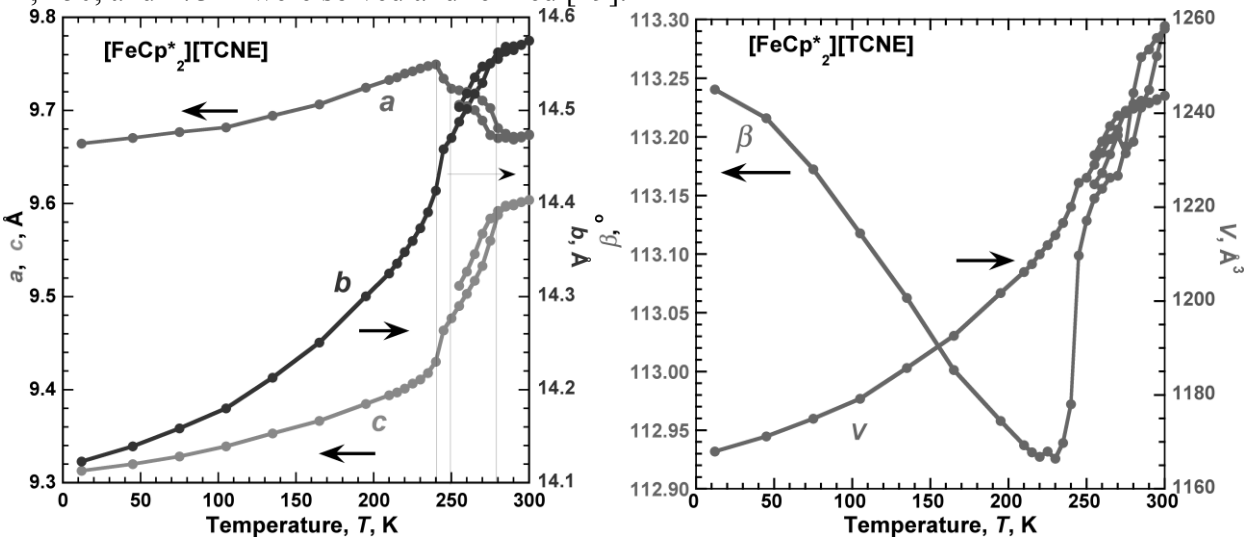


Figure 1. The temperature dependent unit cell parameters for $[Fe(C_5Me_5)_2][TCNE]$. The lines are guiders for the eye.

It is worthwhile to review some of the steps of the structure determination. The 250-K, high-resolution PXRD was readily indexed to a monoclinic unit cell with $a$ = 9.710 Å, $b$ = 14.493 Å, $c$ = 9.500 Å, and $\beta$ = 113.15°, which contains two formula units. In powder diffraction, systematic absences are a much weaker determinant of the space group than in single crystal data sets, because generally it is only a few of the lowest order reflections that can be stated to be missing. In this case, the (010) reflection was not observed, and most likely no (030) reflection, and so the postulate that the space group is $P2_1$ or $P2_1/m$ remained to be confirmed upon successful solution and refinement. A favored technique for structure determination in problems like this is direct space simulated annealing [20], in which a model was hypothesized with the known molecular contents in the unit cell and seeks the arrangement which matches the observed powder diffraction pattern. Frequently, several different guesses with respect to the molecular contents, symmetry, etc. must be modeled before reaching a satisfactory solution. Both molecules could have mirror symmetry, but solutions with the molecules on mirror planes of $P2_1/m$ were not promising. A search in $P2_1$, with one copy of each molecule on a general position, yielded a much better match to the observed pattern, as shown in Figure 2. However, restrained Rietveld refinements were not stable, and could not give acceptable agreement with the measured profile. Furthermore, attempts to Rietveld-refine the structure in $P2_1$ led to unacceptable bond lengths.

This conundrum was solved by recognizing that the structure was disordered, and could be satisfactorily modeled with half occupancy of two orientations of each molecule, related by the mirror in $P2_1/m$. The difference was small (*e.g.,* $R_{wp}$ = 4.74 *vs.* 5.23%), but unmistakable. The disorder vanishes below 250 K, where one axis doubles and the mirror plane becomes a glide plane; details are given in Ref. 19. Examination of Figure 2 shows that the difference between powder patterns of ordered $P2_1$ and disordered $P2_1/m$ is small, and careful evaluation of the

stability of structure solutions and consideration of alternative structural models was necessary to reach the correct conclusion.

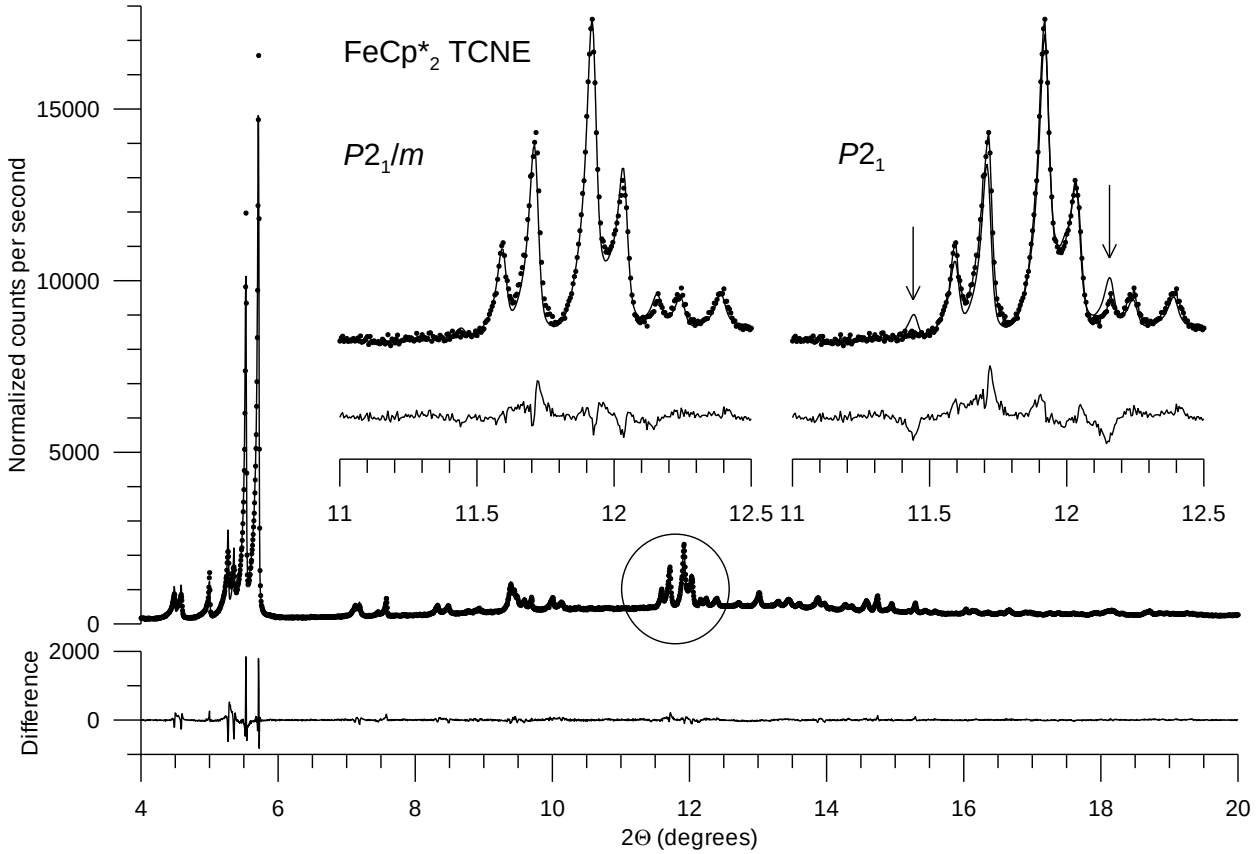


Figure 2. Rietveld refinement of $[Fe(C_5Me_5)_2][TCNE]$ at 250 K. Dots represent raw data, solid lines the computed fit. The insets show regions where the refinements in space groups $P2_1/m$ and $P2_1$ most clearly differ.

The resulting ordered structure consists of chains of alternating $[Fe^{III}(C_5Me_5)_2]^+$ cations and $[TCNE]^-$ anions (see Figure 3), very similar to the structure of the solvate previously known from single crystal measurements. A 1.7% contraction and tilting of the $[Fe^{III}(C_5Me_5)_2][TCNE]$ chains occurs at l2 K relative to room temperature. With knowledge of all of the key inter- and intrachain separations, a computational analysis identifying the key nearest-neighbor spin interactions was executed [19]. This study identified the key interactions as being the intrachain ferromagnetic $[Fe(C_5Me_5)_2]^{+\cdots}[TCNE]^-$ interactions ($J/k_B$ = 26 ± 5 K), but additional antiferro- and ferromagnetic interchain interactions (<|0.1| K) are also evident. These small interchain exchange interactions, however, are insufficient to account for the observed 3-D ferromagnetic ordering. Hence, the simplified models currently used are inadequate to understand the magnetic couplings.

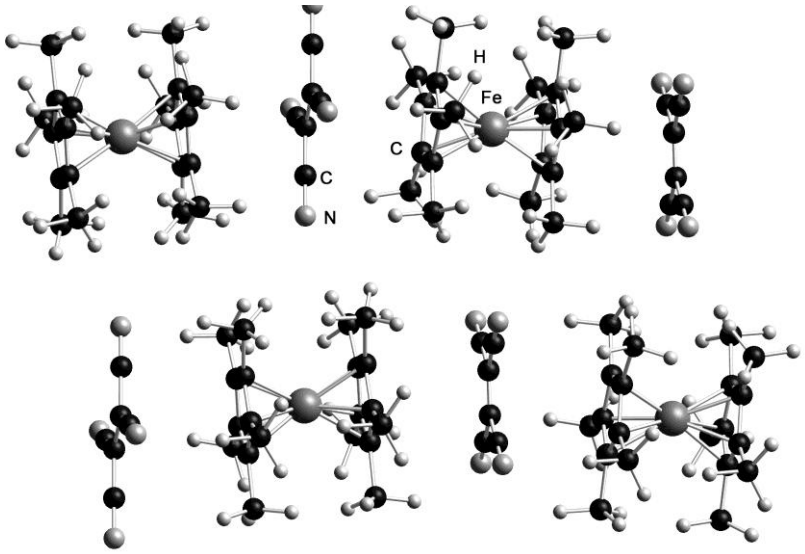


Figure 3. Segment of two adjacent parallel, out-of-registry chains of $[Fe^{III}(C_5Me_5)_2][TCNE]$ at 12 K.

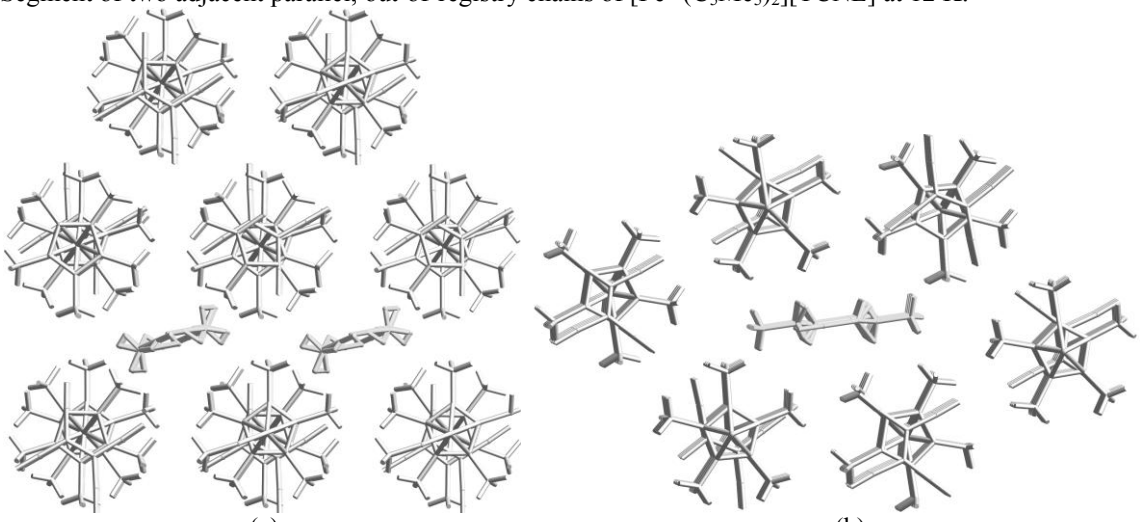

(a) (b)

Figure 4. Structure of $[Fe^{III}(C_5Me_5)_2][TCNE]$•sol [sol = MeCN (a); PrCN/2 (b)] normal to the parallel chains.

Subsequently, the structures of $[Fe(C_5Me_5)_2][TCNE]$•sol (sol = MeCN, EtCN/2, *n*-PrCN/2), which have been challenging due to the facile solvent loss, have been solved [21]. Key was obtaining suitable samples for single crystal X-ray diffraction. Crystals formed upon cooling a saturated solution to -30 $^{o}$C, and the crystals along with their with mother liquor were then poured onto a paper towel while cold. The crystals were quickly covered with Paratone® oil on a needle and relocated to a Paratone drop on a microscope slide, and then mounted for study. This method did not work every time, but this methodology was repeated until suitable crystals were located.

The structure for $[Fe(C_5Me_5)_2][TCNE]$•MeCN at 100 K has a $P\bar{1}$ unit cell [21], whereas at 243 K it has a monoclinic $C2/c$ unit cell [3]. Nonetheless, in both phases, parallel chains of alternating $[Fe^{III}(C_5Me_5)_2]^{\bullet+}$ cations and $[TCNE]^{\bullet-}$ anions, as occurs for $[Fe(C_5Me_5)_2][TCNE]$, are separated by layers of MeCN solvent, Figure 4a. In contrast, the EtCN and *n*-PrCN solvates have half as

many per Fe, and possess columns of solvent parallel to the alternating $[Fe^{III}(C_5Me_5)_2]^{\bullet+}$ cations and $[TCNE]^{\bullet-}$ anions, as occurs for $[Fe(C_5Me_5)_2][TCNE]$, Figure 4b.

The presence of solvent, either layers or columns, for $[Fe(C_5Me_5)_2][TCNE]$•sol reduces the number of and/or lengthens the spin interaction pathways that reduce the average interaction energy and lowers $T_c$. This is observed as $T_c$ is reduced from 4.80 K for $[Fe(C_5Me_5)_2][TCNE]$, to 2.87 K for $[Fe(C_5Me_5)_2][TCNE]$•MeCN and 2.98 K for $[Fe(C_5Me_5)_2][TCNE]$•EtCN/2 [22].

Both $[Fe^{III}(C_5Me_5)_2][TCNE]$ and $[Fe^{III}(C_5Me_5)_2][TCNE]$•sol are best considered as being structurally zero dimensional (0-D) due to the presence of isolated ions, and lack extended bonding. From a magnetic perspective, they have dominant 1-D coupling.

**$[Fe[TCNE](NCMe)_2][FeCl_4]$**

While the reaction of $FeI_2$ [26] or $Fe(CO)_5$ [27] and TCNE formed $Fe^{II}[TCNE]_2$•$zCH_2Cl_2$, the reaction of TCNE and $FeCl_2(NCMe)_2$ in dichloromethane formed a new material that from IR and magnetic data was clearly not $Fe^{II}[TCNE]_2$•$zCH_2Cl_2$. The stoichiometry and structure were unknown. The high-resolution PXRD data was well resolved to nearly atomic resolution, and so direct methods appeared to be a suitable mode to solve this problem. The development of direct methods to phase unknown structures from single crystal diffraction data has been one of the significant milestones in the development of crystallography, and its extension to powder data has likewise been a valuable advance. We used the powder direct methods program EXPO [23] to solve, and TOPAS Academic [12] to refine the structure. Only by determining the crystal structure could the chemical formula be identified as $[Fe^{II}[TCNE](NCMe)_2][Fe^{III}Cl_4]$, and the overall reaction was has TCNE being reduced and $[Fe^{II}Cl_4]^{2-}$ being oxidized [24]:

$$2\ Fe^{II}Cl_2(NCMe)_2\ +\ TCNE\ \rightarrow\ [Fe^{II}[TCNE](NCMe)_2][Fe^{III}Cl_4] + 2\ MeCN$$

$[Fe^{II}[TCNE](NCMe)_2][Fe^{III}Cl_4]$ possesses four $S$ = 1/2 $\mu_4$-$[TCNE]^{\bullet-}$ anions bonded to four octahedrally coordinated $S = 2$ $Fe^{II}$ ions in corrugated layers (Figure 5a).

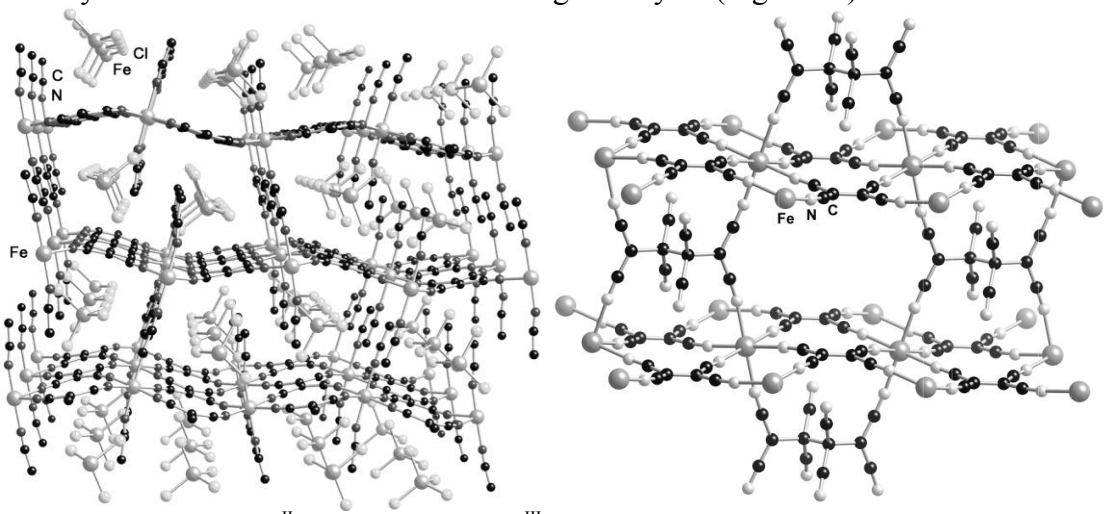


Figure 5. (a) Structures of $[Fe^{II}[TCNE](NCMe)_2][Fe^{III}Cl_4]$ possessing corrugated layers of $\mu_4$-$[TCNE]^{\bullet-}$ bound to four $Fe^{II}$ ions. MeCN coordinates trans to the $Fe^{II}$ ions, and the $[Fe^{III}Cl_4]^-$ anion lies within the lattice. (b) Structure of $Fe(TCNE)_2$•$zCH_2Cl_2$, *i.e.*, $Fe[TCNE][C_4(CN)_8]_{1/2}$•$zCH_2Cl_2$, (z ~ 0.32) possessing corrugated layers of $\mu_4$-$[TCNE]^{\bullet-}$ bound to four $Fe^{II}$ ions that are connected by $\mu_4$-$[C_4(CN)_8]^{2-}$ [29]. The $CH_2Cl_2$ solvent is disordered in the channels and is not shown for clarity.

The $\chi T(T)$ for $[Fe(TCNE)(NCMe)_2][FeCl_4]$ can be fit to the Curie-Weiss expression with $\theta \sim$ 100 K indicative of significant short-range ferromagnetic coupling, and above 200 K $d\chi^{-1}(T)/dT$, decreases characteristic of a ferrimagnet [24]. Both the real, $\chi'(T)$, and complex, $\chi''(T)$, ac susceptibilities exhibit a sharp peak at ~90 K (Figure 6) in accord with an ordering temperature, $T_c$, of 90 K. $S = 5/2$ $[FeCl_4]^-$ contributes to the magnetization, but not to the magnetic ordering. Hence, $[Fe(TCNE)(NCMe)_2][FeCl_4]$ is structurally and magnetically a 2-D system, and due to the anisotropic $Fe^{II}$ ion is an Ising ferrimagnet with weak magnetic coupling between the layers [25].

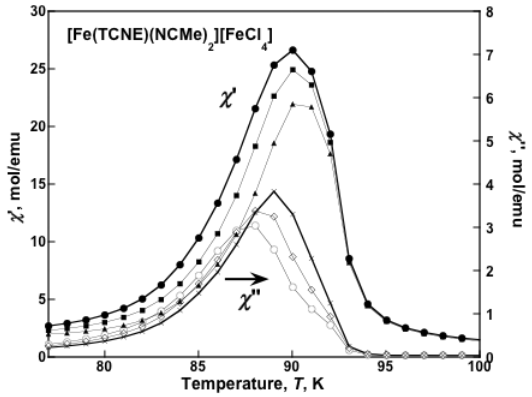


Figure 6. $\chi'(T)$ and $\chi''(T)$ for $[Fe[TCNE](NCMe)_2][FeCl_4]$.

**$M^{II}[TCNE]_2$ (M = Mn, Fe)**

The reaction of $MI_2$ and TCNE in dichloromethane with a little acetonitrile formed magnets with the nominal $M^{II}[TCNE]_2 \bullet zCH_2Cl_2$ (M = Mn, Fe, Co, Ni) composition [26], with $T_c$ = 100 [26b,27], 75 [26c,28], 44, and 44 K [26a] for M = Fe, Mn, Co, Ni, respectively. Prior to this $V[TCNE]_x \bullet zCH_2Cl_2$ (x ~ 2) was established to be a room temperature magnet [15,16,17], however, it is amorphous, and its structure could not determined. In contrast to $V[TCNE]_x \bullet zCH_2Cl_2$, the Mn and Fe compounds diffracted, and the solution and Rietveld refinement of the PXRD data resulted in initially determining the structure for $Fe^{II}[TCNE]_2 \bullet zCH_2Cl_2$. While $M^{II}[TCNE]_2 \bullet zCH_2Cl_2$ (M = Mn, Fe) prepared from $MI_2$ gave a decent powder X-ray diffraction pattern, examination of that pattern revealed that the sample was not pure, and other diffracting phases were also present that limited the refinement of the data. However, $Fe^{II}[TCNE]_2 \bullet zCH_2Cl_2$ prepared from $Fe(CO)_5$ [27] led to a purer product and PXRD data that eventually enabled the structure determination (Figure 7) [29].

One issue frequently encountered in the structure determination from powder data is the influence of preparation conditions on the quality of powder diffraction pattern obtained. Figure 7 shows the patterns of several different samples of $Fe^{II}[TCNE]_2 \bullet zCH_2Cl_2$, all of which had essentially equivalent magnetic properties. The various steps of structure determination from powder diffraction data depend on having sharp, well-resolved peaks. The bottom two traces in Figure 7 are useless for structure determination. The third pattern up could be indexed to an orthorhombic unit cell, but the diffraction pattern still did not contain enough information for a structure solution. Data from the top pattern eventually yielded a solution and refinement of the crystal structure shown in Figure 5b, and Rietveld refinement shown in Figure 8.

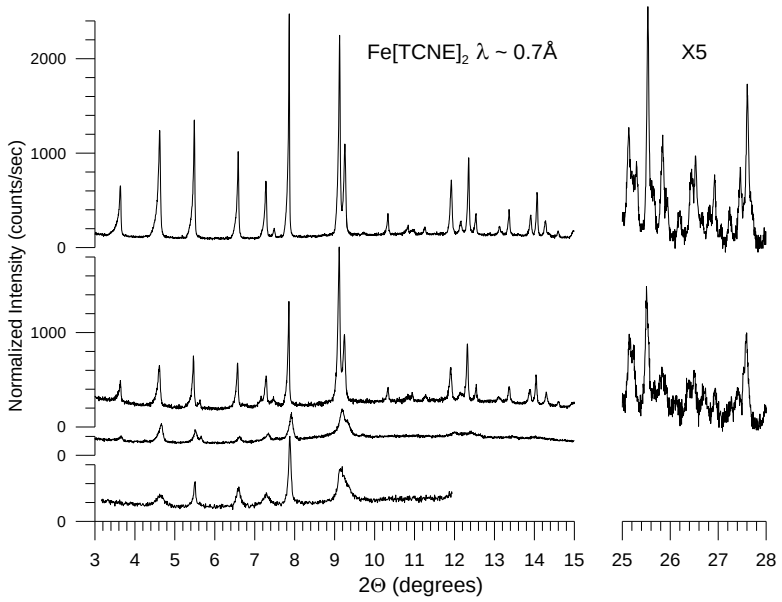


Figure 7. Powder X-ray diffraction patterns of several different samples of $Fe^{II}[TCNE]_2 \bullet zCH_2Cl_2$. All measurements were taken with samples sealed in capillaries.

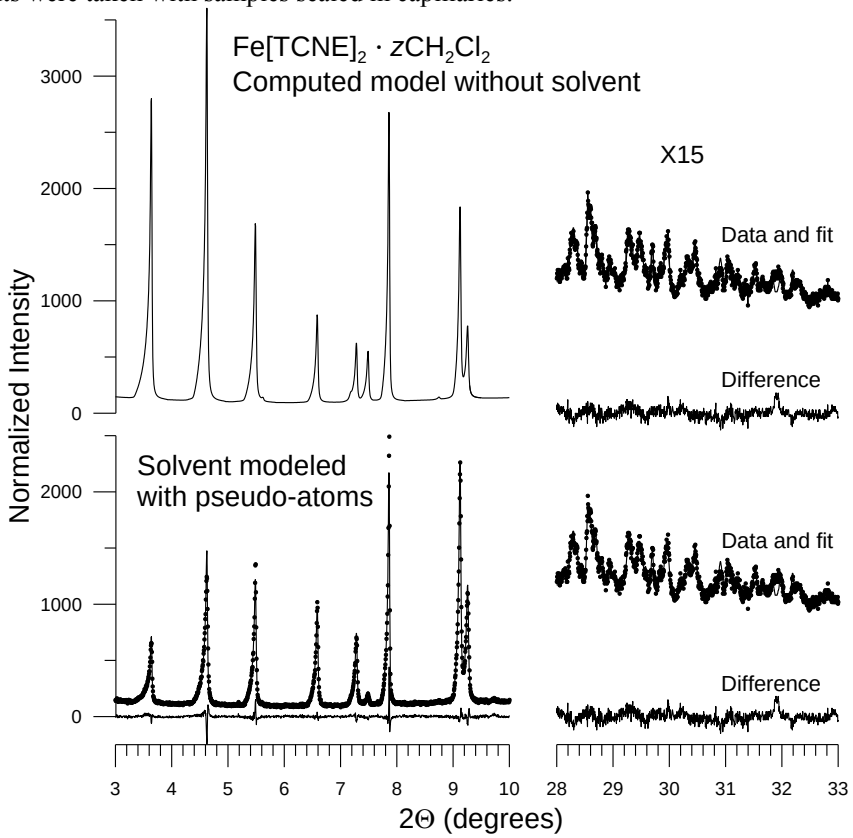


Figure 8. High-resolution synchrotron PXRD data (dots) and Rietveld fit of the data for $Fe(TCNE)_2 \bullet zCH_2Cl_2$ (lines) [29]. The upper panels show the computed model from the $Fe[TCNE][C_4(CN)_8]$ framework only; the lower panels are for the final refinement with solvent described as pseudo-atoms. The vertical axis is expanded by a factor of 15 for the high angle data.

The XRPD pattern was readily indexed as *C*-centered orthorhombic unit cell, and the lack of further systematic absences required the space group to be *Cmmm* or (very unlikely) one of its acentric subgroups. In conjunction with lattice dimensions and simple packing considerations, this suggests that each of the molecular constituents should be centered at special positions at the intersections of mirror planes and/or two-fold rotation axes. Initial attempts to solve this structure by simulated annealing of the expected molecular contents and by direct methods were unsuccessful. In retrospect, this was because of a large degree of disorder in the structure. We were able to solve the structure using FOX [30], in an unconventional mode using independent pseudo-atoms. When molecules were assigned to the charges, it revealed the unexpected reaction of two $[TCNE]^{\bullet-}$ to form $[C_4(CN)_8]^{2-}$ [31], which is disordered about sites of *mmm* symmetry. The structure is illustrated in Figure 5b. Disordered solvent also plays an important role in the diffraction pattern. Even though it is a small fraction of the total charge, if it is left out, the low angle part of the diffraction pattern is computed incorrectly and the correct solution cannot be reached. A comparison of the correct refinement (bottom panels) with the model computed without solvent is shown in Figure 8. Note the very large differences at low angles ($d$ = 13.4 – 4.0 Å) in contrast to the indistinguishable quality of fit for high angle data ($d$ = 1.45 – 1.23 Å). This is because the disordered solvent has a diffuse charge distribution, which acts as a very large thermal parameter, so that it only contributes to low-angle reflections.

The structure of $Fe(TCNE)_2 \bullet zCH_2Cl_2$ consists of $S$ = 1/2 $\mu_4$-$[TCNE]^{\bullet-}$ anions bonded to four octahedrally coordinated $S$ = 2 $Fe^{II}$ ions in corrugated layers (Figure 5b). These magnetic layers are connected by non-spin bearing $S$ = 0 $\mu_4$-$[C_4(CN)_8]^{2-}$ dianions that provide for a porous 3-D extended network structure with the $CH_2Cl_2$ solvent residing within the channels. Hence, the structure is best described as $Fe[TCNE][C_4(CN)_8]_{1/2} \bullet zCH_2Cl_2$ with the $S$ = 2 $Fe^{II}$ ions antiferromagnetically coupled to one, not two, $S$ = 1/2 $\mu_4$-$[TCNE]^{\bullet-}$ anions.

It is noteworthy that $Fe[TCNE][C_4(CN)_8]_{1/2} \bullet zCH_2Cl_2$ and $[Fe^{II}[TCNE](NCMe)_2][Fe^{III}Cl_4]$ have very similar corrugated structures of the magnetically active $Fe^{II}[TCNE]^{\bullet-}$ layers (Figure 5), even though their empirical formulae, $Fe[TCNE]_2$ and $FeCl_2[TCNE]_{1/2}(NCMe)$ have opposite ratios of metal to TCNE. $Mn[TCNE][C_4(CN)_8]_{1/2} \bullet zCH_2Cl_2$ is isostructural with the Fe compound [28].

Prior to the structure determination, the observed saturation magnetization of 16.4 kemuOe/mol at 9 T, 2 K was a puzzle, as 11.2 kemuOe/mol was expected from antiferromagnetic coupling of $Fe^{II}$ to two $[TCNE]^{\bullet-}$ anions [29]. The formation of diamagnetic $[C_4(CN)_8]^{2-}$ from two $S$ = 1/2 $[TCNE]^{\bullet-}$ anions results in only one $[TCNE]^{\bullet-}$ anion per $Fe^{II}$, which has an expected moment of 16.8 kemuOe/mol. Thus, $Fe[TCNE][C_4(CN)_8]_{1/2} \bullet zCH_2Cl_2$ has a 3-D extended network structure, but a layered (2-D) magnetic structure with weak magnetic coupling between the layers.

**$Mn(TCNE)_{3/2}I_{3/2}$**

While the reaction of $MnI_2$ and TCNE formed $Mn^{II}[TCNE]_2 \bullet zCH_2Cl_2$ [26], the replacement of $MnI_2$ with $MnI_2(THF)_3$ (THF = tetrahydrofuran) formed a different material with strong 2231 and 2189 $cm^{-1}$ $\nu_{CN}$ absorptions as well as preliminary magnetic data suggesting magnetic ordering at a fairly high temperature (~170 K). These peaks were suggestive of the presence of $\mu_4$-$[TCNE]^{\bullet-}$ [24]. Nonetheless, the composition of the material and its structure were a mystery. High-resolution PXRD data showed that it had a similar lattice to $M^{II}[TCNE]_2 \bullet z$Sol, which led to the construction of a hypothesized framework of the structure. In successive refinements, other

elements of the structure were added: an additional inequivalent $[TCNE]^{\bullet-}$, $I_3^-$ counterions, and some disordered solvent. The refined structure was identified as $Mn^{II}[TCNE]_{3/2}I_{3/2}$•zTHF, and its 3-D structural-magnetic framework is illustrated in Figure 9

The structure of $Mn^{II}[TCNE]_{3/2}I_{3/2}$ possesses octahedrally coordinated $S = 5/2$ $Mn^{II}$ ions bonded to two different $S = 1/2$ $\mu_4$-$[TCNE]^{\bullet-}$ anions. One $\mu_4$-$[TCNE]^{\bullet-}$ forms corrugated layers, as is observed for $Fe[TCNE][C_4(CN)_8]_{1/2}$•$zCH_2Cl_2$ (Figure 5b) and $[Fe[TCNE](NCMe)_2][FeCl_4]$ (Figure 5a). The other $\mu_4$-$[TCNE]^{\bullet-}$ lies nominally perpendicular, and forms a planar layer (Figure 9). This 3-D network structure has the composition of $[Mn^{II}[TCNE]_{3/2}]^{1/2+}$, and its counteranion is triiodie, $I_3^-$ for which occurs in a 1:1/2::Mn:$I_3$ ratio. $I_3^-$ forms linear chains parallel to the central CC bonds of both types of $\mu_4$-$[TCNE]^{\bullet-}$.

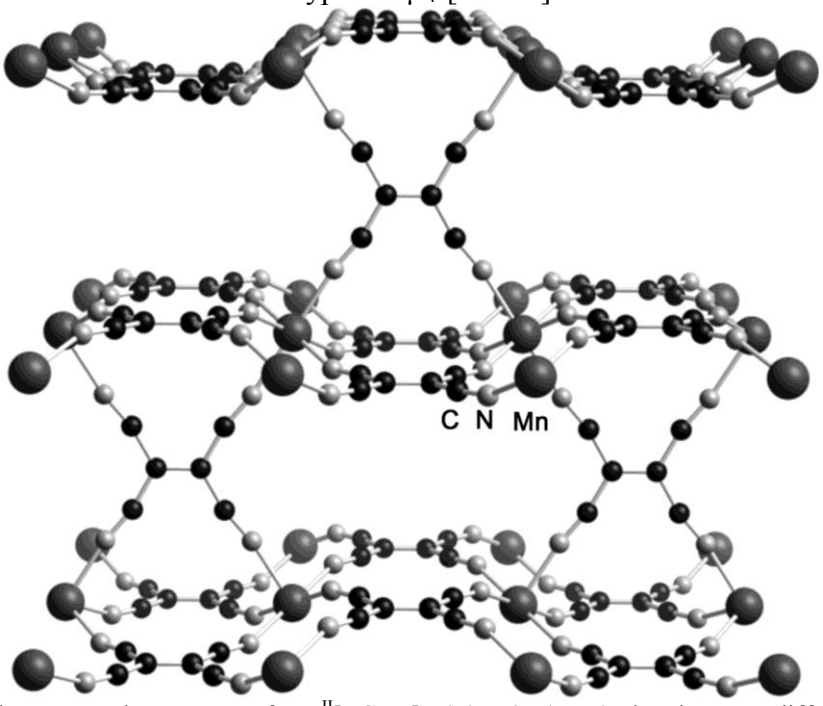


Figure 9. 3-D covalent network structure of $Mn^{II}[TCNE]_{3/2}(I_3)_{1/2}$•0.5(THF) showing two different $\mu_4$-$[TCNE]^{\bullet-}$'s. Disordered solvent and $I_3^-$ are omitted for clarity.

The structure of $Mn^{II}[TCNE]_{3/2}I_{3/2}$ possesses octahedrally coordinated $S = 5/2$ $Mn^{II}$ ions bonded to two different $S = 1/2$ $\mu_4$-$[TCNE]^{\bullet-}$ anions. One $\mu_4$-$[TCNE]^{\bullet-}$ forms corrugated layers, as is observed for $Fe[TCNE][C_4(CN)_8]_{1/2}$•$zCH_2Cl_2$ (Figure 5b) and $[Fe[TCNE](NCMe)_2][FeCl_4]$ (Figure 5a). The other $\mu_4$-$[TCNE]^{\bullet-}$ lies nominally perpendicular, and forms a planar layer (Figure 9). This 3-D network structure has the composition of $[Mn^{II}[TCNE]_{3/2}]^{1/2+}$, and its counteranion is triiodie, $I_3^-$ for which occurs in a 1:1/2::Mn:$I_3$ ratio. $I_3^-$ forms linear chains parallel to the central CC bonds of both types of $\mu_4$-$[TCNE]^{\bullet-}$.

The zero-field/field cooled (ZFC/FC) magnetizations, $M_{ZFC}(T)$ and $M_{FC}(T)$, for $Mn[TCNE]_{3/2}(I_3)_{1/2}$ rise sharply below 172 K (Figure 10) suggestive of magnetic ordering. $M_{ZFC}(T)$ reaches a maximum at 170 K before gradually decreasing toward zero, while, $M_{FC}(T)$ increases on additional cooling. These data diverge at a 171-K bifurcation temperature ($T_b$), while the extrapolated intercept of the $M_{FC}(T)$ data is also 171 K. Likewise, the temperature-dependent remnant magnetization, $M_r(T)$, is coincident to $M_{FC}(T)$, and extrapolation of the initial

rise upon cooling give an intercept of 171 K (Figure 10). Hence, $T_c$ is 171 K for this structural and magnetic 3-D ferrimagnet [28].

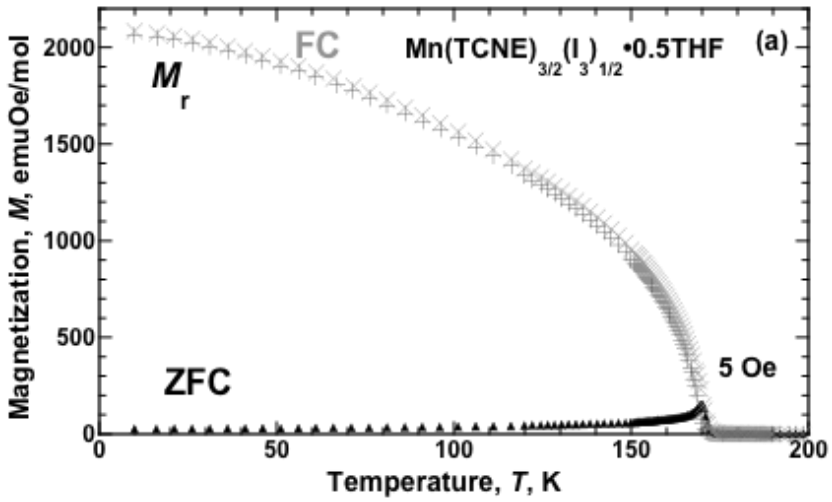


Figure 10. 5-Oe $M_{ZFC}(T)$ (σ), $M_{FC}(T)$ (x), and $M_r(T)$ (+) for $Mn[TCNE]_{3/2}(I_3)_{1/2}$•THF/2.

## SUMMARY

The structures and magnetic behaviors of four structural families of TCNE-based magnets have been reviewed. These examples were selected to emphasize the importance of crystallography, especially via the Rietveld refinement of the synchrotron powder X-ray diffraction data. This embryonic technique has proved invaluable to not only determine the structure of materials whose structure could not be accessed by any other method, but in many cases to identify the chemical stoichiometry. The structure of $[Fe(C_5Me_5)_2]^+[TCNE]^-$ could not have been determined by single crystal X-ray diffraction, as crystals disintegrated upon cooling due to the two phase transition that occur below 273 K. While the composition of $M^{II}[TCNE]_2$•$zCH_2Cl_2$ (M = Mn, Fe) was known from the elemental analyses, the structure, especially the formation of $\mu_4$-$[TCNE]^-$ was unknown. The revelation that $[TCNE]^-$ dimerized to form the σ-dimer, $[C_4(CN)_8]^{2-}$, was unexpected, and was remarkably revealed only through the Rietveld refinement of the PXRD data. Likewise, lacking any perception of what the structure of $[Fe(TCNE)(NCMe)_2][FeCl_4]$ was, the Rietveld refinement of the PXRD data provided this information. Finally, the composition, and structure $Mn^{II}[TCNE]_{3/2}(I_3)_{1/2}$ was revealed only from the Rietveld refinement of the PXRD data. These are several, but not all, examples that illustrate the importance of Rietveld refinement of synchrotron PXRD data to ascertain the structure, and in some cases, the stoichiometry of new materials.


## ACKNOWLEDGMENTS

The research described here was performed with many students and other collaborators. We are pleased to acknowledge the bulk of the PXRD analysis by Jae-Hyuk Her and Kevin Stone. We appreciate the continued partial support by the Department of Energy Division of Material Science (Grant Nos. DE-FG03-93ER45504 and DE-FG02-01ER4593). Use of the National Synchrotron Light Source, Brookhaven National Laboratory, was supported by the U.S. Department of Energy, Office of Basic Energy Sciences, under Contract No. DE-AC02-98CH10886.

**REFERENCES**


[1] R.M. White, J. Appl. Phys., 57, (1985), 2996. W.E. Wallace, J. Less-Common Met., 100, (1984), 85. J.S. Miller and M. Drillon, eds., Magnetism - Molecules to Materials (Wiley-VCH, Weinheim, DE, 2001), Vol. 1 - 5.
[2] a) P.W. Anderson, Concepts in Solids, (W. *A*. Benjamin, Inc., New York, NY, 1963), p 7. b) H.M. McConnell, J. Chem. Phys., 39, (1963), 1910. c) H.M. McConnell, Proc. R. A. Welch Found., Chem. Res., 11, (1967), 144.
[3] J.S. Miller, J.C. Calabrese, H. Rommelmann, S. Chittipeddi, A.J. Epstein, J.H. Zhang and W.M. Reiff, J. Am. Chem. Soc., 109, (1987), 769.
[4] J.S. Miller, J. Mater. Chem., 20, (2010), 1846.
[5] a) D.B. Amabilino, J. Veciana, Magnetism - Molecules to Materials, J.S. Miller and M. Drillon, Eds., 2, (Wiley-VCH, Mannheim, 2001), p 1. b) M. Kinoshita, Phil. Trans. R. Soc. Lond. A, 357, (1999), 2855. c) M. Kinoshita, Jap. J. Appl. Phys., 33, (1994), 5718. d) R. Chiarelli, A. Rassat, Y. Dromzee, Y. Jeannin, M.A. Novak and J.L. Tholence, Phys. Scrip., T49, (1993), 706.
[6] a) S.J. Blundell and F.L. Pratt, J. Phys.: Condens. Matter, 16, (2004), R771. b) V.I. Ovcharenko and R.Z. Sagdeev, Russ. Chem. Rev., 68, (1999), 345. c) W. Plass, Chem. Zeit, (1998), 32, 323. d) J.A. Crayson, J.N. Devine and J.C. Walton, Tetrahedron, 56, (2000), 7829. e) P. Day, J. Chem. Soc., Dalton Trans., (1997), 701. f) J.S. Miller and A.J. Epstein, Chem. Eng. News, 73, (1995), 30. g) J.S. Miller and A.J. Epstein, Adv. Chem. Ser., 245, (1995), 161. h) A.L. Buchachenko, Russ. Chem. Rev., 59, (1990), 307. i) O. Kahn, Struct. Bonding, 68, (1987), 89.
[7] J.S. Miller and A.J. Epstein, Angew. Chem. Int. Ed. Engl., 33, 1994, 385.
[8] O. Kahn, Molecular Magnetism, (VCH Publishers, Inc., New York, NY, 1993).
[9] a) D. Gatteschi, Adv. Mat., 6, (1994), 635. b) A. Caneschi, D. Gatteschi, R. Sessoli and P. Rey, Acc. Chem. Res., 22, (1989), 392. c) A. Caneschi and D. Gatteschi, Progr. Inorg. Chem., 37, (1991), 331.
[10] a) M. Verdaguer, A. Bleuzen, V. Marvaud, J. Vaissermann, M. Seuleiman, C. Desplanches, A. Scuiller, C. Train, R. Garde, G. Gelly, C. Lomenech, I. Rosenman, P. Veillet, C. Cartier and F. Villain, Coord. Chem. Rev., 190-192, (1999), 1023. b) M. Verdaguer, A. Bleuzen, C. Train, R. Garde, F. Fabrizi de Biani and C. Desplanches, Phil. Trans. R. Soc. Lond. A, 357, (1999), 2959. c) M. Verdaguer and G.S. Girolami, Magnetism - Molecules to Materials, J. S. Miller, M. Drillon, Eds., (Wiley-VCH, Mannheim, 2004), 4, 283.
[11] M. Pilkington and S. Decurtins, Magnetism - Molecules to Materials, J.S. Miller and M. Drillon, Eds., (Wiley-VCH, Mannheim, 2001), 2, 339.
[12] A.A. Coelho, http://www.topas-academic.net.
[13] J.S. Miller, Angew. Chem. Internat. Ed., 45, (2006), 2508.
[14] a) G.T. Yee and J.S. Miller, Magnetism - Molecules to Materials, J.S. Miller and M. Drillon, Eds., (Wiley-VCH, Mannheim, 2004), 5, 223. b) E. Coronado, J.R. Galàn-Mascarós and J.S. Miller, Comprehensive Organometallic Chemistry III, R.H. Crabtree and D.M.P. Mingos, Eds, (Elsevier, Amsterdam, Oxford, 2006), 12, 413.
[15] J.S. Miller and A.J. Epstein, J. Chem. Soc., Chem. Commun., (1998), 1319
[16] J.M. Manriquez, G.T. Yee, R.S. McLean, A.J. Epstein and J.S. Miller, Science, 252, (1991), 1415.

[17] J.S. Miller, Polyhed., 28, (2009), 1596.
[18] J.S. Miller, J.C. Calabrese, H. Rommelmann, S. Chittipeddi, A.J. Epstein, J.H. Zhang and W.M. Reiff, J. Am. Chem. Soc., 109, (1987), 769.
[19] J.-H. Her, P.W. Stephens, J. Ribas-Ariño, J.J. Novoa, W.W. Shum and J.S. Miller, Inorg. Chem., 48, 2009, 3296.
[20] K.D.M. Harris, M. Tremayne, P. Lightfoot, and P.G. Bruce, J. Am. Chem. Soc., 116, (1994), 3543.
[21] J.S. Miller, P.K. Gantzel, A.L. Rheingold and M.L. Taliaferro, Inorg. Chem., 48, (2009), 4201.
[22] M.L. Taliaferro, T.D. Selby and J.S. Miller, Chem. Mater., 15, (2003), 3602.
[23] A. Altomare, M.C. Burla, M. Camalli, B. Carrozzini, G.L. Cascarano, C. Giacovazzo, A. Guagliardi, A.G.G. Moliterni, G. Polidori, and R. Rizzi, Journal of Applied Crystallography, 32, (1999), 339-340.
[24] K.I. Pokhodnya, M. Bonner, J.-H. Her, P.W. Stephens and J.S. Miller, J. Am. Chem. Soc., 126, (2006), 15592.
[25] a) J.-W. Yoo, V.N. Prigodin, W.W. Shum, K.I. Pokhodnya, J.S. Miller and A.J. Epstein, Phys. Rev. Lett., 101, (2008), 197206. b) W.W. Shum, A.J. Epstein and J.S. Miller, Phys. Rev. B, 80, (2009), 064403.
[26] (a) J. Zhang, J. Ensling, V. Ksenofontov, P. Gütlich, A.J. Epstein and J.S. Miller, Angew. Chem. Internat. Ed., (1998), 37, 657. (b) M.A. Girtu, C.M. Wynn, J. Zhang, J.S. Miller and A.J. Epstein, Phys. Rev. B, 61, (2000), 492. (c) C.M. Wynn, M.A. Girtu, J. Zhang, J.S. Miller and A.J. Epstein, Phys. Rev. B, 58, (1998), 8508.
[27] K.I. Pokhodnya, N. Petersen and J.S. Miller, Inorg. Chem., 41, (2002), 1996.
[28] K.H. Stone, P. W. Stephens, A.C. McConnell, E. Shurdha, K.I. Pokhodnya and J.S. Miller, Adv. Mater., 22, (2010), 2514.
[29] J.-H. Her, P.W. Stephens, K.I. Pokhodnya, M. Bonner and J.S. Miller, Angew. Chem. Internat. Ed., 46, (2007), 1521.
[30] N. Favre-Nicolin and R. Cherny, J. Appl. Crystallog., 35, (2002), 734.
[31] J. Zhang, L.M. Liable-Sands, A.L. Rheingold, R.E. Del Sesto, D.C. Gordon, B.M. Burkhart and J.S. Miller, J. Chem. Soc., Chem. Commun., (1998), 1385.

# FEMTOSECOND MOLECULAR CRYSTALLOGRAPHY WITH ULTRABRIGHT ULTRASHORT ELECTRON BUNCHES

Meng Gao, Hubert Jean-Ruel, Ryan R. Cooney, Cheng Lu, German Sciaini, Gustavo Moriena, and R. J. Dwayne Miller
*Max Planck Research Department for Structural Dynamics at the University of Hamburg, CFEL/DESY, Notkestrasse 85, 22607 Hamburg, Germany*
*Departments of Chemistry and Physics, University of Toronto, 80 st. George st. Toronto, ON M5S3H6, Canada*

Sergei Kruglik
*Departments of Chemistry and Physics, University of Toronto, 80 st. George st. Toronto, ON M5S3H6, Canada*
*Present address: Laboratoire Acides Nucléiques et Biophotonique, Université Pierre et Marie Curie, 5 rue Henri Desbruères, 91030 Evry Cedex, France*

Maher Harb
*Departments of Chemistry and Physics, University of Toronto, 80 st. George st. Toronto, ON M5S3H6, Canada*
*Present address: Department of Physics, Lund University, P.O. Box 118, SE-221 00 Lund, Sweden*

Jonathan Stampe and Mark de Jong
*Canadian Light Source Inc., 101 Perimeter Road, Saskatoon, SK S7N 0X4, Canada*

## 1. ABSTRACT

Femtosecond electron diffraction (FED) is used to directly monitor the photoinduced cyclization reaction of a diarylethene derivative in its crystalline phase. A femtosecond (fs) UV pulse converts the molecules from their open-ring conformation to their closed-ring state, while the optically induced structural changes are followed by a variably delayed ultrabright 15 picosecond (ps) photoelectron burst. Both a slow dynamic, associated with lattice strain during the molecular transformation, and a fast dynamic (<15 ps, instrument response limited), associated with the cyclization reaction itself, are observed. Femtosecond (fs) all optical pump-probe measurements are also applied to determine the timescale of the reaction, and support the assignments of the time-resolved diffraction experiment. From the optical measurements, a sub-ps timescale is associated to the ring-closing reaction. Due to the ultrafast nature of the photoinduced cyclization and its limited reversibility, ultrabright electron pulses with improved temporal resolution are required to fully resolve its structural dynamics. In this regard, electron guns synchronized to radio-frequency (RF) compression cavities are discussed as a method to achieve ultrabright, sub-100 fs electron bunches. A scheme for a RF photoelectron compression system is presented.

## 2. INTRODUCTION

Diarylethenes are a class of molecules that undergo classic photoinduced cyclization reactions with conserved stereochemistry [1]. The photoreversible conformational changes involve ring-closing and opening of the molecular system when illuminated with ultraviolet (UV) and visible (VIS) light, respectively (see **Figure 1**). Recently, several new classes of diarylethenes have been developed to show thermal stability and high fatigue resistance in both solution and crystalline forms, allowing the isomerization reaction to be repeated more than $10^4$ times [2]. This opens diarylethenes for applications in optoelectronic devices, such as memories and switches.

Optical transient absorption (pump-probe) measurements have established that the ring-closing reaction in crystalline diarylethenes occurs on the ps to sub-ps timescale [3,4]. However, unambiguous determination of the timescales from optical methods is difficult to achieve without a complete spectral analysis along the reaction pathway. In contrast, femtosecond electron diffraction (FED) can directly follow the atomic motions during the reaction, and map the molecular structure of the initial to final states with the appropriate temporal resolution [5]. Here we report the results of a FED experiment for the cyclization reaction of single crystal 1,2-bis(2,4-dimethyl-5-pheny-3-thienyl) perfluorocyclopentene. Complementary fs all optical results are also presented.

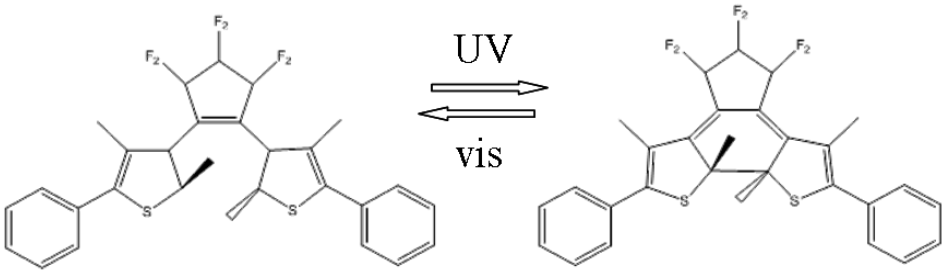


**Figure 1.** A schematic representation of the reversible photo-cyclization of 1,2-bis(2,4-dimethyl-5-pheny-3-thienyl) perfluorocyclopentene (a diarylethene derivative). Exposure of the open-ring conformation (left hand side structure) to UV light initiates ring-closure, while exposing the closed ring isomer (right hand side structure) to visible light induces cycloreversion.

## 3. EXPERIMENTAL TECHNIQUE

### 3.1 Sample Preparation

For all experiments, a commercially available diarylethene derivative [1,2-bis(2,4-dimethyl-5-pheny-3-thienyl) perfluorocyclopentene] (TCI America) was used to grow single crystals from solution. In the optical pump-probe experiments these crystals were mounted on a copper plate with a 400 micron pinhole to facilitate transmission. For FED experiments, the crystals were microtomed to approximately 100 nm and mounted on standard TEM copper grids held at room temperature.

### 3.2 Femtosecond Optical Pump-Probe

fs optical pump-probe measurements were employed to determine the appropriate fluence to induce cyclization of the single crystalline diarylethene derivative and to confirm the timescales

associated with the ring-closing conformational change. In these measurements femtosecond pump pulses centered at 405 nm and 270 nm, derived from either a frequency doubled or tripled Ti:Saph regenerative amplifier (810 nm, 1 kHz, 70 fs) respectively, were used to impulsively initiate the ring-closure. Variably delayed probe pulses, derived from a dispersion compensated continuum at single wavelengths, monitored the spectral changes resulting from the cyclization. A third beam (CW He-Ne) was used to return the sample to its initial open-ring state before each successive pump-probe measurement. The instrument response function of the optical system was approximately 200 fs.

### 3.3 Femtosecond Electron Diffraction

In FED, an ultrashort laser pulse (270 nm wavelength) excites the sample under study and a femtosecond electron bunch ($10^5$ electrons, 100 keV) probes the structural changes by recording time delayed diffraction patterns. As in the optical measurements, a CW He-Ne was used to return the diarylethene derivative to its initial open-ring state for each new measurement. Here, the electron pulses were uncompressed (see section 5), yielding a temporal electron pulse width at the sample of about 15 ps.

## 4. RESULTS

### 4.1 Optical Pump-Probe

The UV/visible linear absorption spectra for the open- and closed-ring conformations of the single crystalline diarylethene derivative are shown in **Figure 2a**. The ring closure results in an increased delocalization of the valence electron density which is manifested as increased absorption in the visible spectral region. The temporally resolved development of this increase in absorption for a probe centered at 620 nm is presented in **Figure 2b**. This transient absorption trace reflects the dynamics of the cyclization, where the persistence of the photoinduced absorption measured at infinite time-delay, $\tau_\infty$, from the optical pump (measured approximately 15 seconds after excitation) demonstrates the thermal stability of the conformational change.

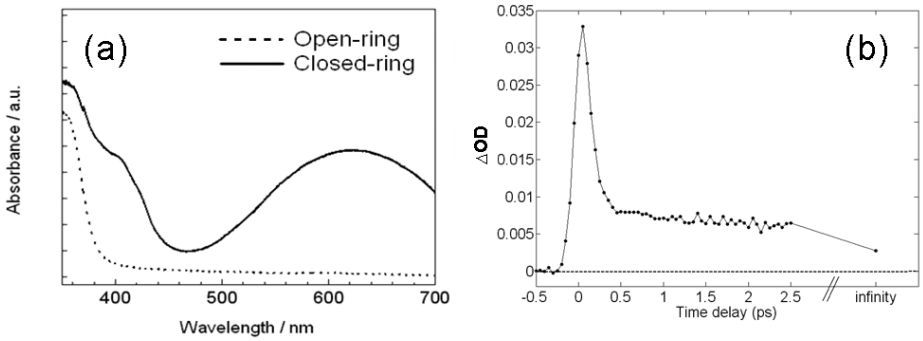


**Figure 2**. (a) UV-Visible spectrum of the open-ring (---) and closed-ring (—) isomers. (b) Transient absorption trace reflecting the ring-closing dynamics, probed at 620 nm and pumped at 405 nm with a fluence of 0.7 mJ/cm$^2$.

We assign the initial response of the dynamics observed in **Figure 2b** to absorption arising from the pump induced excited state of the open-ring conformation. The following dynamics on sub-ps timescales originate from the decay of this excited state absorption and, since the quantum

yield for the cyclization is close to unity [6], the rapid decay of this signal is associated with the attendant increase in the ground state absorption of the closed ring photoproduct. The dynamics on the ps timescale are attributed to the relaxation of the vibrationally hot, newly formed, closed-ring conformation, while the absorption differences between 2 ps and $\tau_\infty$ reflect the subsequent development of strain in the crystal. These assignments are confirmed by the electron diffraction studies that demonstrate a change in molecular structure (see section 4.2). Thus, the cyclization reaction was found to occur on the sub-ps time scale, which is within the upper estimates previously reported for the ring-closing reaction of diarylethene derivatives in the crystalline phase [3,4].

### 4.2 Femtosecond Electron Diffraction

The reversibility of the structural changes associated with the cyclization reaction in crystalline diarylethene was confirmed by electron diffraction studies. **Figure 3a** shows the diffraction pattern of a diarylethene single crystal in the initially open-ring conformation. The measured diffraction following exposure of the sample to multiple pulses of 270 nm is presented in **Figure 3b**. Multiple pulses were used to accentuate the resulting changes. It must be emphasized that upon cyclization, there are significant changes in diffraction peak intensities, mainly suppression of high order peaks, but not in peak positions. This fact implies that there is no conversion into the corresponding closed-ring crystal's lattice. The photo-reversible nature of the diffraction changes resulting from cyclization is demonstrated in **Figure 3c**, which presents the diffraction pattern resulting from exposure of the same sample, shown in **Figure 3b**, to CW-HeNe. As can be noted, the initial pattern of **Figure 3a** is recovered.

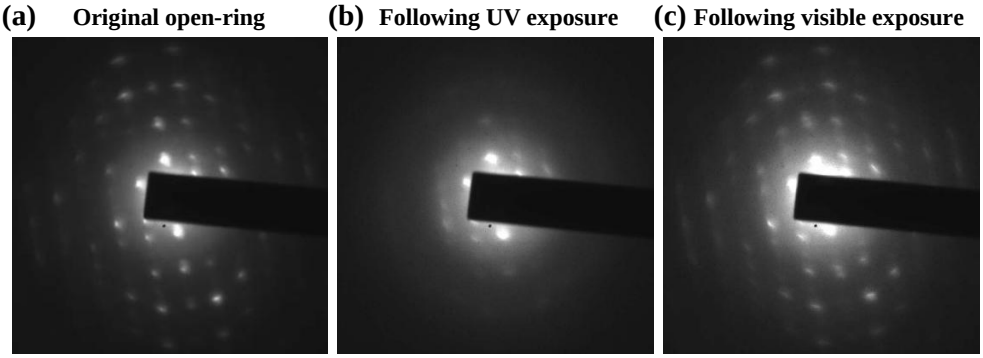


**Figure 3**. (a) Diffraction pattern of single crystalline diarylethene initially in the open-ring conformation. (b) Diffraction pattern following UV driven cyclization, and (c) cycloreversion to the ring-open form upon visible radiation.

In order to perform a temporally-resolved investigation of the cyclization dynamic the reversibility of subsequent cyclization and cycloreversion reactions must be confirmed, with the ring-closing reaction being induced by a single UV pulse. The inset of **Figure 4a** presents a typical diffraction pattern of the initially open-ring conformation. The normalized intensity of the (7 -1 -6) diffraction peak (circled) at $\pm \tau_\infty$ as the crystal undergoes subsequent ring-closing and ring-opening cycles is presented in **Figure 4a**. Here the peak intensities are acquired before and after exposure to a single 270 nm pulse with sufficient fluence to photoexcite approximately 5 % of the molecules within the probed volume. Following each measurement the close-ring

conformation is returned to its initial structure by exposure to a CW-HeNe. The reversibility of the structural change is apparent, and, with exception to the first cycle, the ring-closing and ring-opening reactions are completely repeatable up to at least 100 cycles.

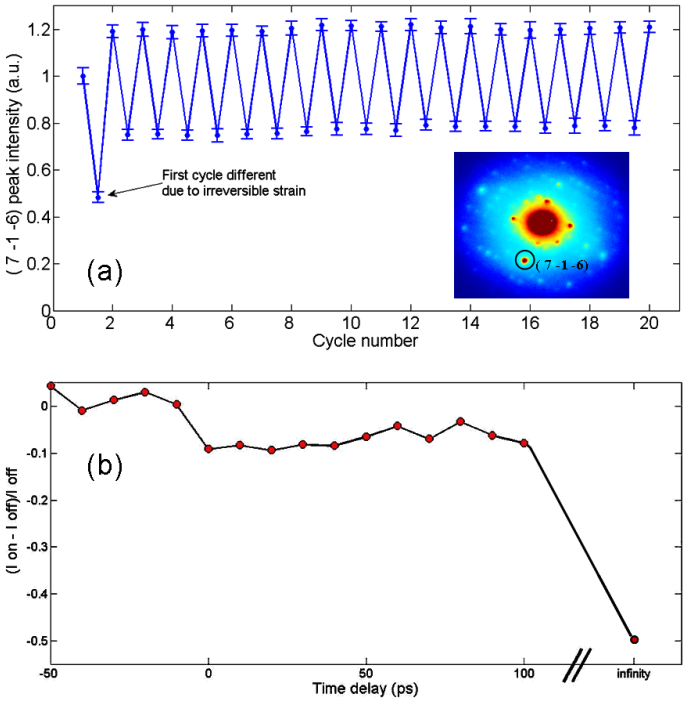


**Figure 4.** (a) Normalized integrated intensity of the peak ( 7 -1 -6), see inset, following successive exposure to single pulses of 270 nm andCW-HeNe photoreversion. Only the first 20 cycles are shown but more than 100 cycles could be repeated before the onset of crystal damage. (b) Time resolved change of the normalized ( 7 -1 -6) peak intensity following excitation of 5 % of the molecules with 270 nm pump pulse. The reported intensity is normalized to its initial value.

Representative results for the temporally resolved changes in the diffraction intensity of the peak (7 -1 -6) following 270 nm excitation are shown in **Figure 4b**. Here the change in peak intensity is normalized to its initial value in the open-ring state. Rapid changes in diffraction intensity on the ps timescale are observed, which we attribute to a combination of the ring-closing reaction and heating effects (Debye-Waller). Our results also indicate the presence of a second phenomenon on longer time scales which we associate with the build up of lattice strain upon formation of the ring closed photoproduct. Due to the longer timescale associated with this strain it can be readily separated from the reaction dynamics. As it was observed in the steady state diffraction patterns of **Figure 3**, the structure does not convert into the corresponding closed-ring single crystalline form. Rather, the presence of ring-closed molecules, inside the open-ring host lattice, results in strains which both reduce the long range order and macroscopically distort the crystal [7] causing further changes in diffraction intensity. Apart from strain effects, the dynamics on the ps timescale are characterized by most orders decreasing in intensity, in agreement with expectations based on a defect model for the diffraction process. However, as suggested by the optical results presented in section 4.1, these dynamics are expected to occur on sub-ps timescales and can not be resolved by our uncompressed 15 ps electron pulses. This suggests the need for improved temporal resolution to reliably determine

the time constant associated with the cyclization. The temporal resolution of a high charge density electron bunch can be dramatically improved by implementing radio frequency compression, and will be the subject of section 5.

## 5. RF PULSE COMPRESSION

In order to temporally resolve the atomic dynamics in question, sub-ps electron pulses containing about $10^5$ to $10^6$ particles are needed to achieve the required signal-to-noise ratio for this experiment. However, for high density bunches (>$10^4$ electrons), space-charge broadening governs the electron pulse duration [8]. This fact makes it very difficult to obtain ultrabright and sub-ps electron pulses. Therefore, there is a trade-off between pulse duration and electron flux. Previous electron guns that attempted to circumvent the space-charge problem include the use of ultracompact designs [9], where space-charge broadening is reduced by minimizing the electron pulse propagation distance to the sample, and the high repetition rate, low flux gun designs, where sub-ps electron bunches can be easily achieved by substantially reducing the number of electrons [10, 11] per bunch. However, due to the limited reversibility of these single crystalline diarylethene derivatives, neither of the aforementioned solutions is suitable. Recently, van Oudheusden *et al.* [12] proposed a novel approach to create ultrabright (> $10^6$ electrons), ultrashort (< 100 fs) electron bunches using a phase synchronized RF cavity to rebunch the electron pulses.

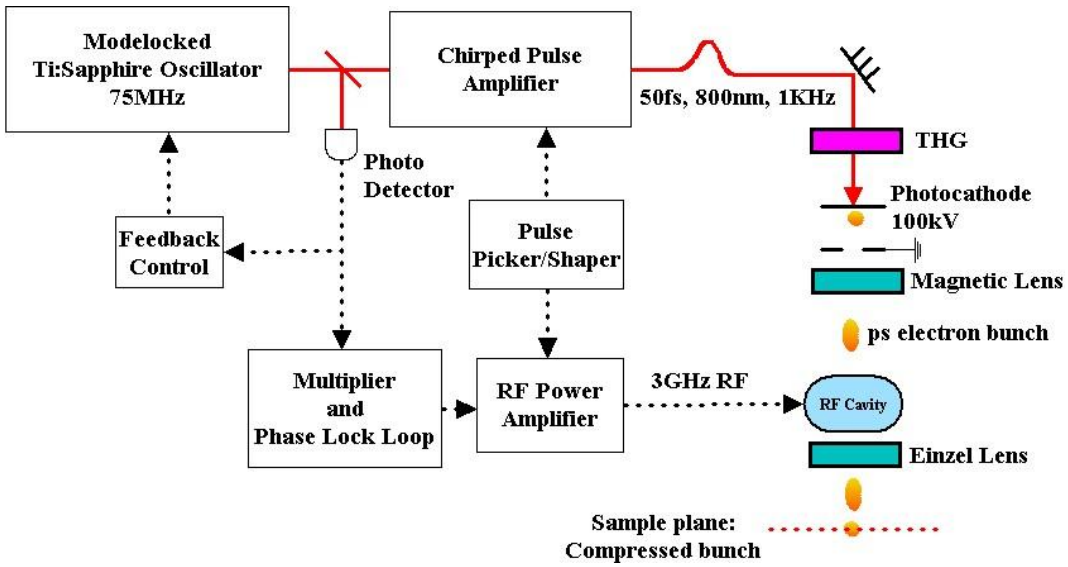


**Figure 5.** Simplified schematic of the electron pulse compression system at University of Toronto. A 3GHz RF signal is phase locked to a 75 MHz oscillator. The RF signal is then amplified and then used to drive a cylindrical cavity in the $TM_{010}$ mode. The oscillating field of the RF cavity induces a reversal in the longitudinal velocity distribution of the electron bunch resulting in a temporal focus at the sample plane.

Siwick *et al.* [8] showed that a nonrelativistic electron bunch develops a near perfect linear chirp after some free space propagation. That is, the velocity of electrons at the front edge of the bunch increases while that for those at the back decreases leading to a linear momentum-space

distribution. If a time-varying electric field can be applied such that the front edge electrons are decelerated and the back edge electrons are accelerated, then the electrons can be rebunched. Practically, this can be achieved by the electric field of a 3 GHz cylindrical RF cavity in $TM_{010}$ mode. **Figure 5** shows a simplified schematic of our pulse compression system. A fraction of the output of the 75 MHz mode-locked oscillator signal is monitored by a fast photodiode. The remaining signal seeds a regenerative amplifier to produce the optical pulses for generating 100 keV photoelectrons and pumping the sample. A high harmonic of the photodiode signal is used to produce a phase locked narrowband RF pulse centered at 3 GHz. The RF signal is then amplified and coupled into the cylindrically symmetric RF cavity. The phase difference between the RF field and the oscillator can therefore be adjusted to match the arrival time of the electron bunch with the slope of the RF field.

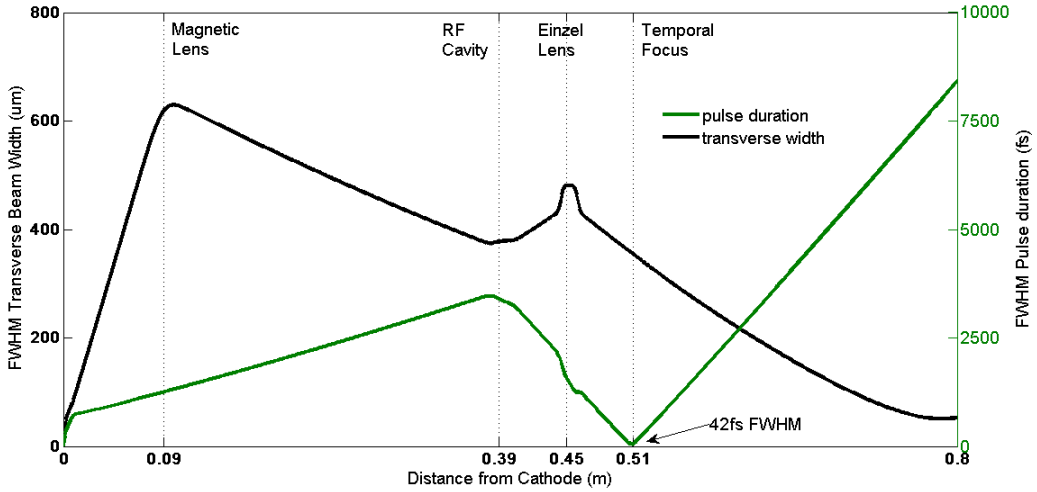


**Figure 6.** General Particle Tracer (GPT) simulation for the propagation of a $10^5$ photoelectron bunch through a RF cavity. The left-hand axis monitors the transverse dimensions of the bunch in μm (black curve), while the right-hand axis monitors the effective pulse duration in fs (green curve). Following the RF induced reversal of the longitudinal velocity distribution, the electron bunch reaches a temporal focus of 42 fs (FWHM).

General Particle Tracer (GPT) [13] simulations were used to predict the characteristics of the electron bunch as it propagates down the beam line and passes through the RF cavity. **Figure 6** shows the simulated results for an electron bunch containing $10^5$ particles and initialized with a gaussian tranverse and longitudinal profile representative of the intial laser pulse generating the photoelectrons. The photoelectrons are first accelerated by an applied DC field (100 kV) and the influence of space-charge effects dramatically broadens the effective bunch size in both the longitudinal and transverse dimensions. In particular, expansion in the longitudinal dimension from the space-charge induced linear chirp translates to an effective expansion of the 70 fs electron bunch to more than a ps by the time it has exited the anode. The transverse profile of the electron pulse is then focused by a magnetic lens through the RF cavity. The oscillating field of the RF cavity induces a reversal in the longitudinal phase distribution of the electron bunch, such that on exiting the cavity the leading edge of the pulse is travelling slower than the trailing edge. In addition, the field from the cavity re-expands the transverse profile of the electron pulse so that a second electrostatic lens is required to refocus the beam. As the electron pulse continues its propagation, the RF induced phase reversal causes the pulse to rebunch in the longitudinal

dimension at approximately 50 cm from the cathode with an effective pulse duration of 42 fs (FWHM). The implementation of a phase-locked RF compression cavity holds great expectations for the development of high charge density and sub-100 fs electron bursts for FED.

## 6. CONCLUSION

These results demonstrate the potential for diffraction experiments to offer an atomic perspective of passage through a transition state region, over all relevant length and time scales, to provide a complete picture of the reaction coordinate for a molecular system. The optical studies have determined the operating dynamics for diarylethene derivatives and suggest the need to implement electron bunch compression in order to temporally resolve the structural change of interest. In addition, the inversion of the diffraction to real space requires a full treatment of the diffraction process with the inclusion of the effect of the photoproduct within the host lattice and will be reported separately.

## 7. ACKNOWLEDGEMENTS

This research was supported by the Natural Science and Engineering Research Council and the Canadian Foundation for Innovation. We would like to thank Philip Coppens and his group for helpful discussions.

## 8. REFERENCES

[1] M. Irie, *Chem. Rev.*, **100** (2000), 1685.
[2] M. Irie, T. Lifka, S. Kobatake, and N. Kato, *J. Am. Chem. Soc.*, **122** (2000), 4871.
[3] H. Miyasaka, T. Nobuto, A. Itaya, N. Tamai, and M. Irie; *Chem. Phys. Lett.*, **269** (1997), 281.
[4] K. Tani, Y. Ishibashi, H. Miyasaka, S. Kobatake, and M. Irie; *J. Phys. Chem. C*, **112** (2008), 11150.
[5] R.J.D. Miller; *Can. J. Chem.*, **80** (2002), 1.
[6] K. Shibata, K. Muto, S. Kobatake, and M. Irie, *J. Phys. Chem. A*, **106** (2002), 209.
[7] M. Irie, S. Kobatake, M. Horichi, *Science*, **291** (2001), 1769.
[8] B.J. Siwick, J.R. Dwyer, R.E. Jordan, R.J.D. Miller; *J. Appl. Phys.*, **92** (2002), 1643.
[9] R.J.D. Miller, R. Ernstorfer, M. Harb, M. Gao, C.T. Hebeisen, H. Jean-Ruel, C. Lu, G. Moriena and G. Sciaini; *Acta. Cryst.*, **A66** (2010). 137.
[11] J.D. Geiser and P.M. Weber, *Proc. SPIE*, **2521** (1995), 136.
[12] T. van Oudheusen, E.F. de Jong, S.B. van der Geer, W.P.E.M. Op't Root, O.J. Luiten, and B.J. Siwick; *J. Appl. Phys.*, **102** (2007), 093501.
[13] http://www.pulsar.nl/gpt/

# NEUTRON PROTEIN CRYSTALLOGRAPHY. HYDROGEN- AND HYDRATION-SENSITIVE STRUCTURAL BIOLOGY

Nobuo Niimura

*Frontier Research Center for Applied Atomic Sciences, Ibaraki University, Shirakata, 162-1, Tokai-mura, Ibaraki-ken, 319-1106, Japan*

Abstract

Neutron protein crystallography (NPC) has not substantially contributed to the determination of the folding structures of biological macromolecules. It takes the next step beyond the folding structure of proteins. This paper demonstrates how hydrogen atoms can be seen by NPC and how NPC can explore protonation and deprotonation of amino acid residues, hydration structures, and hydrogen-to-deuterium exchange ratios. The contribution of NPC to solving the classical problems in insulin will be given as an example. The structure of the insulin monomer is the hormonally active form and $Zn^{2+}$ ions promote the hexamerization of insulin molecules by constructing the octahedrally coordinated structure of the zinc ions when insulin is stored in pancreas. To understand the coordination mechanism thereof, it is essential to know the protonation and/or deprotonation states of not only HisB10 $N^{\varepsilon 2}$ but also HisB10 $N^{\delta 1}$. Moreover, it is of interest to understand how the zinc positive charge is balanced by negatively charged glutamic acid carboxylates or other groups. When crystals grown in $H_2O$ solution are soaked in a deuterated solution for different periods of time, the time evolution of the H/D exchange is obtained. An example of the time evolution of H/D exchange of the hexamer insulin has been reported.

## INTRODUCTION

Since the beginning of the PDB, the number of folding structures registered in the PDB has increased exponentially year by year; by 2009, it was over 60,000. Most of these structures have been determined by X-ray Protein Crystallography (XPC) or by nuclear magnetic resonance (NMR). In contrast, the number of structures determined by

Neutron Protein Crystallography (NPC) is very small (less than 50 as of 2010). Thus, it could be said that NPC has not substantially contributed to the determination of the folding structures of biological macromolecules.

Neutrons can provide unique information about hydrogen atoms, protonation states, and hydrogen orientations in water molecules as the recent review papers presented. [1-5] As an example, Fig.1 compares sample results obtained by XPC and by NPC. Figure 1(a) shows the structure of myoglobin as determined by XPC (2blh); Figure 1(b) shows the same structure as determined by NPC (1l2k). The clear difference is that the NPC structure includes the hydrogen atoms, which are shown as red spheres in the figure. In general, about half of the constituent atoms of a protein are hydrogen, and in principle, all the hydrogen atoms (protonation states) can be identified by neutron diffraction. So, the purpose of NPC is not to determine the folding structure of biomolecules but rather the structure that is "beyond the folding structure." In other words, by identifying the hydrogen atoms in and around the biomolecule, NPC takes the next step beyond the folding structure and gives information about the hydrogen bonding, protonation states, and hydration configuration of the biomolecule—all of which are critical features for understanding how the it actually functions. This unique information makes NPC a valuable tool for researchers.

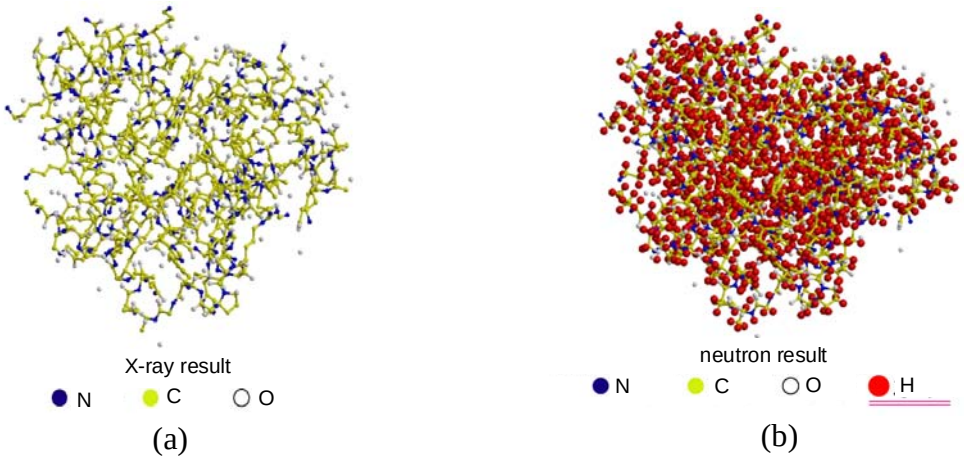


Figure 1: (a)The structure of myoglobin as determined by X-ray protein crystallography (XPC), (b) The same structure as determined by NPC.

**Observation of hydrogen atoms in macromolecules**

The positions of hydrogen atoms in proteins and nucleci acids can be identified very well using NPC. The structures of rubredoxin wild type (Rb-w) [6] is a good example of this use of NPC. Figure 2(a) shows a (2|*Fo*|-|*Fc*|) nuclear density map of Phe48 of Rb-w at 1.5Å resolution. The neutron scattering length of hydrogen atoms is negative, and their density contours in nuclear Fourier maps are shown in red; while deuterium, carbon, nitrogen and oxygen atoms all have positive neutron scattering lengths, and their contours are shown in blue. In this map, the hydrogen atoms bonded to carbon atoms are clearly visible. Figure 2(b) shows a similar nuclear density map for Tyr12 of Rb-w, also at 1.5Å resolution. Here, the contours of the hydrogen atom of the O-H bond in Tyr12 are shown in blue, and thus it can be concluded that it has been replaced by a deuterium atom. Figure 2(c) shows the (2|*Fo*|-|*Fc*|) nuclear density of Trp36 of Rb-w at 1.5Å resolution, and it is clearly seen that the N-H bond of the indole ring, which is shown in blue, has become an N-D bond.

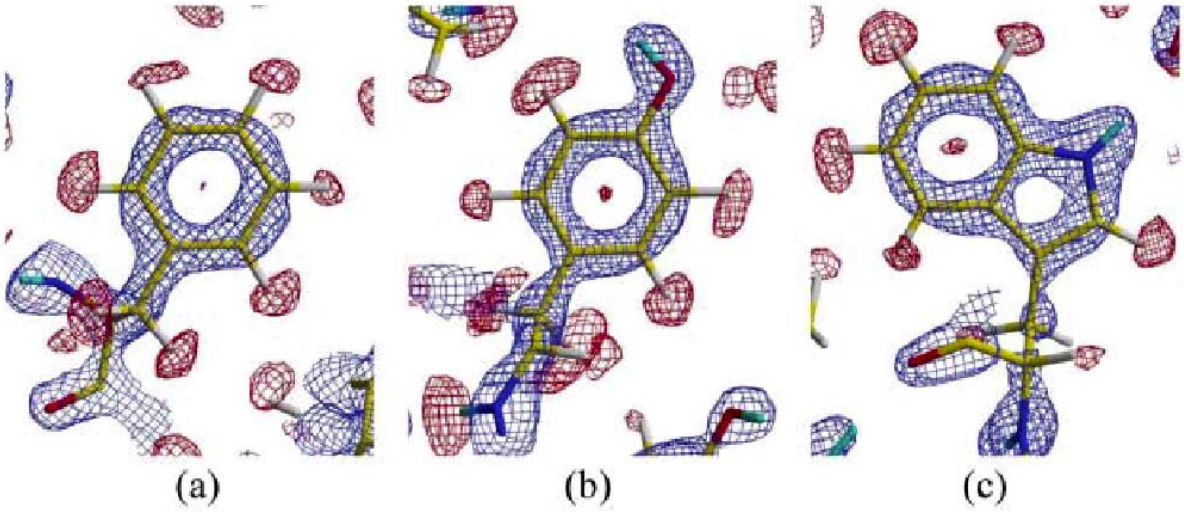


Figure 2: 2|Fo|-|Fc| nuclear density maps of (a) Phe48 of Rb-w, (b) Tyr12 of Rb-w, and (c) Trp36 of Rb-w.

**Observation of hydration in macromolecules**

Figure 3 displays one region of the hydration structure around myoglobin and shows that all of the hydration water molecules are independently defined.[7] In some cases, hydrogen (deuterium) atoms in water molecules can be clearly identified in triangular (boomerang) shaped peaks, and the formation of the hydrogen bonds between two water molecules can be recognized as well. At the same time it is interesting to note that, near the two triangular-shaped contours, a spherically-shaped water molecule can be found (Fig.3). Moreover, water molecules with other shapes, such as ellipsoidal (stick-shaped) ones, can be found in other regions of the map.

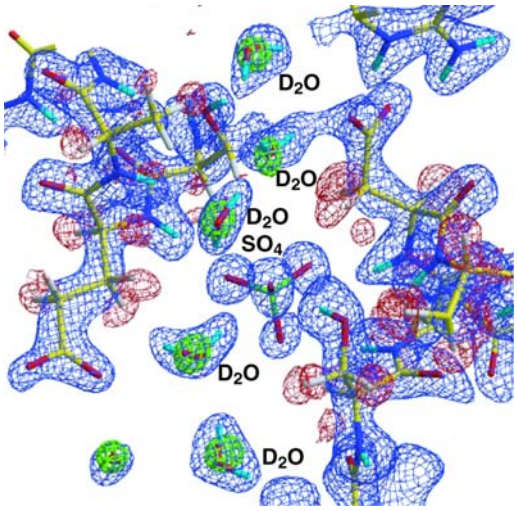


Figure 3: Nuclear and X-ray maps in a region of the hydration structure around myoglobin. Blue contours: positive 2Fo-Fc nuclear map. Red contours: negative 2Fo-Fc nuclear map. Green contours: positive Fo-Fc X-ray omit-water map.

The observed water molecules were categorized into the following classes, based on their appearance in Fourier maps as shown in Fig. 4: (i) triangular shape, (ii) ellipsoidal stick shape, and (iii) spherical shape; in the second category, ellipsoidal stick shapes were further sub-classified as (iia) short and (iib) long. This classification conveniently reflects the degree of disorder and/or the dynamic behavior of a water molecule.[8]

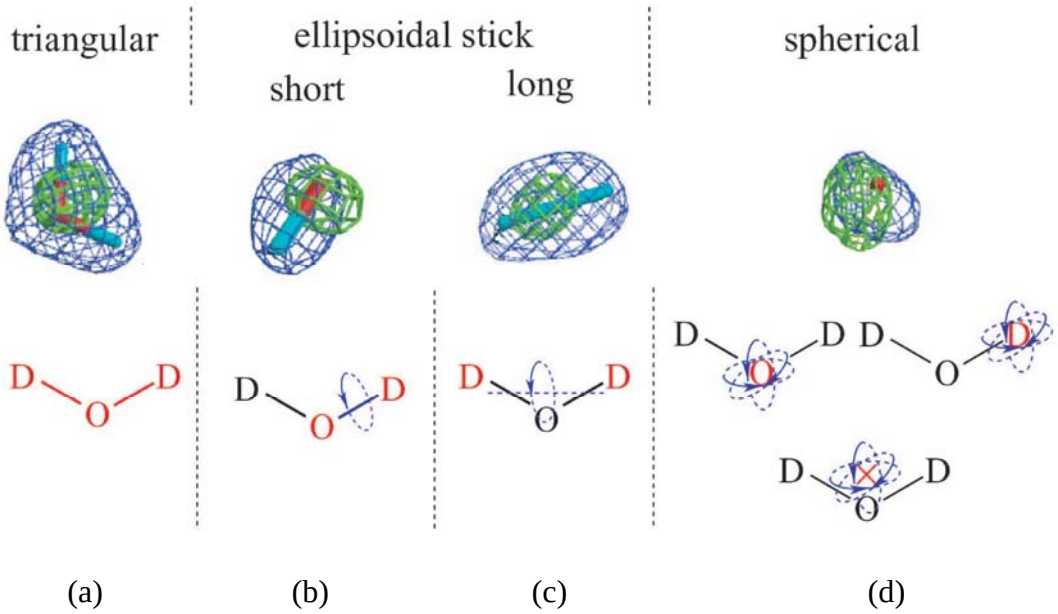


Figure 4: Classification of water molecules of hydration from (2Fo-Fc) neutron Fourier maps. Blue contours: positive 2Fo-Fc nuclear map. Green contours: positive Fo-Fc X-ray omit-water map.

**H/D exchange**

For most neutron experiments, in order to reduce background scattering from H atoms (which have a large incoherent scattering cross section), protein solutions are either subjected to $H_2O/D_2O$ exchange prior to crystallization, or crystals are soaked in $D_2O$ after crystallization from $H_2O$ solution. These techniques allow D atoms to be substituted for many of the H atoms, not only in the solvent water molecules, but also in the protein molecules at sites containing “exchangeable” hydrogen atoms (mostly H atoms of N-H and O-H bonds exposed to the solvent). Nevertheless, some potentially exchangeable sites resist deuteration and remain hydrogenated, as shown in Fig.5. Figure.5 shows the region around some of the backbone N-H bonds of wild-type rubredoxin[6]; negative densities (red peaks) can be clearly seen at the H-containing sites, while positive densities (blue) are visible at the D-containing sites. Presumably, some N-H groups resist H/D exchange because of their poor solvent accessibility.

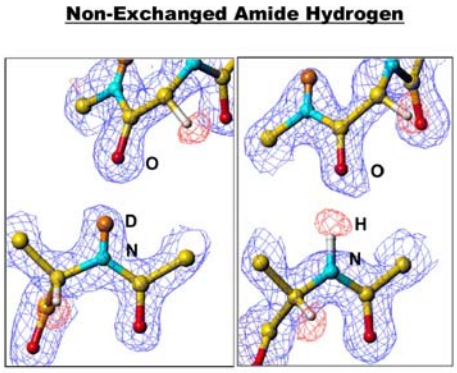


(a) (b)

Figure 5: Nuclear density maps (blue:positive contour ; red:negative contour) showing the difference between (a) H/D-exchanged hydrogen in an amide. (b) Non-H/D-exchanged hydrogen in an amide.

**Protonation/Deprotonation**

The charges of various amino-acid side chains depend on the pH. For example, at a high pH (low acidity conditions), carboxylic acids tend to be negatively charged (deprotonated), and amines tend to be uncharged (unprotonated). At a low pH (high acidity), the opposite is true. The pH at which exactly half of any ionized amino acid is charged in solution is called the $pK_a$ of that amino acid. These $pK_a$ values of such ionizable amino-acid side chains are tabulated in standard textbooks. However, the protonation state of a given amino-acid side chain in a protein cannot be estimated from standard $pK_a$ values measured from isolated amino acids in solution, because inside a protein it may vary significantly depending on the local environment. The electrically charged states of the amino-acid residues are very important in understanding the physiological function of the protein, the interaction between ligands and proteins, molecular recognition, structural stability, and so on.

## THE CONTRIBUTION OF NPC TO SOLVING THE CLASSICAL PROBLEMS IN INSULIN

Insulin is a polypeptide hormone critical for the metabolism of glucose. The insulin monomer consists of two chains—a 21-residue A-chain and a 30-residue B-chain—linked by a pair of disulfide bonds, A7-B7 and A20-B19, respectively; furthermore, an additional intra-chain disulfide bond links A6 and A11. In a solution

free of metal ions, insulin exists as a mixture of monomer, dimer, tetramer, hexamer, and higher aggregates depending on its concentration. The structure of hexameric insulin, the form in which it is stored in the pancreas β-cells, was reported first in 1969 [9]; and a comprehensive description of the room-temperature structure at 1.5Å resolution, as well as the biological implications thereof, was published afterwards[10]. The structure of the insulin monomer is the hormonally active form. $Zn^{2+}$ ions promote the hexamerization of insulin in pancreas. In the case of the hexamer state, the crystal asymmetric unit contains two insulin monomers (a dimer) related by a pseudo-two-fold axis as shown in Fig.6(a); the crystallographic three-fold axis generates the insulin hexamer from three dimers, as shown in Fig.6(b). Two zinc ions, on opposite sides of the hexamer, are situated on the crystallographic three-fold axis; each is octahedrally coordinated by the three crystallographically related HisB10 $N^{\varepsilon 2}$ atoms and three water molecules. The coordination of metal ions is intrinsically the problem of protonation/deprotonation of the polar amino acid residues, and only NPC can reveal the protonation states.

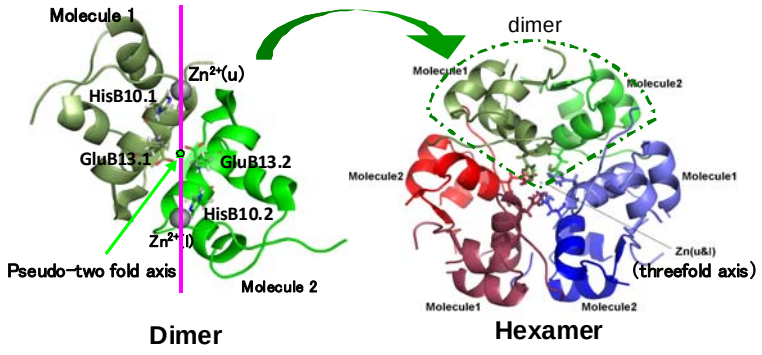


Figure 6: (a) Model of the crystal asymmetric unit showing two insulin monomers (a dimer) related by a pseudo-two-fold axis. (b) Model of the insulin hexamer from three dimers generated by the crystallographic three-fold axis.

## The protonation/deprotonation of histidine

To understand the octahedrally coordinated structure of the zinc ions and the coordination mechanism thereof, it is essential to know the protonation and/or deprotonation states of not only HisB10 $N^{\varepsilon 2}$ but also HisB10 $N^{\delta 1}$. [11-14]Moreover, it

is of interest to understand how the zinc positive charge is balanced by negatively charged glutamic acid carboxylates or other groups. The most appropriate method to study the protonation and/or deprotonation states of these polar amino acid residues is neutron diffraction. In the hexamer insulin crystals, three dimers are assembled around two zinc ions (upper Zn (u) and lower Zn (l)), 16.4 Å apart on the three-fold axis. Figure 7(a) and (b) show (2*Fo-Fc*) maps of the areas around upper Zn (u) and lower Zn (l), respectively. The $N^{\varepsilon 2}$ atom of HisB10 is deprotonated and coordinated to Zn, whereas $N^{\delta 1}$ of HisB10 is protonated, making the net charge of HisB10 neutral. The two molecules in the dimer are designated molecule 1 and molecule 2, as shown in Fig.6 (a) and (b). Residues belonging to either molecule 1 or molecule 2 are distinguished by the suffix .1 or .2 after the residue number. Thus, the upper zinc is coordinated to three symmetry-related $N^{\varepsilon 2}$ atoms of HisB10.1 (i.e., from molecule 1) and three water molecules, while the lower Zn is coordinated to the three symmetry-related $N^{\varepsilon 2}$ atoms of HisB10.2 and three water molecules, as shown in Fig.7(a) and (b), respectively. From the top, three water molecules can be seen coordinating the upper Zn (u) and from the bottom, another three water molecules can be seen coordinating the lower Zn (l). The former three water molecules are classified as triangular, since the deuterium atoms of these water molecules could be placed. On the other hand, the latter three water molecules are classified as stick-shaped and are presumably rotating about OD axis. These facts are well supported by the B-factors, which are smaller for the triangular molecules (36.5$Å^2$) than for the ball-shaped ones (74.0$Å^2$). Differences in the dynamic behavior of the coordinated water molecules, between the upper and lower Zn ions, can be observed in the structure of hexamer human insulin at 1.0 Å resolution, at 120K, in which the unambiguous electron density of three water molecules coordinating the upper Zn ion was observed [15]. Continuous electron density for the three water molecules coordinating the lower Zn ion can also be observed, suggesting that it would be possible for a disordered anion—such as a citrate—to occupy this site. [15] Furthermore, in the structure of a dried crystal of hexamer human insulin at 100K, the upper Zn ion binds three water molecules and adopts an octahedral coordination in the crystal, whereas the lower zinc ion adopts a tetrahedral coordination, with the three water molecules being replaced by a single chloride ion. [15] In the neutron crystallography results, a difference in the temperature

factor of $N^{\varepsilon 2}$ of HisB10 coordinating with Zn ions was also observed: The temperature factors were 9.3Å$^2$ for $N^{\varepsilon 2}$ of HisB10.1 coordinating the upper Zn ion and 14.6Å$^2$ for $N^{\varepsilon 2}$ of HisB10.2 coordinating the lower Zn ion.

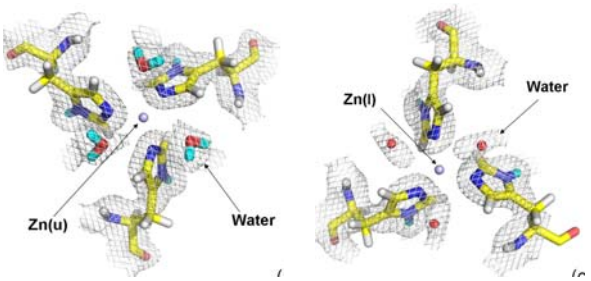


(a) (b)

Figure 7: 2Fo-Fc maps of the areas around upper Zn (u) and lower Zn (l) of insulin.

Porcine insulin can crystallize in a cubic space group without zinc, and neutron crystallographic studies of this cubic insulin at pD values of 6.6 and 9.0 have been carried out. The crystal structures of pD6.6 and pD9 are almost the same. The overall root-mean-square differences of non-hydrogen atoms and all atoms between pD6.6 [9] and pD9 are 0.67Å$^2$ and 1.04Å$^2$, respectively. Porcine insulin has two histidines (HisB5 and HisB10) in the B chain. As for HisB5, both of $N^{\delta 1}$ and $N^{\varepsilon 2}$ atom of the imidazole ring are protonated at pD6.6, and only the $N^{\delta 1}$ atom was protonated at pD9 : Fig.8 (c) and (d)). This fact indicates that the $pK_a$ value of HisB5 has the range between pD6.6 and pD9, which is plausible because of the $pK_a$ value (=6.5) of a simple histidine moiety. However, HisB10 was confirmed to be protonated at both the $N^{\delta 1}$ and $N^{\varepsilon 2}$ atoms at both pDs. (See Fig.8 (a) and (b).) Figure 8 (b) shows that HisB10 is doubly protonated and positively charged even at the alkaline pH of 9.0. There are two possible reasons for this double-protonation state; a hydrogen bonding network and an electrostatic potential. In HisB10, two D atoms of the imidazole ring are anchored to the surrounding water molecules and amino acids by hydrogen bonds. At both pD6.6 and pD9, the $N^{\varepsilon 2}$-D group was hydrogen bonded to a carbonyl group of the main chain of TyrA14. (The δD-O bond lengths were 2.3Å and 2.1Å for pD9 and pD6.6, respectively.) The abnormal $pK_a$ value of HisB10 higher than 9.0 indicates the high affinity for positive

ions. This property would be effective to the polymerization of insulin depending on various cations. HisB10 captured the $D^+$ atom instead of the divalent metal cation in the absence of $Zn^{2+}$ ion. This structure would be the active form of insulin at biological pH levels. This mechanism would be achieved by the cation capturing of HisB10; therefore, HisB10 is essential for polymerization of insulin in organisms.

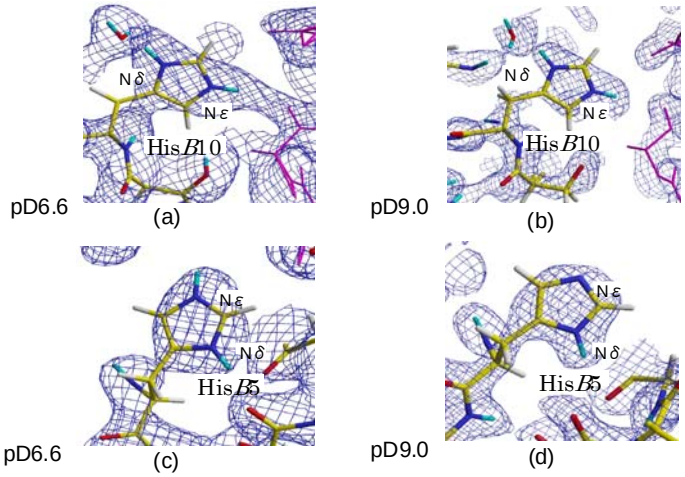


(Ishikawa et al,2007,2008)

Figure 8: 2Fo-Fc positive nuclear density maps in insulin of (a) His *B*10 at pD 6.6, (b) His *B*10 at pD 9.0, (c) His *B*5 at pD 6.6, and (d) His *B*5 at pD 9.0.

**Charge balance of the zinc positive charges**

The bivalent positive charge on the zinc should be balanced by separate but correlated negative ions.[10,16] It seems most probable that here the positive charges of the zinc ions are balanced by negatively charged glutamic acid B13 carboxyl groups that lie in a layer mid-way between them as shown in Fig.9. Two zinc ions have four positive charges. If all the glutamic acid B13 residues (in the hexamer) would be negatively charged (i.e., six negative charges), the proposed hexamer molecular arrangements would give two extra net negative charges as shown in Fig.9. To solve the problem, Iwai et al. carried out a neutron crystallographic analysis of hexamer porcine insulin at 2.1Å resolution, using 4,824 independent reflections from 13,038 observed reflections. The (2*Fo-Fc*) positive nuclear density at room temperature was studied; the map is given in Fig.10. The carboxyl group of GluB13 in molecule 1 is found to be deprotonated, it has one negative charge; therefore, the net charge of GluB13 in molecule 1 is –3. On the

other hand, the side chain of GluB13 in molecule 2 also has a double conformation in which one of the carboxyl groups of this double conformation is protonated but the other is deprotonated, as shown in Fig.10. Thus 50% of this carboxyl group has no charge and the other 50% has a negative charge; consequently, the net charge of GluB13 in molecule 2 is –3/2 and the net charge of GluB13 in the hexamer becomes –4.5 (= –3 – 3/2). (See Fig.11) Strictly speaking, the charge balance is still not completely fulfilled, but if the accuracy of the occupancy of the double conformation is considered along with other factors, the 0.5 charge difference might be within the acceptable error range. The balance between the positive charge of the Zn ions and the negative charge of the GluB13 residues is thus explained by the identification of a proton bound to one of the carboxyl groups of double conformation.

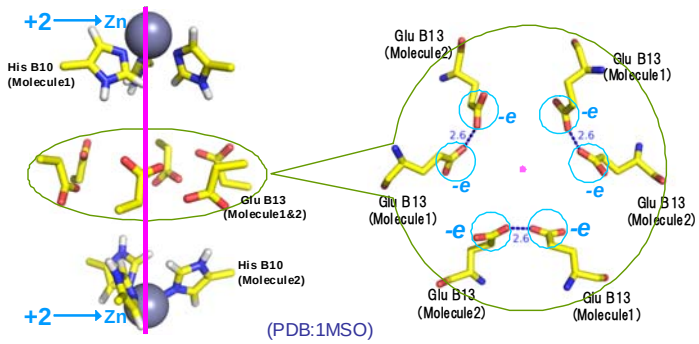


Figure 9: Model showing the two net negative charges resulting from the difference between the four positive charges from the two zinc ions and the six negatively charged glutamic acid B13 carboxyl groups between the zinc ions.

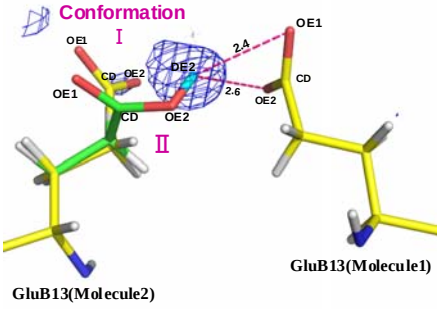


Figure 10: The 2Fo-Fc positive nuclear density map of the carboxyl group of Glu *B*13 in molecule 2 of insulin.

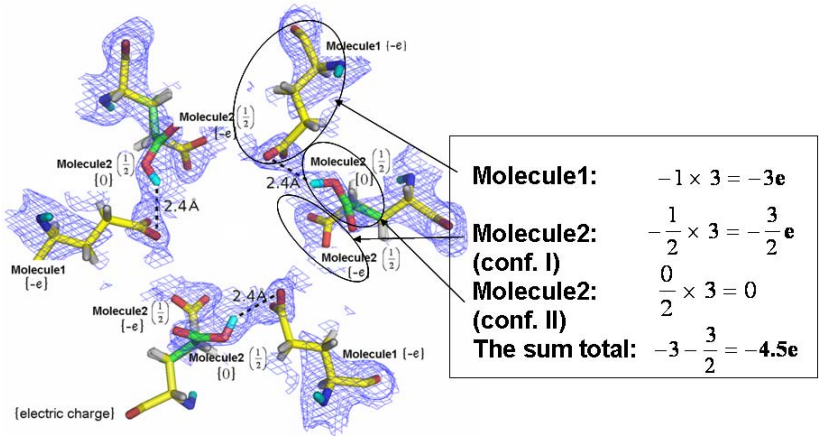


Figure 11: The net charge of Glu *B*13 in the insulin hexamer. Blue contours: 2Fo-Fc nuclear map.

**Time evolution of H/D exchange of hexmer insulin**

When crystals grown in $H_2O$ solution are soaked in a deuterated solution for different periods of time, the time evolution of the H/D exchange is obtained. An examples of the time evolution of H/D exchange of hexamer insulin has been reported.

$T_6$ porcine insulin crystals were soaked in $D_2O$ for one month[14] and for 4.5 months[17] . The hydrogen/deuterium (H/D) exchange ratios of the amide hydrogen atoms of $T_6$ porcine insulin for the one-month and 4.5-months soaking periods are presented in Fig.12 (a) and (b), respectively. The error of the H/D exchange ratio was assumed to be about 25%. There were 18 hydrogen atoms that were highly protected from H/D exchange, and these were found to be concentrated in the center of a helical region of the B-chains. From the viewpoint of soaking time versus H/D exchange ratios, the amide hydrogen atoms in $T_6$ porcine insulin could be classified into three categories, as shown in Fig.13: 1) those hydrogen atoms that were fully or partially exchanged after one month (shown as open symbols in Fig.13; 2)those in which H/D exchange occurred between one and 4.5 months (lightly-shaded symbols inFig.13; and 3) those which are not exchanged (highly protected), even after 4.5 months (dark-filled symbols in Fig.13. The greatest protection of amide H atoms was in the center of a helical region in each of the B-chains (residues 14–19 in molecule 1 and 12–19 in molecule 2). This result indicates that H/D exchange in secondary structures depends on their location in the molecule. Moreover, it was found that the H/D exchange rates for amide hydrogen atoms in the interior of the protein molecule are rather slow, i.e., on the order of a month.

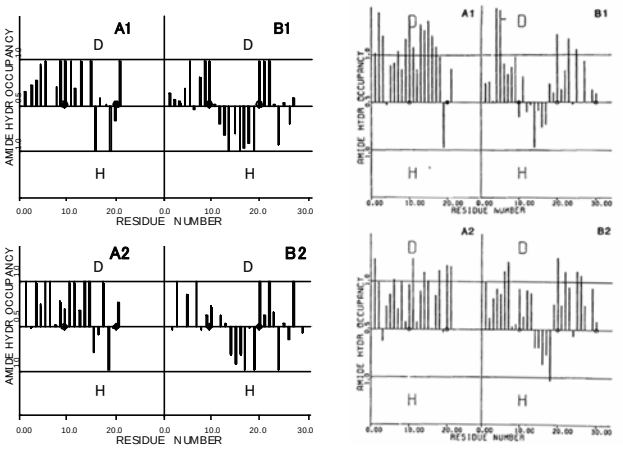


Figure 12: The hydrogen/deuterium (H/D) exchange ratios of the amide hydrogen atoms of T6 porcine insulin for (a) one-month and (b) 4.5-months soaking periods.

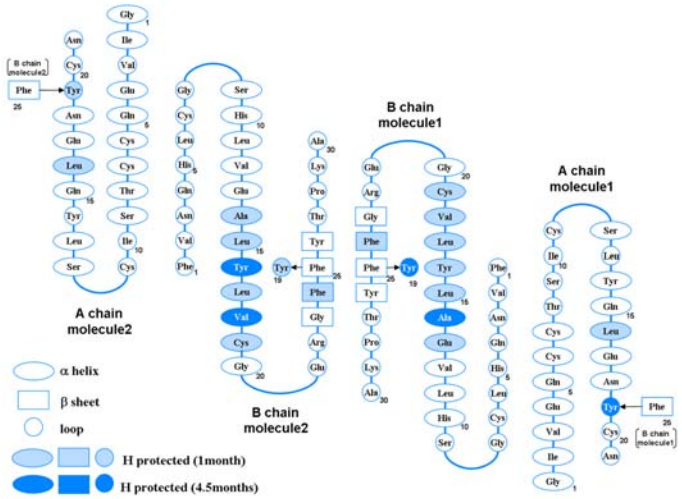


Figure 13: A diagram summarizing the time evolution of H/D exchange of amide hydrogen atoms in T6 porcine insulin.

## ‘NEXT GENERATION ‘ SPALLATION NEUTRON SOURCE

An exciting new development currently under way is the construction of high-intensity, state-of-the-art, pulsed neutron facilities. These are the Spallation Neutron Source (SNS) at Oak Ridge, Tennessee in the U.S.A. and the Japan Proton Accelerator Research Complex (J-PARC) in Ibaraki prefecture in Japan. Both SNS and J-PARC

promise to deliver neutron intensities that are at least an order of magnitude (or more) higher than those at existing sources: traditional nuclear reactors such as those at ILL in Grenoble (France) and JRR-3 in JAEA (Japan), as well as existing pulsed (spallation) neutron sources such ISIS at Didcot (England) and LANSCE at Los Alamos (U.S.).

At both new high-intensity spallation sources, diffractometers for macromolecular crystallography are either being built. At J-PARC, construction of the so-called iBIX instrument has been almost finished [18] and has been operated since 2008. As of April 2010, it is operated with 200kW accelerator power ; while at SNS, a corresponding instrument, to be called MaNDi (Macromolecular Neutron Diffractometer), has been funded. [19] The instruments will differ somewhat in the type of moderator used. (The moderator is the material situated between the neutron target source and the sample crystal; its choice determines the intensities and wavelength distribution of the neutrons used in the diffraction experiment.) iBIX is using neutrons from a coupled moderator, which has a higher intensity but a wider pulse in time; while MaNDi is expected to use a decoupled moderator, which is less intense but has a sharper pulse in time. One reason for this difference is that J-PARC has a lower pulsing frequency (25 Hz) than SNS (60 Hz). Overlap between pulses is therefore less serious of a problem with the more widely separated (in time) pulses at J-PARC than with the closely-spaced pulses at SNS.

Regardless of these technical differences, the implications of the development of SNS and J-PARC on macromolecular research are obvious: If intensities can be increased by an order of magnitude or two, then in principle it will be possible to study crystals that are correspondingly smaller in volume. The consequences of this development will be a dramatic decrease in crystal size, which should have a very significant effect on the usefulness of single-crystal neutron diffraction in the field of structural biology.

**ACKNOWLEDGEMENT**

Most of the works were supported by a grant-in-aid for scientific research from the Ministry of Education, Culture, Sports, Science and Technology of Japan and by the Human Frontiers Science Program (under grant number RGP0021/2006-C).

REFERENCES


[1] I. Tsyba, R. Bau, Chemtracts 2002, 15, 233.

[2] N. Niimura, S. Arai, K. Kurihara, T. Chatake, I. Tanaka, R. Bau, Cell Mol Life Sci 2006, 63, 285.

[3] M. P. Blakeley, P. Langan, N. Niimura, A. Podjarny, Curr Opin Struct Biol 2008, 18, 593.

[4] N. Niimura, R. Bau, Acta Crystallogr A 2008, 64, 12.

[5] M. P. Blakeley, Crystallography Reviews 2009, 15, 157

[6] K. Kurihara, I. Tanaka, T. Chatake, M. W. Adams, F. E. Jenney, Jr., N. Moiseeva, R. Bau, N. Niimura, Proc Natl Acad Sci U S A 2004, 101, 11215.

[7] A. Ostermann, F. G. Parak, in Hydrogen- and Hydration-Sensitive Structural Biology (Eds.: N. Niimura, H. Mizuno, J. R. Helliwell, E. Westhof), KubaPro, Tokyo, 2005, pp. 87.

[8] T. Chatake, A. Ostermann, K. Kurihara, F. G. Parak, N. Niimura, Proteins 2003, 50, 516.

[9] M. J. Adams, T. L. Blundell, E. J. Dodson, G. G. Dodson, M. Vijayan, E. N. Baker, M. M. Harding, D. C. Hodgkin, B. Rimmer, S. Sheat, Nature 1969, 224, 491.

[10] E. N. Baker, T. L. Blundell, J. F. Cutfield, S. M. Cutfield, E. J. Dodson, G. G. Dodson, D. M. Hodgkin, R. E. Hubbard, N. W. Isaacs, C. D. Reynolds, et al., Philos Trans R Soc Lond B Biol Sci 1988, 319, 369.

[11] M. Maeda, T. Chatake, I. Tanaka, A. Ostermann, N. Niimura, J Synchrotron Radiat 2004, 11, 41.

[12] T. Ishikawa, T. Chatake, Y. Ohnishi, I. Tanaka, K. Kurihara, R. Kuroki, N. Niimura, Chemical Physics 2008, 345, 152.

[13] T. Ishikawa, T. Chatake, Y. Morimoto, M. Maeda, K. Kurihara, I. Tanaka, N. Niimura

[14] W. Iwai, T. Yamada, K. Kurihara, Y. Ohnishi, Y. Kobayashi, I. Tanaka, H. Takahashi, R. Kuroki, T. Tamada, N. Niimura, Acta Crystallogr D Biol Crystallogr 2009, 65, 1042.

[15] G. D. Smith, R. H. Blessing, Acta Crystallogr D Biol Crystallogr 2003, 59, 1384.

[16] N. Sakabe, K. Sakabe, K. Sasaki, Journal of Biosciences 1985, 8, 45.

[17] A. Wlodawer, H. Savage, G. Dodson, Acta Crystallogr B 1989, 45 ( Pt 1), 99.

[18] I. Tanaka, K. Kusaka, K. Tomoyori, N. Niimura, T. Ohhara, K. Kurihara, T. Hosoya, T. Ozeki, Nuclear Instruments and Methods in Physics Research Section A: Accelerators, Spectrometers, Detectors and Associated Equipment 2009, 600, 161.

[19] L. Coates, A. D. Stoica, C. Hoffmann, J. Richards, R. Cooper, Journal of Applied Crystallography 2010, 43.

# NEW MICROPOROUS CRYSTALLINE MATERIALS: MOFS, COFS, AND ZIFS

**Michael O'Keeffe**

***Center for Reticular Chemistry at the California NanoSystems Institute, University of California, Los Angeles, CA 90095, USA, and Department of Chemistry and Biochemistry, Arizona State University, Tempe AZ 85287, USA.***

**Omar M. Yaghi**

***Center for Reticular Chemistry at the California NanoSystems Institute, and Department of Chemistry and Biochemistry, University of California, 607 Charles E. Young Drive East, Los Angeles, CA 90095, USA.***

## 1. ABSTRACT

We give examples from our own work of metal-organic frameworks (MOFs), covalent organic frameworks (COFs) and zeolitic imidazolate frameworks (ZIFs). In MOFs in general, polyatomic and cationic metal-containing clusters (secondary building units) are linked by ditopic or polytopic anionic organic linkers (often carboxylates) to form robust porous periodic frameworks. In COFs all the linked groups are organic. ZIFs are special cases of MOFs in which transition metal ions are linked by substituted imidazolate ions into frameworks with a topology that is either that of a known zeolite or zeolite-like. Reticular chemistry is the design and synthesis of such materials. However to implement designed synthesis the principal topologies possible must be known. We indicate how these are known and where they are available.

## 2. INTRODUCTION

About sixty tears ago a number of groups, particularly in Japan, started systematically investigating crystalline materials in which metal atoms were held together by ditopic and, less frequently, polytopic coordinating ligands, particularly those containing cyanide groups. Such materials have generally been termed *coordination polymers*. These have been defined in a recent book with that title [1] in the terms: "A coordination polymer contains metal ions linked by coordinated ligands into an infinite array". It had long been noted that the topology of such structures could be abstracted as simple periodic graphs termed *nets*. These nets were also found in the topology of simple inorganic crystals such as diamond, cristobalite and rutile and were often named after them. Indeed one of the leading pioneers in this field, Toschitake Iwamoto, proposed the term *mineralomimetic chemistry* [2], a term that did not catch on (try saying it!).

More recently we, and others, have developed related classes of materials in which metal-containing inorganic groups, generally *polyatomic* clusters, are joined by polytopic organic linkers into periodic structures. These are often salts of carboxylic acids and, in contrast to coordination polymers, generally have neutral frameworks. Also in contrast to coordination polymers, all the links in the new materials are strong bonds leading to robust frameworks which can be freed from occluded solvent and other guest molecules to produce permanent porosity. The new materials are termed *metal-organic frameworks* (MOFs) — a term that is widely accepted, if not yet very precisely defined.

It was also long recognized that relatively few simple nets predominated in coordination polymers, so that in favorable cases structures with predetermined topologies could be produced by design [3]. However although many nets were known, largely from the work of A. F. Wells [4,5], there was no systematic catalog of preferred (*default*) nets, although we early made a first attempt [6].

In this article we describe our approach to what we term *reticular chemistry* [7] — the design and synthesis of materials by linking together molecular building blocks (clusters, molecules, etc.) by strong bonds into polyhedral or periodic frameworks. In order to target a particular topology we have to know the possibilities — in the words of G. O. Brunner "The synthesis of new structures requires not only chemical skill but also some knowledge of the principal topological possibilities" [8].

We first give some examples of the new microporous materials from our own work. These are MOFs and the related (metal-free) covalent organic frameworks (COFs). Then we describe examples of a special class of MOF termed zeolitic imidazolate frameworks (ZIFs) to which special conditions apply for designed synthesis. These materials have enormous potential especially for clean energy applications involving storage and separations of gases such as dihydrogen, methane and carbon dioxide, and are currently under active large-scale development for these and other purposes [9]. Finally we indicate briefly how the nets important for design have been enumerated and characterized using tiling theory.

## 3. METAL-ORGANIC FRAMEWORKS (MOFS)

The iconic MOF is MOF-5 [10], Fig. 1. In this structure $Zn_4O$ groups are linked by terephthalate = 1,4-benzenedicarboxylate (BDC) to form a neutral framework of composition $Zn_4O(BDC)_3$. This material has large pores (one is shown with a yellow ball inside it in the figure) which are filled with solvent in the as-prepared state but which can readily be emptied. The 'activated' material now has unprecedentedly large surface area and can reversibly absorb large quantities of gases such as nitrogen, methane, etc. It also has excellent thermal stability.

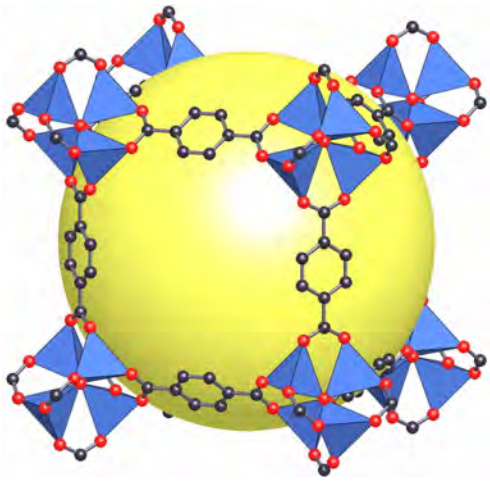

**Figure 1**. A fragment of the structure of MOF-5. $ZnO_4$ tetrahedra are shown in blue. Carbon atoms are black and oxygen atoms are red.

The metal carboxylate cluster has composition $Zn_4O(CO_2)_6$ and it may be seen (Fig. 2) that the six carboxylate C atoms are at the vertices of a regular octahedron. It is interesting that the cluster was known much earlier in basic zinc acetate $Zn_4O(OAc)_6$ (here $OAc^-$ is the acetate anion) and its congener basic beryllium acetate. With hindsight it seems remarkable that one had to wait about 50 years for the periodic structure to be produced.

The geometry of the structure can be abstracted as linked octahedra as shown in Fig. 2. The topology of the linked octahedra is a 6-coordinated net in which in fact the vertices correspond to the nodes of the primitive cubic lattice and the edges coincide with the shortest lattice vectors. As discussed below, we identify this net by the symbol **pcu**. Replacing a vertices in a net by a polygon or polyhedron corresponding to the vertex figure (in this example an octahedron) gives the *augmented* net which has symbol **pcu-a**.

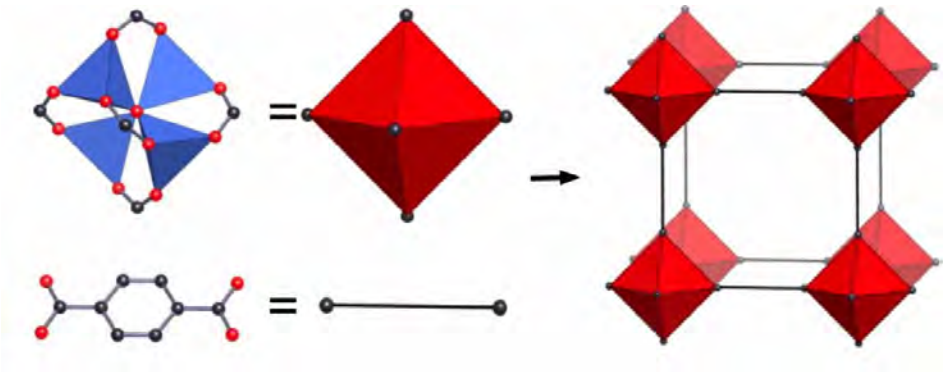

**Figure 2.** Left: showing that the carboxylate carbon atoms (black) of the basic zinc acetate cluster are at the vertices of an octahedron and that the same carboxylate carbon atoms in the terephthalate anion in MOF-5 form a linear linker. On the right the **pcu-a** net discussed in the text formed from these units.

It was an obvious next step to replace the terephthalate by other dicarboxylate linkers and an *isoreticular* (based on the same net topology) series of compounds were produced [11]; representative examples are shown in Fig. 3. Thus it was demonstrated that materials could be produced with cavities of predetermined size and functionality.

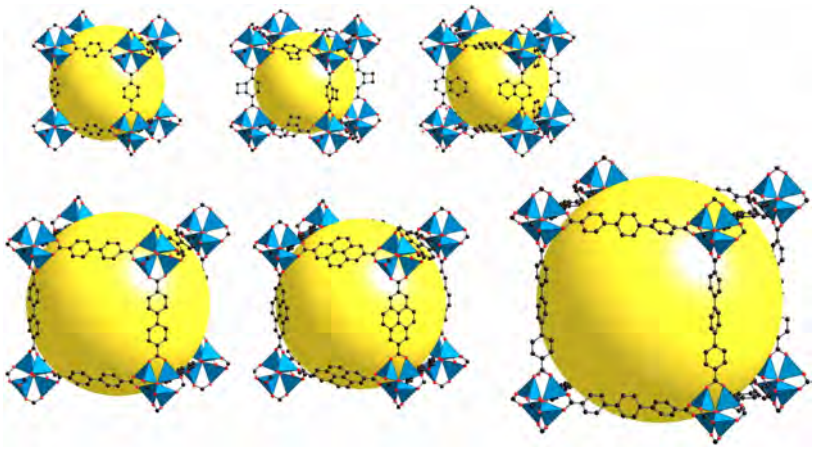

**Figure 3**. A series of MOFs isoreticular with MOF-5 (top left) [11].

One can also use tritopic organic units to link the same units. An early example of this was MOF-150 [12] in which the organic linker is tricarboxytriphenylamine (Fig. 4). This crystal has a simple cubic structure with a underlying topology that is a (6,3)-coordinated net (symbol **pyr**) named for the Fe-S bond network in pyrite. In fact as shown in Fig. 5, two separate networks occur interpenetrating.

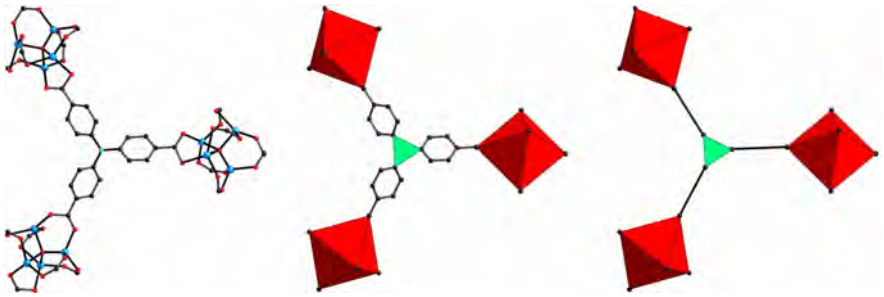

**Figure 4.** Left: a fragment of the MOF-150 structure centered on the N atom of the organic linker with three $Zn_4O$ clusters shown. Middle: the inorganic units condensed to an octahedron as in Fig. 2 and the organic unit shown as a triangle. Right: the phenyl groups condensed to a single rod as in Fig. 2 showing the structure as part of an augmented (6,3) coordinated net.

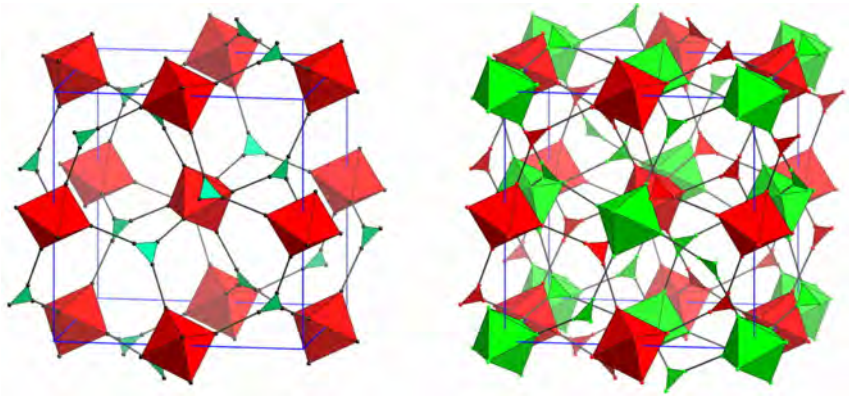

**Fig. 5.** Left: connection of the units in Fig. 4 to form the **pyr-a** net, Right: two such nets interpenetrating as in the structure of MOF-150.

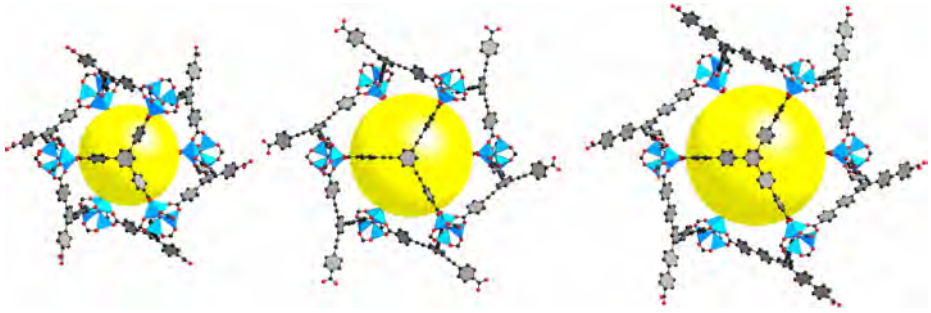

**Fig. 6.** Fragments of the structures of MOF-177 (left), MOF-180 (center) and MOF-200 (right,)

A pleasant surprise occurred in attempting to make a second isoreticular series with

extended linkers when it was found in MOF-177 that a related, but different topology (symbol **qom**) was obtained [13]. This material occurs as a single (i.e. not an interpenetrating pair) net and set records for porosity and surface area. Indeed it is a particularly attractive material for storing permanent gases such as hydrogen and methane and is a leading candidate for industrial development [9]. This new topology does permit isoreticular expansion and recently we reported MOF-180 and MOF-200 with the same topology. The isoreticular series is illustrated in Fig. 6. These and related materials have set new records for porosity and surface area [14].

Another metallic (cationic) secondary building unit (SBU) commonly used in MOF chemistry is the 'paddlewheel' found in copper acetate $Cu_2(OAc)_4$. The metal-carboxylate SBU has composition $Cu_2(CO_2)_4$ and now the four carboxylates C atoms are at the vertices of a square (Fig. 7).

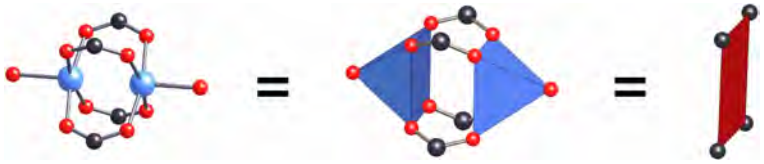

**Fig. 7.** Left: the copper acetate paddle wheel (Cu blue. O red, C black; methyl groups not shown. Middle: the same with blue $CuO_5$ pyramids (the apex O is from water). Right; the square formed by the carboxylate carbon atoms.

We have systematically explored the different topologies and dimensionalities (periodicities) that can be obtained by combining this SBU with variously shaped ditopic linkers [15]. Fig. 8 shows two extreme examples: a 0-periodic metal-organic polyhedron, MOP-1 [16] and a 3-periodic framework MOF-101 [17]. Many more isoreticular examples have been published more recently [18]. The 3-periodic structure has a topology of a 4-coordinated net with vertices in the positions of the atoms in crystalline NbO that has the symbol **nbo**.

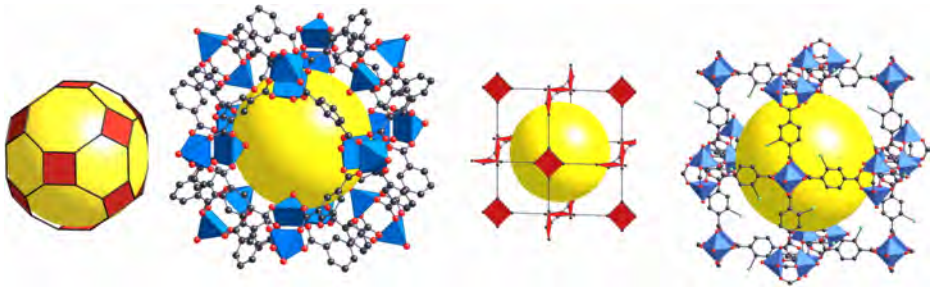

**Fig. 8.** From left: an augmented (truncated) cuboctahedron, MOP-1, the **nbo-a** net, MOF-101.

The best MOFs [14] have surface areas > 5000 $m^2/g$, significantly higher than any other crystalline materials. The surface-area/volume ratio for the same materials is typically 2000 $m^2/cm^3$; this ratio corresponds to the external surface-area/volume ratio of cubes of 3 nm edge. The examples given here are merely representative examples from our work. A good place to start for more information is a recent themed issue of *Chem. Soc. Reviews* [19].

## 4. COVALENT-ORGANIC FRAMEWORKS (MOFS)

In COFs SBUs are again linked into a periodic framework, but now all the components

are organic. The first such material (COF-1) was made by condensing benzene 1,4-diboronic acid to produce a layer structure in which six-membered boroxane rings (B-O-B-O-B-O-m see Fig. 10) were linked by benzene rings [20]. Later an analogous material was made from condensation of 1,4-dicyanaobenzene; here 6-membered triazine (C-N-C-N-C-N-) rings are linked to a 2-periodic array again by benzene rings. [21]

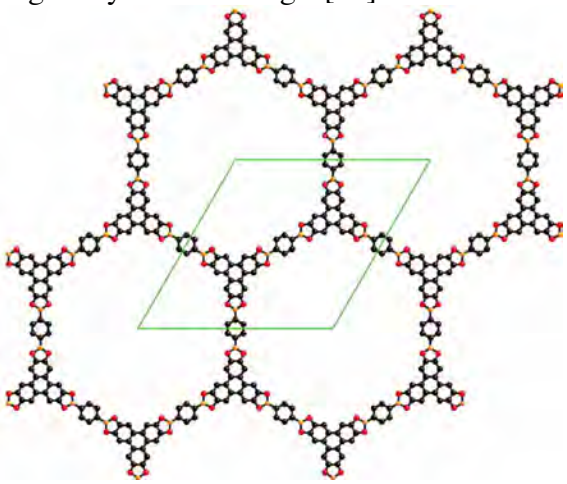

**Figure 9**. A layer of COF-5. Oxygen atoms are red.

In COF-5, reported at the same time as COF-1, benzene diboronic acid was linked to a trigonal hexahydroxy SBU (see Fig. 10 below) by eliminating water in an esterification reaction [20]. Again a 2-periodic layer results (Fig. 9); now with large diameter (27 Å) pores. These materials did not yet challenge the best MOFs for porosity and surface area but subsequent work [22] produced related materials with even larger pores (COF-10).

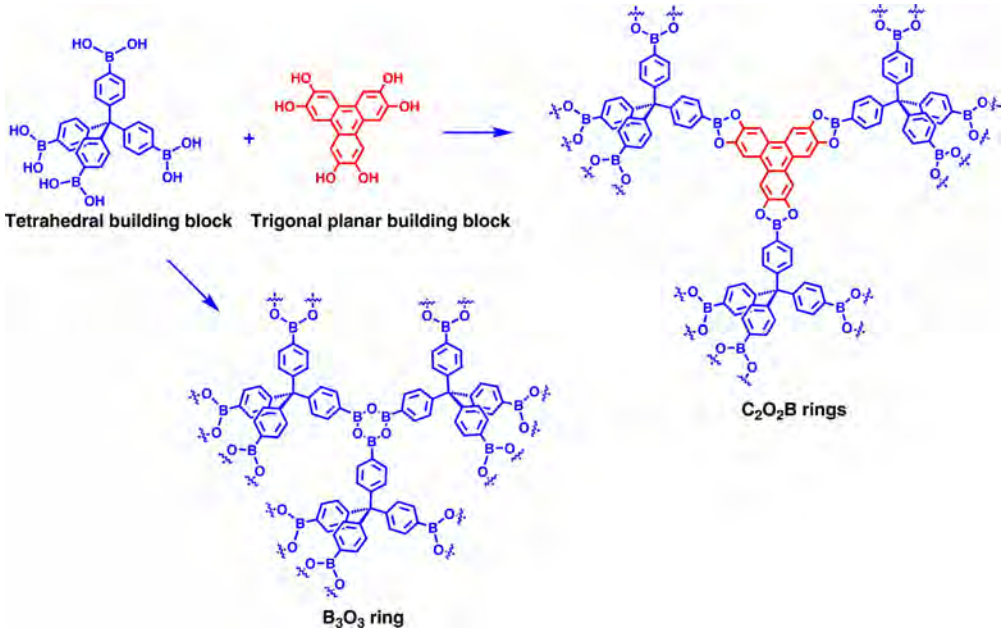


**Figure 10**. The combination of tetrahedral and trigonal SBUs to make COFs based on (3,4)-coordinated nets.

The first COFs with 3-periodic frameworks followed shortly thereafter [23]. Now tetrahedral tetraboronic acids were linked as COF-1 and COF-5 either by self condensation or with the triangular hexahydroxy SBU (Fig. 10) to form structures based on (3,4)-coordinated nets. There are only two nets of this sort with just one kind of link and both are found (Fig. 11). It might be noted that these materials are obtained as powders and have diffraction patterns of relatively poor quality and knowing the expected structures, which give distinctive cubic diffraction patterns, was essential to identifying their structures.

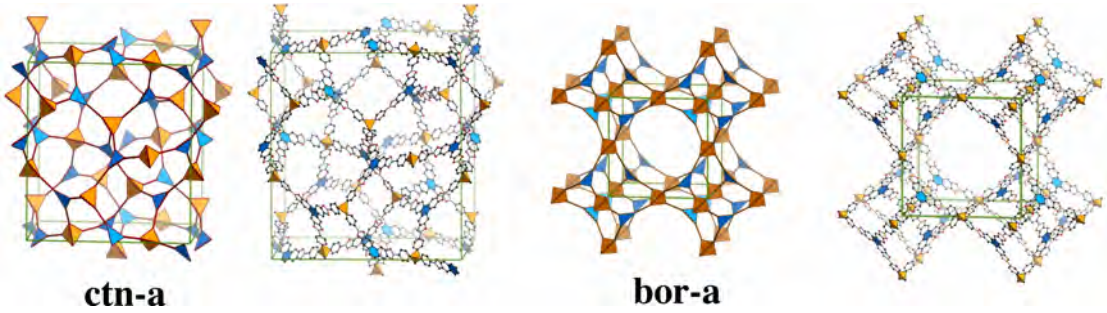


**Figure 11**. COFs based on (3,4)-coordinated nets (shown in augmented form). Left COF-105; right MOF-108

Subsequent work has shown that COFs are highly competitive for sorption and storage of small molecules such as dihydrogen, methane and carbon dioxide [22, 24] and ammonia [25].

## 5. ZEOLITIC IMIDAZOLATE FRAMEWORKS (ZIFS)

Imidazole (ImH) is usually thought of as a base, but it is amphoteric and Cu, Zn and Co imidazolates have been known for many years but these were non-porous materials of relatively high density. However the M-Im-M link has a large angle (ca 145°, see Fig. 12) and it was realized that with tetrahedral M one has a situation similar to silicates in which Si-O-Si angles are generally also around 145°.

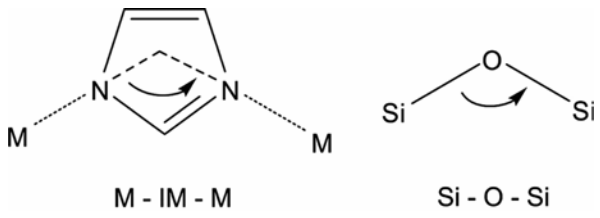


**Figure 12**. Comparing an imidazolate link with that in a silicate.

Accordingly one might expect under suitable conditions to mimic silicon zeolite synthesis. Indeed this is the case, but it was found, much like zeolite synthesis and unlike carboxylate MOF synthesis, the routes to a wide variety of ZIFs with zeolite structures were best discovered by high-throughput methods [26]. Two representative examples are shown in Fig. 13. A recent review [27] covers all ZIFs prepared by us and by others to date. It might be noted that in both the examples shown the same large cage appears, but replacing just one C of the linker by N results in a structure of different topology. This illustrates the subtle structure-directing

effect of the linker in ZIFs [28].

ZIFs can have pores with a wide range of functional groups because of the ready availability of substituted imidazoles (examples can be seen in the figure). The 5-membered imidazole ring controls the scale of the ZIF structure but the topology is driven mainly by the linker (to a lesser extent by solvent). With careful control particularly of the shape of the linker isoreticular series can be prepared with the topology of the zeolite gmelinite (zeolite framework code **GME**) [29] and zeolite rho (**RHO**) [30].

Occasionally "rogue" structures are observed with colossal cages. The one in ZIF-100 is based on a polyhedron with 264 vertices and is made up of 7524 vertices [31].

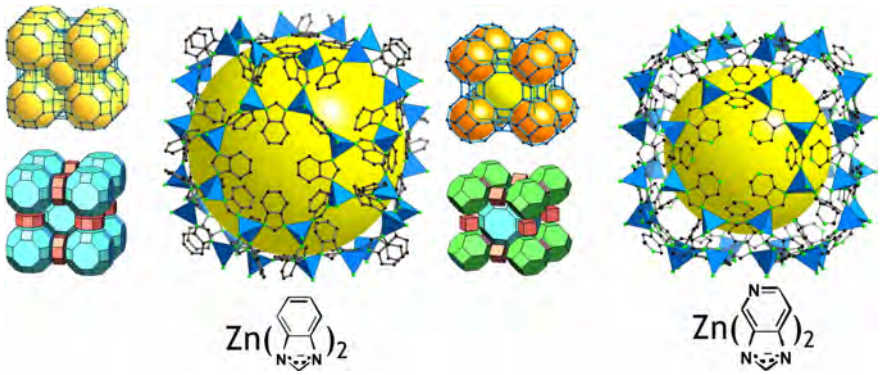


**Figure 13**. Left ZIF-20 with the zeolite **LTA** topology, right ZIF-11 with the zeolite **RHO** topology; The underlying nets are shown as a stick model and as a tiling (space-filling packing of polyhedra). Only the largest cage of the ZIFs are shown.

ZIFs have generally excellent chemical and thermal stability and are excellent candidates for selective absorption of carbon dioxide from gas streams [16, 30, 31].

## 6. THREE-PERIODIC NETS AND TILINGS AND RETICULAR CHEMISTRY

As already remarked, if we are to synthesize periodic structures by design we must know the basic possibilities. In fact we now know quite a bit about the basic periodic nets. Mathematically periodic nets are special cases of graphs and are conveniently considered within the framework of graph theory [32]. For computational purposes it is sometimes convenient to assign the vertices in a repeat unit of a periodic net *barycentric coordinates* in which each vertex has coordinates that are the average of those of all its neighbors. An important result [33] is that for nets in which no two vertices have the same barycentric coordinates, the combinatorial symmetry of the graph is isomorphic to a space group symmetry, and such nets are referred to as *crystallographic*. For such nets the true symmetry can be determined from any input embedding, and a unique signature identified – so for this class of graph the isomorphism problem (graph identification problem) is solved. This is easily done using a generally-available program Systre written by Olaf Delgado-Friedrichs. An account of the theoretical methods is available [34].

The nets of interest in crystal chemistry are all (so far!) crystallographic and most of them admit a *natural tiling* [35]. A tiling in this context is a space filling by generalized polyhedra or *cages* that fit together face to face. A tiling for the diamond net (symbol **dia**) is shown in Fig. 14. The tiles have a skeleton (framework) corresponding to the ten C vertices of adamantane and

have divalent and trivalent vertices. A natural tiling is required to have the symmetry of the net; further, if necessary (i.e. there is more than one tiling with the symmetry of the net), the tiles are made as small as possible subject to the constraint that no one face is bigger than all the rest.

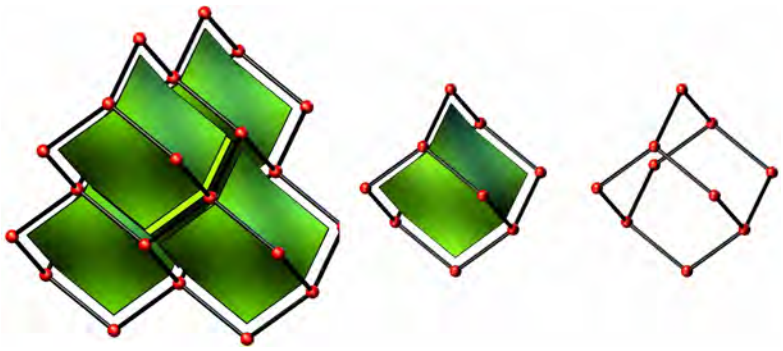

**Figure 14**. Tiling for the diamond (**dia**) net. The tiles (green) are slightly shrunken for clarity - in reality they fill space. On the right the skeleton of one tile (center) is shown. It has the carbon framework of adamantane $C_{10}H_{14}$.

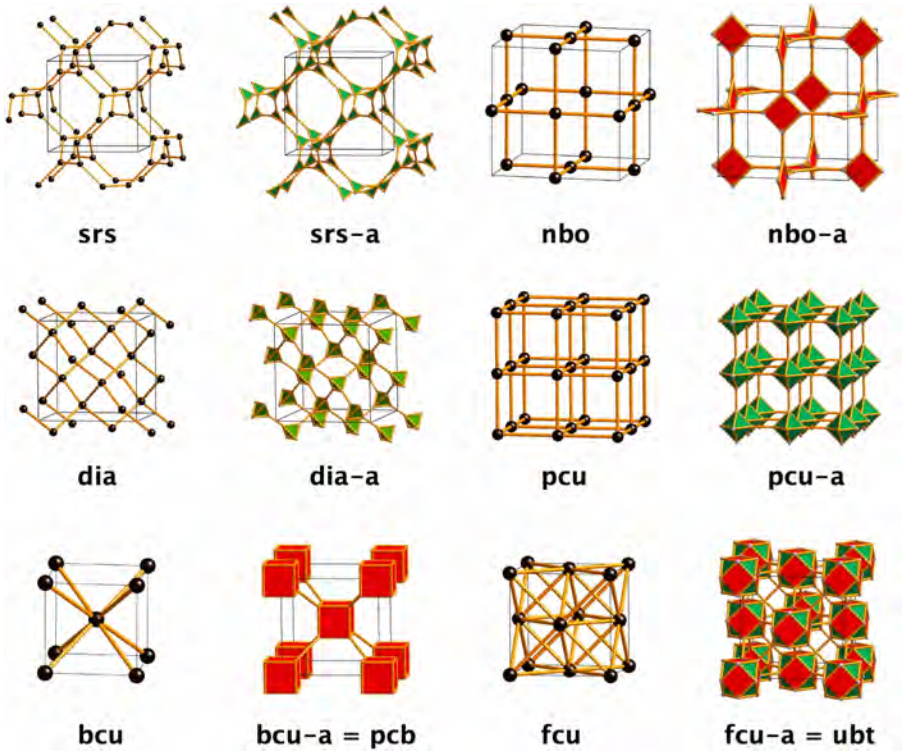


**Figure 15**. The five regular nets and the on quasiregular net (**fcu**). The nets are also shown in their augmented forms (**xxx-a**).

It would take us too far afield to go into the uses of tiling theory in crystal chemistry (but see [35]). Here we just call attention to the fact that of special interest in reticular chemistry are nets with just one kind of edge (*edge transitive* in the jargon). Subject to the restriction that there is an embedding in which there are no inter-vertex distances shorter than edges, it has been possible to identify all edge-transitive nets [36]. Tilings of nets provide a nice measure of

regularity. There are five *regular* nets (Fig. 15) for which the tiling has just one kind of vertex, one kind of edge, one kind of face and one kind of tile, i.e. *transitivity* 1111. In the most symmetric form the vertex figure of a regular net is a regular polygon or polyhedron – specifically triangle, square, tetrahedron, octahedron or cube [37]. The nets all have cubic symmetry.

There is one *quasiregular* net with a vertex figure that is a quasiregular polyhedron (one with one kind of vertex and edge, but two kinds if face). This is the net of the face-centered cubic lattice and it is no surprise that the natural tiling has two kinds of tile (tetrahedra and octahedra) and the transitivity is 1112. These nets are generally well known, but for the fascinating story of the redicovery of the three-coordinated net **srs** see reference [38].

An account of the taxonomy of periodic nets, and its relevance to designed synthesis of materials has been given recently [39]. We have also established a searchable database of nets (RCSR = Reticular Chemistry Structure Resource) [40].

## 7. ACKNOWLEDGEMENTS

In this article we have called attention to some highlights of our work on porous crystals over the last dozen years. We have been aided by many talented students and distinguished colleagues, too many to list here, but the names of many of them appear in the references below.

## 8. REFERENCES

[1] S. R. Batten, S. M. Neville and D. R. Turner, *Coordination Polymers* (RSC Publishing, 2009).
[2] T. Iwamoto, S. Nishikiori, T. Kitazawa and H. Yuge, J. Chem. Soc. Dalton Trans. (1997), 4127.
[3] R. Robson, J, Chem. Soc. Dalton Trans. (2000), 3735.
[4] A. F. Wells, *Three-dimensional nets and polyhedra* (Wiley, New York, 1977).
[5] A. F. Wells, *Further studies of three-dimensional nets* (Amer. Crystallogr. Assoc. Monograph 8, 979).
[6] M. O'Keeffe, M. Eddaoudi, H. Li, T. Reineke and O. M. Yaghi, J. Solid State Chem. **152**, (2000), 2.
[7] O. M. Yaghi, M. O'Keeffe, N. W. Ockwig, H. K. Chae, M. Eddaoudi and J. Kim, Nature 423, (2003), 705.
[8] G. O. Brunner, Zeits. Kristallogr. 156 (1981), 295.
[9] A. U. Czada, N. Trukhan and U. Müller, Chem. Soc. Revs. 38 (2009), 1284.
[10] H. Li., M. Eddaouddi, M. O'Keeffe, O. M. Yaghi, Nature, 402 (1999), 276.
[11] M. Eddaoudi, J. Kim, N. Rosi, D. Vodak, J. Wachter, M. O'Keeffe and O. M. Yaghi, Science, 295 (2002), 469.
[12] H. K. Chae, J. Kim, O. Delgado Friedrichs, M. O'Keeffe and O. M. Yaghi, Angew. Chem. Int. Ed**.** 42 (2003), 3907.
[13] H. K. Chae, D. Y. Siberio-Pérez, J. Kim, Y. Go, M. Eddaoudi, A. J. Matzger, M. O'Keeffe and O. M. Yaghi, Nature, 427 (2004), 523.
[14] H. Furukawa, N. Ko, Y. B. Go. N. Aratani, S. B. Choi, E. Choi. A. O. Yazaydin, R. Q.

Snurr, M. O'Keeffe, J. Kim and O. M. Yaghi, Science, 329, (2010), 424.
[15] M. Eddaoudi, J. Kim, D. Vodak, A. Sudik, J. Wachter, M. O'Keeffe and O. M. Yaghi, Proc. Nat. Acad. Sci. 99 (2002), 4900.
[16] M. Eddaoudi, J. Kim, J. B. Wachter, H. K. Chae, M. O'Keeffe and O. M. Yaghi, J. Am. Chem. Soc. 123 (2001), 4368.
[17] M. Eddaoudi, J. Kim, M. O'Keeffe and O. M. Yaghi, J. Am. Chem. Soc. 124 (2002), 376.
[18] H. Furukawa, J. Kim. N. W. Ockwig, M. O'Keeffe and O. M. Yaghi, J. Am. Chem. Soc. 130 (2008), 11650-11661.
[19] J. R. Long and O. M. Yaghi, eds., *The Pervasive Chemistry of Metal-Organic Frameworks*. Chem. Soc. Revs. 38 (1009), 1201.
[20] A. P. Côté, A. I. Benin, N. W. Ockwig, M. O'Keeffe, A. J. Matzger and O. M. Yaghi, Science 310, (2005), 1166.
[21] P. Kuhn, M. Antionietti and A. Thomas, Angew, Chem. Int. Ed. 47 (2008), 6909.
[22] H. Furukawa and O. M. Yaghi. J. Amer. Chem. Soc.131 (2009), 8875.
[23] H. M. El-Kaderi, J. R. Hunt. J. L. Mendoza-Cortés, A. P. Côté, R. E. Taylor, M. O'Keeffe and O. M. Yaghi, Science 316, (2007), 268.
[24] S. S. Han, H. Furukawa, O. M. Yaghi and W. A. Goddard, J. Amer. Chem. Soc. 130 (2008), 11580.
[25] C. J. Doonan, D. J. Tranchemaontaigne, T. G. Glover, J. R. Hunt and O. M. Yaghi, Nature Chemistry 2 (2010) 235.
[26] R. Banerjee, A. Phan, B. Wang, C. B. Knobler, H. Furukawa. M. O'Keeffe and O. M. Yaghi, Science 319 (2008) 939.
[27] A. Phan, C. J. Doonan, F. J. Uribe-Romo, C. B. Knobler. M. O'Keeffe and O. M. Yaghi, Accts. Chem. Res. 43 (2010), 58.
[28] H. Hayashi, A. P. Côté, H. Furukawa, M. O'Keeffe and O. M. Yaghi. Nature Materials 6, (2007), 501.
[29] R. Banerjee, H. Furukawa, D. Britt, C. B. Knobler, M. O'Keeffe and O. M. Yaghi, J. Am. Chem. Soc. 131 (2009), 3875.
[30] W. Morris, B. Leung, H. Furukawa and O. M. Yaghi, J. Am. Chem. Soc. 132 (2010), 11006.
[31] B. Wang, A. P. Côté, H. Furukawa, M. O'Keeffe and O. M. Yaghi, Nature, 453 (2008), 207.
[32] O. Delgado-Friedrichs and M. O'Keeffe, J. Solid State Chem. 178 (2005), 2480.
[33] O. Delgado-Friedrichs, Discr. Comput. Geom. 33 (2005), 67.
[34] O. Delgado-Friedrichs and M. O'Keeffe, Acta Crystallogr. A59 (2003), 351.
[35] V. A. Blatov, O. Delgado-Friedrichs, M. O'Keeffe and D. M. Proserpio, Acta Crystallogr. A63 (2007), 418.
[36] O. Delgado-Friedrichs, M. O'Keeffe and O. M. Yaghi, Acta Crystallogr. A63 (2007), 344.
[37] O. Delgado-Friedrichs, M. O'Keeffe and O. M. Yaghi, Acta Crystallogr. A59, (2003), 22.
[38] S. T. Hyde. M. O'Keeffe and D. M. Proserpio, Angew. Chem. Int. Ed. 47(2008), 7996.
[39] O. Delgado-Friedrichs, M. O'Keeffe and O. M. Yaghi, Phys. Chem. Chem. Phys. 9 (2007), 1035.
[40] M. O'Keeffe, M. A. Peskov, S. J. Ramsden and O. M. Yaghi, Accts. Chem. Res. 41 (2008), 1782.

# BIG METALS, SMALL LIGANDS: CHARACTERIZATION OF THE 15-COORDINATE COMPLEX THORIUM AMINODIBORANATE $[Th(H_3BN(CH_3)_2BH_3)_4]$ BY SINGLE CRYSTAL NEUTRON DIFFRACTION

Paula M. B. Piccoli and Arthur J. Schultz
*Intense Pulsed Neutron Source, Argonne National Laboratory, Argonne, IL 60439 (USA)*

Tanya K. Todorova
*Department of Physical Chemistry, Sciences II, University of Geneva*
*30, Quai Ernest Ansermet, 1211 Geneva 4 (Switzerland)*

Laura Gagliardi
*University of Minnesota, Department of Chemistry, 207 Pleasant St. SE*
*Minneapolis, MN 55455-0431 (USA)*

Scott R. Daly and Gregory S. Girolami
*School of Chemical Sciences, University of Illinois at Urbana-Champaign*
*600 South Matthews Avenue, Urbana, IL 61801 (USA)*

## 1. ABSTRACT

The anionic borohydride ligand, $[BH_4]^-$, is known to bind to metals by means of unidentate, bidentate, and tridentate binding modes, making it a useful ligand for the achievement of high coordination numbers in inorganic and organometallic complexes. Combinations of borohydride ligands with metal centers having large atomic radii often leads to complexes with coordination numbers higher than 12. Although 14-coordinate actinide complexes such as $[U(BH_4)_4(thf)_2]$ have been previously reported, no complex with a coordination numbers higher than 14 has been unambiguously characterized. Due to the low sensitivity of X-rays for the detection of hydrogen atoms and the domination of the heavy metal in the scattered X-ray data, neutron diffraction data is invaluable for accurately characterizing such complexes.

Reaction of $ThCl_4$ with $Na(H_3BNMe_2BH_3)$ in tetrahydrofuran produces the monomeric complex $[Th(H_3BNMe_2BH_3)_4]$ (**1**), a molecule for which DFT calculations predict a theoretical maximum coordination number of 16 in the gas phase. Neutron diffraction data collected at the IPNS at low temperature reveal that fifteen of the hydrogen atoms on the chelating aminodiboranate ligands coordinate to the thorium center. The Werner coordination number of 15 in the solid state is the highest for any structurally characterized complex to date. Upon heating, complex **1** undergoes a thermal reaction to produce the sterically less crowded 14-coordinate $[Th(H_3BNMe_2BH_3)_2(BH_4)_2]$ (**2**).

Herein we describe the structural characterization of **1**, an analysis of its structure by DFT methods, and comparisons to analogous high coordination actinide complexes containing hydride or borohydride ligands.

## 2. BACKGROUND

In 1913, Alfred Werner became the first inorganic chemist to receive the Nobel Prize in Chemistry for his important work on coordination compounds and stereochemistry in inorganic complexes. His first paper on coordination chemistry, published in 1893 [1], built the foundation for modern inorganic chemistry as we know it. It defined a property that he called primary valence, but which is now known as coordination number. In all classical Werner coordination complexes, each coordination site involves a two-electron bond between the metal and a single atom of a ligand; the total number of such two-electron bonds formed by the metal is its coordination number. Later studies of organometallic complexes led to a revision of the coordination number concept: for ligands such as ethylene two atoms jointly occupy a single coordination site [2]. As an extension of this concept, the cyclopentadienyl ligand, $C_5H_5^-$, is generally not regarded as occupying five coordination sites, but instead it is considered to be a 6-electron donor that occupies three coordination sites. Figure 1 illustrates two complexes, a classical Werner complex and an organometallic complex; even though different numbers of atoms are directly linked to the metal center, both complexes are classified as 6-coordinate.

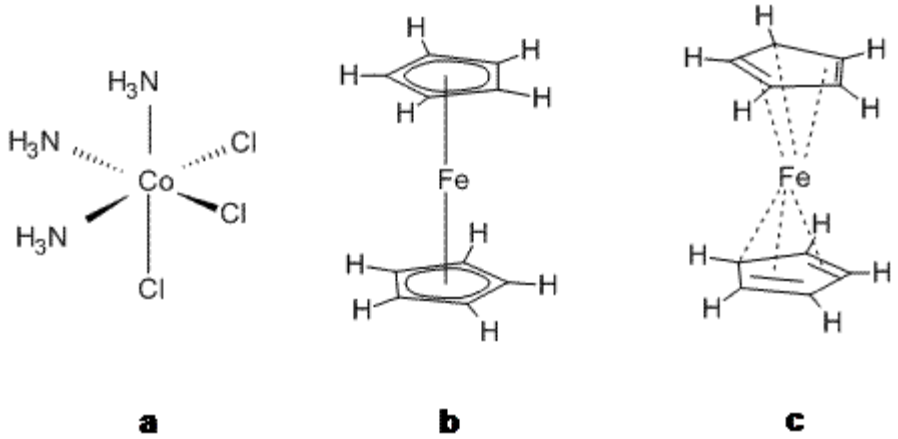


**Figure 1.** Two 6-coordinate, 18-electron complexes: (a) the Werner complex *fac*-$[CoCl_3(NH_3)_3]$, (b) ferrocene ($Cp_2Fe$). Figure 1(c) at right illustrates the 6-electron donating nature of the $Cp^-$ ligand and how it behaves as a tridentate ligand.

As coordination numbers increase, geometries beyond common tetrahedral and octahedral shapes can be achieved. The 1977 review of high coordination number complexes by Drew is a superb analysis of the regular polyhedral shapes as they apply to inorganic and organometallic complexes [3]. At the time of the publication, only a scant number of very high coordinate complexes (coordination number > 10) had been reported. Most of these examples are complexes of lanthanides and actinides, as well as zirconium; these metals all have some of the largest radii in the periodic table. Several factors may influence the overall coordination number of a complex, among them being the atomic or ionic radius of the central atom, the electronic structure as alluded to above, and the sizes of the ligands. Shannon and Prewitt have illustrated,

for example, that the effective ionic radii of common cations increases with coordination number but decreases with increasing oxidation state, two important factors to consider when building high coordinate complexes [4]. A recent paper on proposed covalent atomic radii* reconfirm the long-known trend that the radii across a period of elements decrease with atomic number [5]. Figure 2, created from the data in Cordero et al., illustrates this trend well over the periodic table. To maximize the number of ligands about a metal center, therefore, we look for the largest possible metal with the smallest possible ligands, as shown by Hermann and coworkers in a theoretical investigation of the gas phase $[Pb(He)_{15}]^{2+}$ [6].

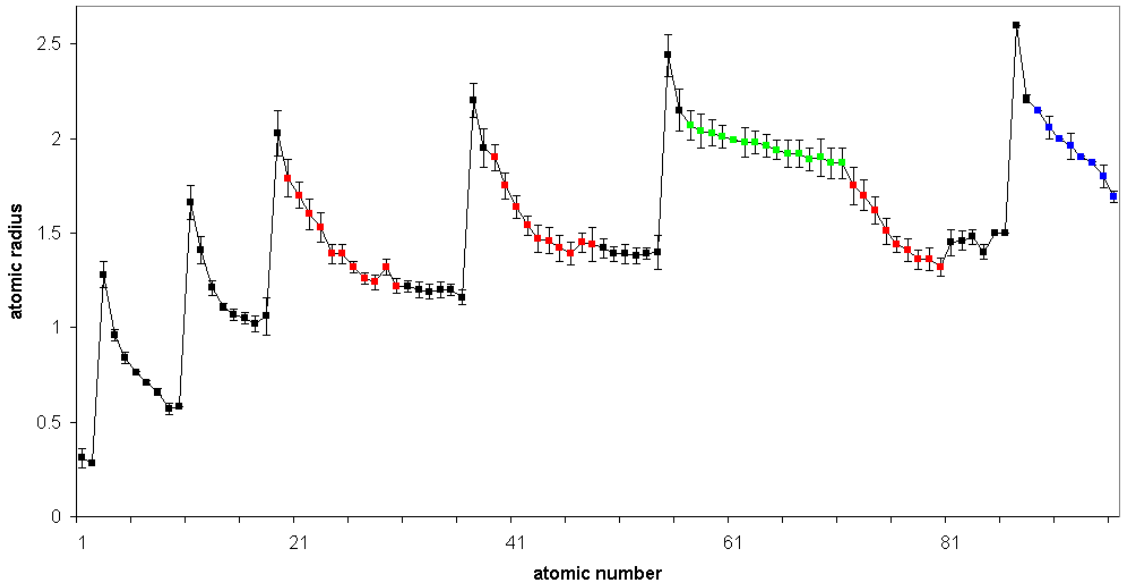


**Figure 2.** A graph of the proposed atomic radii in Angstroms (Å) as a function of atomic number through Z = 96, reconstructed from data compiled from Cordero et al. **[5]**. The red data points are for each transition metal series, green points are for the lanthanide series, and blue points indicate the actinides.

One of the smallest ligands per coordination site is the chelating borohydride anion, $[BH_4]^-$. This versatile ligand can bind to a single metal center through up to three of its own hydrides in a monodentate, bidentate or tridentate fashion (see Figure 3). Additionally the $[BH_4]^-$ anion can bridge two or more metal centers in a polymeric or three-dimensional fashion in order to utilize all four of its hydrogen atoms. Electronically, like most agostic [7] or σ complexes [8], each B-H-M interaction can be counted as a separate three-center, two-electron bond [9,10]. In this way the borohydride anion has produced complexes possessing some of the highest Werner coordination numbers to date. Borohydride complexes with a Werner coordination number of 12 include $[Zr(BH_4)_4]$ [11-13], $[Hf(BH_4)_4]$ [11,12,14], $[Np(BH_4)_4]$ [15] and $[Pu(BH_4)_4]$ [15]. Even more impressively, the polymeric complexes $[Th(BH_4)_4]$ [11,12], $[Pa(BH_4)_4]$ [15] and

* Author's note: Such data are often determined from a survey of the crystallographic literature and databases using bond distances to common atoms such as H, N, C and O. For these reasons it may still be wise, even though many journals no longer require it, to deposit published crystallographic structures of small molecules and extended solids to databases such as the Cambridge Structural Database or the Inorganic Crystal Structure Database.

$[U(BH_4)_4]$ [16,17] and the monomeric compound $[U(BH_4)_4(thf)_2]$ [18-20], have coordination numbers of 14. To date, however, no structurally characterized molecular complex has a Werner coordination number higher than 14.

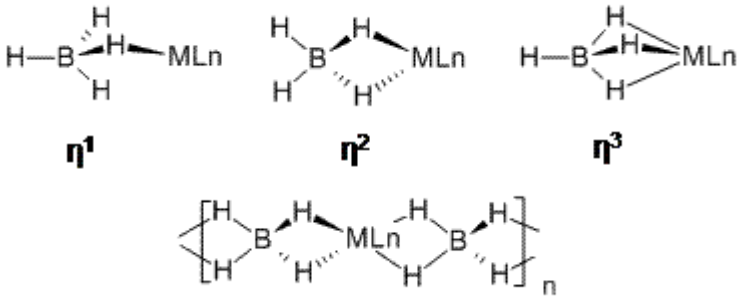


**Figure 3.** Binding modes of the $[BH_4]^-$ anion, from left to right: monodentate, bidentate and tridentate. The figure at bottom illustrates how the $[BH_4]^-$ anion can act as a bridging ligand in order to create a polymeric structure.

Recently, we published a preliminary communication giving details of the first 15-coordinate complex to be structurally characterized, $[Th(H_3BNMe_2BH_3)_4]$ (**1**) [21]. An analog of the borohydride anion, the chelating N,N-dimethylaminodiboranate ligand [22,23] was used to achieve this high coordination number. This manuscript describes the characterization of the complex, with particular emphasis on the structural determination using X-ray and neutron diffraction, as well as a comparison to similar lanthanide and actinide complexes that utilize this class of ligands. DFT calculations suggest that, in the gas phase, compound **1** adopts a coordination number of 16.

## 3. RESULTS

### 3.1 EXPERIMENTAL [21]

$[Th(H_3BNMe_2BH_3)_4]$ (**1**) was produced from the reaction of $ThCl_4$ with four equivalents of $Na(H_3BNMe_2BH_3)$ [23] in tetrahydrofuran (thf) at −78 °C and crystallized from toluene as described elsewhere [21]. Single crystal X-ray and neutron diffraction studies were carried out at -80 °C (193 K) in order to achieve the joint refinement of the neutron structure in the space group *Pnma* (no. 62, see below).

DFT quantum mechanical calculations on the geometry optimized molecules of **1** were carried out using the TURBOMOLE 5.9.1 package [24]. Periodic DFT calculations were carried out using the Vienna ab initio Simulation Package (VASP) [25,26]. A plane-wave basis set with a kinetic energy cutoff of 400 eV was used along with the Perdew-Burke-Ernzerhof (PBE) exchange-correlation functional. The interaction between the ionic cores and the valence electrons was described by the projector augmented wave (PAW) method [27]. The integrations in the Brillouin zone employed a (2x3x4) Monkhorst-Pack grid [28]. All atoms were allowed to relax while keeping the lattice parameters fixed at the experimentally determined values ($a$ = 18.8309, $b$ = 13.4269, $c$ = 9.6636 Å, $\alpha = \beta = \gamma = 90°$).

### 3.2 NEUTRON DIFFRACTION

Neutron diffraction data were collected using the Single Crystal Diffractometer (SCD) at the Intense Pulsed Neutron Source (IPNS) at Argonne National Laboratory (decommissioned, 2008; the SCD is currently installed at the Lujan Neutron Scattering Center at Los Alamos National Laboratory [29]). Because of the high atom percentage of boron in the molecule and boron's large cross section for neutron absorption (767 barns for natural abundance boron; 1 barn = $10^{-24}$ $cm^2$), the crystals for the neutron diffraction experiment were limited in size. Owing to the low number of resultant neutron data, the data were collected at the same temperature as the X-ray diffraction experiment to enable a joint refinement of X-ray and neutron data using GSAS [30]. In the joint refinement, the unit cell metrics and positions of the heavy (non-hydrogen) atoms were determined first from the X-ray structure, and their positions and thermal parameters were fixed at those values. Hydrogen atom locations were first approximated from the X-ray structure and subsequently also located in the neutron Fourier maps; any differences were corrected according to the neutron-determined data. To increase the number of observations and improve the quality of the neutron refinement, soft restraints were included to restrain all terminal B-H bond distances to be equal and all B-H bond distances for B-H units bridging to Th to be equal. C-H bond distances were also restrained to be equal.

The crystallographic structure of $[Th(H_3BNMe_2BH_3)_4]$ (**1**) as determined by X-rays and neutrons is shown in Figure 4. All four aminodiboranate ligands are chelating in a bidentate fashion to the metal center. Compound **1** is monomeric with the boron atoms distributed about the Th center in a distorted $D_{2d}$ dodecahedral arrangement. The Th···B distances (for B1 through B5) range from 2.882(3) to 2.949(3) Å, however the Th···B6 distance is appreciably longer and falls outside of this range at 3.193(5) Å. The molecule lies on the mirror plane at (*x, ¼, z*), and atom B6 was shown by neutron Fourier mapping to be disordered; it lies just off the mirror plane. One of its hydrogen atoms, H62, was shown to lie on the mirror plane so that the pendant $–BH_3$ portion of the B5-N3-B6 chelating ligand is disordered. No other disorder of the molecule was found.

For the seven short Th···B contacts (B1-B5), two hydrogen atoms bridge between B and Th (as in the bidentate mode for $BH_4^-$). However for the long contact between Th and B6, only one H atom is bridging, bringing the total coordination number of the Th center to 15. The bridging Th-H distances range from 2.37(2) to 2.539(18) Å for **1**.

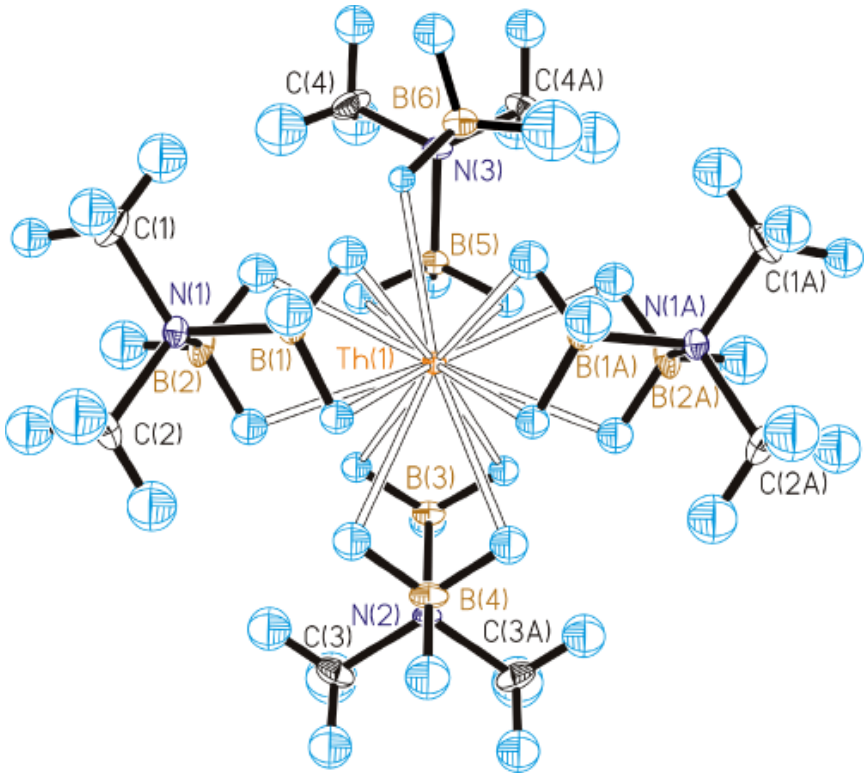


**Figure 4.** ORTEP diagram of the neutron structure of the 15-coordinate $[Th(H_3BNMe_2BH_3)_4]$ (**1**), as viewed along the direction of the mirror plane at (*x, ¼, z*). From this view it can be seen that only one of the hydrogen atoms belonging to B6 is coordinated to the Th atom and that the other two H atoms are terminal. Reprinted from S. R. Daly, P. M. B. Piccoli, A. J. Schultz, T. K. Todorova, L. Gagliardi, and G. S. Girolami, Angew. Chem. Int. Ed. **49**, 3379-338 1 (2010). Copyright Wiley-VCH Verlag GmbH & Co. KGaA. Reproduced with permission.

### 3.3 SPECTROSCOPIC CHARACTERIZATION

The various covalent (Figure 3) and ionic metal-tetrahydroborate bonding modes each has a distinctive vibrational signature [31]. The infrared spectrum of **1** features a terminal B-H stretch as a strong band at 2420 $cm^{-1}$ and bridging B-H stretches at 2264 and 2208 $cm^{-1}$ [21]. These values compare well with those seen for $[Th(BH_4)_4]$, which exhibits a terminal B-H stretch at 2530 $cm^{-1}$ and bridging stretches at 2270, 2200, and 2100 $cm^{-1}$ [12]. The $[Th(BH_4)_5]^-$ anion is proposed to have tridentate $BH_4$ groups as judged from its IR spectrum, but this compound has not yet been investigated crystallographically.

As with many tetrahydroborate complexes, the terminal and bridging hydrogens exchange rapidly on the NMR time scale [31] and results in a broad quartet at $\delta$ 4.23 ($^1H$, 1:1:1:1 q, $J_{BH}$ = 90 Hz, $BH_3$) [21]. These hydrogen atoms couple with the natural abundance $^{11}B$ to give rise to a binomial quartet at $\delta$ -2.75 in the $^{11}B$ NMR spectrum [21]. By contrast, the $^{11}B$ spectrum of $[Th(BH_4)_4]$ shows a quintet at δ -8.0 but with a similar $J_{BH}$ coupling constant of 86.5 Hz [12].

### 3.3 DFT CALCULATIONS

The DFT calculations, undertaken by the Gagliardi group at the University of Minnesota, show that isolated molecules of **1** adopt a completely symmetric structure with $D_{2d}$ symmetry that

lacks the lengthened Th-B6 bond seen in the solid state structure. This result suggests that in the gas phase **1** possesses an unprecedented coordination number of 16. To investigate if crystal structure packing forces result in the disruption of the totally symmetric structure and disorder of the -$B6H_3$ group, geometry optimizations were carried out on larger clusters cut out of the experimental crystal structure. In these clusters, which consisted of two, three, four, and six [$Th(H_3BNMe_2BH_3)_4$] units, molecules of **1** still possess the fully symmetric $D_{2d}$ structure seen for the isolated molecule. However, when periodic boundary conditions are imposed on the molecular array, the molecules distort and one of the Th···B bonds lengthens significantly from a previous value of 2.85 – 2.93 Å to 3.08 Å, in relatively good agreement with the diffraction results. This elongated distance lies in the crystallographic *ac* plane, which is also consistent with the experimental result.

## 4. DISCUSSION

### 4.1 OTHER THORIUM COMPLEXES CONTAINING BRIDGING HYDRIDE LIGANDS OR Th-H-B INTERACTIONS

A search of the Cambridge Structural Database [32] returns 32 X-ray diffraction structures in which an actinide element is bound to a hydrogen atom. Of these, 28 have a B-H-An linkage, 5 of which are pyrazolylborate derivatives, and only 4 of the 32 contain thorium (there are two neptunium structures and the remaining complexes are uranium based). Only one of these 32 structures, $(Cp^*_2ThH)_2(\mu\text{-}H)_2$, has been characterized by neutron diffraction although some of the actinide tetrahydroborate compounds in the Inorganic Crystal Structure Database (ICSD) have been characterized in this way. The Th-H distances found for **1** are slightly longer than those to hydrides that bridge between Th centers, but are comparable to Th complexes in which the hydrides bridging between B and Th. Table 1 compares the Th-H distances in **1** with those in other molecules containing Th-H-Th or B-H-Th linkages.

| TABLE 1 | | | |
|---|---|---|---|
| Comparison of Th-H distances for some structurally characterized thorium hydride or borohydride complexes. Hydride distances of interest are in bold type. | | | |
| Complex | Th-H distance, Å | Diff. method | Reference |
| $[Th(\mathbf{H_3B}NMe_2BH_3)_4]$ | 2.37(2)- 2.539(18) | Neutron | [21] |
| $[(Cp^*_2ThH)_2(\mu\text{-}\mathbf{H})]$ | 2.29(3) | Neutron | [33] |
| $[Cp^*_3Th\mathbf{H}]$ | 2.33(13) | X-ray | [34] |
| $[Th_3(\mu_3\text{-}\mathbf{H})_2(\mu_2\text{-}\mathbf{H})_4(O\text{-}2,6\text{-}{}^tBu_2C_6H_3)_6]$ | 2.0(1)–2.3(1) | X-ray | [34] |
| $[Th(\mathbf{H_3B}CH_3)_4]_2(Et_2O)]$ | 2.27(6) - 2.72(1) | X-ray | [35] |
| $[Th(\mathbf{H_3B}CH_3)_4(thf)]_2$ | 2.27(6) - 2.72(1) | X-ray | [35] |
| $(Ind^*)_2Th(BH_4)_2$ ($Ind^* = C_9Me_7$) | 2.466 – 2.531 | X-ray | [36] |

## 4.2 OTHER AMINODIBORANATE COMPLEXES OF LARGE METALS

The aminodiboranate ligand has been recently employed to synthesize a large number of complexes of the lanthanides [37] and uranium [38]. For example, the reaction of $LnCl_3$ (Ln = Pr, Sm, Er) with three equivalents of $Na(H_3BNMe_2BH_3)$ in tetrahydrofuran (thf) affords complexes of stoichiometry $Ln(H_3BNMe_2BH_3)_3(thf)$, which loses thf upon sublimation [37]. The size of the Ln atom has a significant effect on the resulting chemical structure of the base-free $Ln(H_3BNMe_2BH_3)_3$ complexes; none of the structures is monomeric and the aminodiboranate ligands exhibit a variety of different binding modes (Figure 5). In the Pr complex, each 14-coordinate Pr atom is bound to 2 chelating ligands and 2 ligands that bridge between metal centers to form a polymeric structure; each boron atom in the chelating ligands forms two B-H-Pr bonds and each boron atom in the bridging ligands forms three B-H-Pr bonds. For Sm, all three of its ligands are chelating to the metal center but it is also coordinated datively to one hydrogen atom from a neighboring molecule in the polymeric chain for a coordination number of 13. $Er(H_3BNMe_2BH_3)_3$ is a dimer in which each 12-coordinate Er atom is bound to two chelating ligands and two bridging ligands each bound in an $Er(\kappa^2\textit{H}\text{-}H_3BNMe_2BH_3\text{-}\kappa^2\textit{H})Er$ manner. The sizes of these atoms are progressively smaller, and the effect on the structures is marked.

The reaction of $UCl_4$ with four equivalents of $Na(H_3BNMe_2BH_3)$ in an $Et_2O$ suspension results in the evolution of gas and the formation of the trivalent compound $U(H_3BNMe_2BH_3)_3$ [38]. A similar reduction of $U^{IV}$ to $U^{III}$ is observed in the decomposition of $U(BH_4)_4$, which when heated changes color from green to brown and evolves $B_2H_6$ and $H_2$, likely resulting in the formation of

$U(BH_4)_3$ [16]. Depending on the solvent used for crystallization, $U(H_3BNMe_2BH_3)_3$ crystallizes in two structural isomers having different coordination numbers and ligand binding modes.

Table 2 outlines the binding modes of the three complexes in the lanthanide study and compares them to the uranium and thorium complexes. Figure 5 offers an illustration of the complex arrangements of the chelating aminodiboranate ligands around the respective metal centers as described above.

**TABLE 2**

Comparison of structures and ionic or covalent radii (*r*, Å) for lanthanide and actinide diaminoboranate complexes [37,38]. Ionic radii from Shannon [4] are for a coordination number (CN) of six.

| Complex | $r_{ionic}$ [4] | $r_{cov}$ [5] | Ligand binding mode | Structure | CN |
|---|---|---|---|---|---|
| $Er(H_3BNMe_2BH_3)_3$ | 0.89 | 1.89 | 2 $\kappa^2,\kappa^2$ chelating, 1 $\kappa^2,\kappa^2$ bridging | dinuclear | 12 |
| $\alpha$-$U(H_3BNMe_2BH_3)_3$ | 1.025 | 1.96 | 3 $\kappa^2,\kappa^2$ chelating + 1 $\kappa^1H$ dative | polymeric | 13 |
| β-$U(H_3BNMe_2BH_3)_3$ | 1.025 | 1.96 | 2 $\kappa^2,\kappa^2$ chelating, 1 $\kappa^3,\kappa^3$ bridging | polymeric | 14 |
| $Sm(H_3BNMe_2BH_3)_3$ | 0.96 | 1.98 | 3 $\kappa^2,\kappa^2$ chelating + 1 $\kappa^1H$ dative | polymeric | 13 |
| $Pr(H_3BNMe_2BH_3)_3$ | 0.99 | 2.03 | 2 $\kappa^2,\kappa^2$ chelating, 1 $\kappa^3,\kappa^3$ bridging | polymeric | 14 |
| $Th(H_3BNMe_2BH_3)_4$ | 0.94* | 2.06 | 3 $\kappa^2,\kappa^2$ chelating, 2 $\kappa^2,\kappa^1$ chelating | monomeric | 15 |

*calculated for $Th^{IV}$ with CN = 6; for CN = 7, *r* = 1.05 from radii-unit cell volume plots and for CN = 12, *r* = 1.21 (calculated)

The increase in the coordination number of the metal center with increasing atomic radius is well precedented in f-metal chemstry; Shannon makes this observation in his review of effective ionic radii [4], and a 1980 study of cyclopentadienyl compounds of the lanthanides and actinides [39] also supports the trend seen in the aminodiboranate complexes highlighted here. Surprisingly, Shannon found that $r_{ionic}$ for Th is far smaller than that of any of the other listed lanthanides or actinides in the table, which is the opposite result expected from periodic trends.

In Shannon and Prewitt's review, the only coordination number for which radii are given for all the elements in Table 2 is coordination number 6. It should be noted that, because of the lack of structural data for six-coordinate $Th^{IV}$ complexes, the radius for six-coordinate Th in Shannon and Prewitt's table is calculated and not derived from radii-unit cell volume plots [4]. For higher coordination numbers, Shannon and Prewitt do not include radii for all the elements, so comparisons become more difficult to make, but even so the effective ionic radius for Th still appears to be smaller than those of the other ions in this discussion (for example: for CN = 9, $r_{ionic}$ = 1.179 for $Pr^{III}$, 1.132 for $Sm^{III}$, 1.062 for $Er^{III}$ and 1.09 for $Th^{IV}$, all radii in Å).

In contrast to Shannon and Prewitt's results, data for covalent radii compiled by Cordero et al. in 2006 from structures in the CSD and ICSD databases show a clear trend in which Th has the largest covalent radius of the elements in question, followed closely by Pr which achieves a high coordination number of 14 (see Figure 2 and Table 2). Over the years there has been much discussion about the relative contributions of ionic and covalent bonding in actinide complexes (see, for example, Raymond's discussion in [39]). The small number of lanthanide and actinide compounds in the CSD makes it difficult to compare bond distances, and the extremely small number of such compounds that have been characterized by neutron diffraction (essential in the case of hydrogen atoms bound to a large metal center), makes a definitive comparison even more problematic.[*]

Spectroscopic rather than structural studies are currently affording the most informative evidence about the bonding in actinide complexes. A fine feature article, published in 2007 by Denning [40], illustrates the use of optical spectroscopy, X-Ray absorption and emission spectroscopies, NMR spectroscopy as well as supporting computational methods to explore the degree of covalency in actinyl ions and their analogs. X-ray absorption spectroscopy (XAS), a technique useful in determining the percentage of orbital mixing between metal and ligand through analysis of the pre-edge absorption features, has more recently been employed by Kozimor et al. in the study of a series of analogous transition metal and actinide $Cp^*_2MCl_2$ molecules ($Cp^* = C_5Me_5$; M = Ti, Zr, Hf, Th and U) [41]. In this study, analysis of the clear pre-edge absorption features arising from excitation of a Cl 1s electron to the 3d, 4d or 5d antibonding orbitals of the group 4 transition metals, respectively, leads to a covalent character of 25%, 23% and 22%, respectively. Analysis of similar pre-edge features in the U spectrum yields a result of 9% Cl 3p covalent character for the U-Cl bond. Although the degree of covalency for U is less than that found for the group 4 metals, it is still a significant finding for the actinides in which such covalency has been highly debated, and the result lends support for the presence of some covalency in complexes such as **1**. Pre-edge XAS features for $Cp^*_2ThCl_2$ unfortunately could not be resolved to enable an evaluation of Cl 3p orbital mixing and determination of Th-Cl covalency. Such further spectroscopic studies, as they become available, will prove more illuminative than simple structural studies of the true extent of covalency in actinide complexes.

[*] Of 203 total structures in the CSD that contain a Ln-H linkage, 120 of these are characterized by a B-H-Ln bond. Of those 120, a total of 57 of these are borohydrides or borohydride analogs. Only one of these 203 structures has been characterized by neutron diffraction, and it does not contain a B-H-Ln bond. See the discussion under section 4.1 of this manuscript for similar statistics of the actinides.

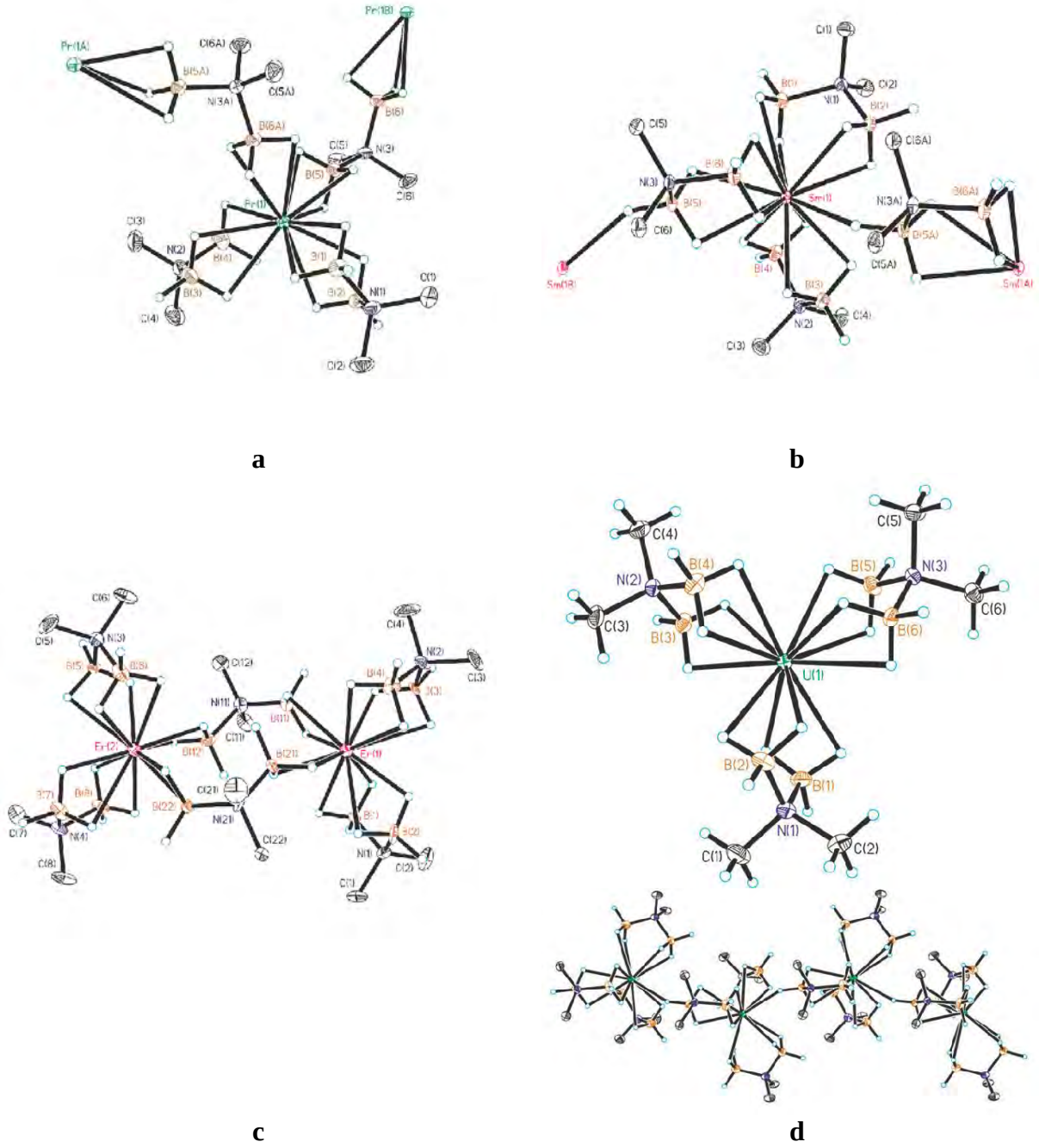


**Figure 5.** Complexes of lanthanides and actinides illustrating the various binding modes of the aminodiboranate ligand, also listed in Table 2 and described in the text: (a) 14-coordinate $Pr(H_3BNMe_2BH_3)_3$, (b) 13-coordinate $Sm(H_3BNMe_2BH_3)_3$, (c) 12-coordinate $Er(H_3BNMe_2BH_3)_3$, (d) the 13-coordinate "$\alpha$" phase of $U(H_3BNMe_2BH_3)_3$. Figures (a-c) reprinted with permission from S. R. Daly, D. Y. Kim, Y. Yang, J. R. Abelson, and G. S. Girolami, J. Am. Chem. Soc. **132**, 2106-2107 (2010), copyright 2010 American Chemical Society. Figure (d) S. R. Daly and G. S. Girolami, Chem. Commun. **46**, 407 (2010) – Reproduced by permission of The Royal Society of Chemistry.

## 4.2 STERIC OVERCROWDING

As described above, the DFT results indicate that the aminodiboranate ligands must be crowded about the Th center, because weak intermolecular packing forces can cause a distortion from the idealized 16-coordinate "gas-phase" structure to a less sterically demanding 15 -coordinate structure. In the latter structure, one of the Th···B contacts is elongated, and only one hydrogen atom (instead of two) bridges between the B and Th centers. In fact, reactivity studies suggest that even the 15-coordinate structure is also somewhat crowded, as evidenced by the chemical change that takes place when **1** is heated to 100° C. One equivalent of $(NMe_2BH_2)_2$ is evolved, and the new thorium complex $[Th(H_3BNMe_2BH_3)_2(BH_4)_2]$ (**2**) is generated. This monomeric complex, which has been structurally characterized by X-ray diffraction (see Figure 6), possesses two chelating $\kappa^2,\kappa^2H$ aminodiboranate ligands and two tetrahydroborate ligands bound in a $\kappa^3H$ mode. The boron atoms are distributed about Th in a distorted octahedral fashion. The Th··· B distances to the aminodiboranate ligand of 2.848(9) to 2.882(9) Å are slightly shorter than observed for the parent molecule **1**, probably because **2** is less sterically crowded. Accordingly, the Th-H distances are also shorter at 2.43(2) and 2.35(3)–2.36(3) Å for the aminodiboranate and borohydride ligands, respectively.

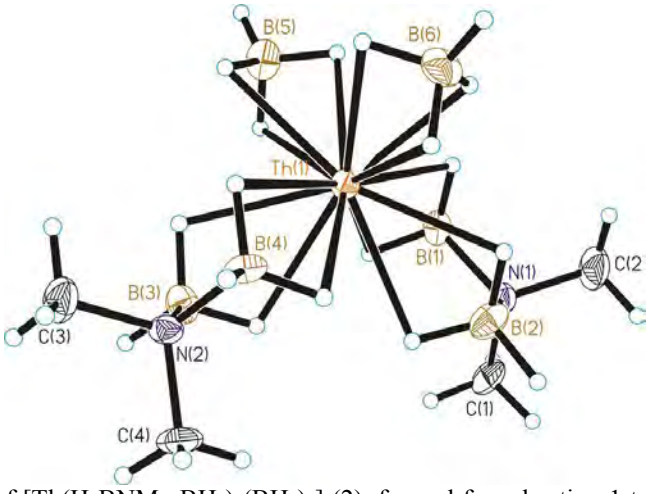


**Figure 6.** X-ray structure of $[Th(H_3BNMe_2BH_3)_2(BH_4)_2]$ (2), formed from heating 1 to 100° C. The 14-coordinate complex contains two chelating aminodiboranate ligands and two tridentate tetrahydroborate ligands. Reprinted from S. R. Daly, P. M. B. Piccoli, A. J. Schultz, T. K. Todorova, L. Gagliardi, and G. S. Girolami, Angew. Chem. Int. Ed. **49**, 3379-338 1 (2010). Copyright Wiley-VCH Verlag GmbH & Co. KGaA. Reproduced with permission.

## 5.0 CONCLUSIONS

The first complex possessing a Werner coordination number of 15, $[Th(H_3BNMe_2BH_3)_4]$ (**1),** has been structurally characterized by both X-ray and neutron diffraction, which are essential tools in accurately characterizing metal hydride and borohydride complexes. Although DFT calculations predict a totally symmetric 16-coordinate geometry in the gas phase, the steric bulk of the chelating aminodiboranate ligand combined with intermolecular packing forces result in a change in the coordination geometry, breaking of one Th-H interaction, and a lessening of the coordination number to 15. Comparisons of the structures of a series of related lanthanide and actinide aminodioboranate complexes show that the atomic radius of the metal has a large

influence on the metal-ligand bonding mode, resulting in complexes having a diverse array of both coordination number and number of chelating or bridging ligands. The thermal reactivity of **1,** i.e., the loss of $(NMe_2BH_2)_2$ to yield the 14- coordinate $[Th(H_3BNMe_2BH_3)_2(BH_4)_2]$ **(2),** suggests that even the 15 coordinate structure of **1** seen in the solid state is still sufficiently crowded to promote conversion to a geometry with a lower coordination geometry. However, with a judicious choice of large metal and small ligands, complexes with stable 16-coordinate geometries do not seem implausible.

## ACKNOWLEDGEMENTS

Work at Argonne National Laboratory was supported by the US Department of Energy, BES-Materials Science, under contract DEAC02-06CH11357. Work at the University of Illinois was supported by the U.S. National Science Foundation (CHE 07-50422) and the PG Research Foundation. We thank Scott R. Wilson and Teresa Prussak-Wieckowska for collecting the XRD data.

## REFERENCES

[1] A. Werner, *Z. Anorg. Chem*. **3**, 267-330 (1893).
[2] P. Pfeiffer, in: *Organische Molekulverbindungen*, 2nd ed. (Stuttgart, 1927), p. 18.
[3] M. Drew, *Coord. Chem. Rev*. **24**, 179-275 (1977).
[4] R. D. Shannon, *Acta Crystallogr. A* **32**, 751-767 (1976).
[5] B. Cordero, V. Gómez, A. E. Platero-Prats, M. Revés, J. Echeverría, E. Cremades, F. Barragán, and S. Alvarez, *Dalton Trans*. 2832 (2008).
[6] A. Hermann, M. Lein, and P. Schwerdtfeger, *Angew. Chem. Int. Ed*. **46**, 2444-2447 (2007).
[7] M. Brookhart, *J. Organomet. Chem*. **250**, 395-408 (1983).
[8] R. H. Crabtree, *Angew. Chem. Int. Ed. Engl*. **32**, 789-805 (1993).
[9] M. Green, *J. Organomet. Chem*. **500**, 127-148 (1995).
[10] Z. Xu, *Coord. Chem. Rev*. **156**, 139-162 (1996).
[11] H. R. Hoekstra and J. J. Katz, *J. Am. Chem. Soc*. **71**, 2488-2492 (1949).
[12] M. Ehemann and H. Nöth, *Z. Anorg. Allg. Chem*. **386**, 87-101 (1971).
[13] K. Hedberg and V. Plato, *Inorg. Chem*. **10**, 590-594 (1971).
[14] R. W. Broach, I. S. Chuang, T. J. Marks, and J. M. Williams, *Inorg. Chem*. **22**, 1081-1084 (1983).
[15] R. H. Banks, N. M. Edelstein, R. R. Rietz, D. H. Templeton, and A. Zalkin, *J. Am. Chem. Soc*. **100**, 1957-1958 (1978).
[16] H. I. Schlesinger and H. C. Brown, *J. Am. Chem. Soc*. **75**, 219-221 (1953).
[17] E. R. Bernstein, W. C. Hamilton, T. A. Keiderling, S. J. La Placa, S. J. Lippard, and J. J. Mayerle, *Inorg. Chem*. **11**, 3009-3016 (1972).
[18] R. R. Rietz, A. Zalkin, D. H. Templeton, N. M. Edelstein, and L. K. Templeton, *Inorg. Chem*. **17**, 653-658 (1978).
[19] R. R. Rietz, N. M. Edelstein, H. W. Ruben, D. H. Templeton, and A. Zalkin, *Inorg. Chem*. **17**, 658-660 (1978).
[20] A. Zalkin, R. R. Rietz, D. H. Templeton, and N. M. Edelstein, *Inorg. Chem*. **17**, 661-663

(1978).
[21] S. R. Daly, P. M. B. Piccoli, A. J. Schultz, T. K. Todorova, L. Gagliardi, and G. S. Girolami, *Angew. Chem. Int*., **49**, 3379 –3381 (2010).
[22] P. C. Keller, *Inorg. Chem*. **10**, 2256-2259 (1971).
[23] H. Nöth and S. Thomas, *Eur. J. Inorg. Chem*. **1999**, 1373-1379 (1999).
[24] R. Ahlrichs, M. Bar, M. Haser, H. Horn, and C. Kolmel, *Chem. Phys. Lett*. **162**, 165-169 (1989).
[25] G. Kresse, *Comp. Mater. Sci*. **6**, 15-50 (1996).
[26] G. Kresse, *Phys. Rev. B* **54**, 11169-11186 (1996).
[27] G. Kresse, *Phys. Rev. B* **59**, 1758-1775 (1999).
[28] H. J. Monkhorst and J. D. Pack, *Phys. Rev. B* **13**, 5188-5192 (1976).
[29] A. J. Schultz, P. M. De Lurgio, J. P. Hammonds, D. J. Mikkelson, R. L. Mikkelson, M. E. Miller, I. Naday, P. F. Peterson, R. R. Porter and T. G. Worlton, Physica B **385-386**, 1059-1061 (2006). The IPNS SCD is currently operating on a beam line at the Lujan Neutron Center at Los Alamos National Laboratory, http://lansce.lanl.gov/lujan/.
[30] A. C. Larson and R. B. von Dreele, Los Alamos Nat. Lab. Rep. LAUR **86-748**, (2000).
[31] T. J. Marks and J. R. Kolb, *Chem. Rev*. **77**, 263-293 (1977).
[32] F. H. Allen, *Acta Crystallogr. B* Struct Sci **58**, 380-388 (2002).
[33] R. W. Broach, A. J. Schultz, J. M. Williams, G. M. Brown, J. M. Manriquez, P. J. Fagan, and T. J. Marks, *Science* **203**, 172-174 (1979).
[34] D. L. Clark, S. K. Grumbine, B. L. Scott, and J. G. Watkin, *Organometallics* **15**, 949-957 (1996).
[35] R. Shinomoto, J. G. Brennan, N. M. Edelstein, and A. Zalkin, *Inorg. Chem*. **24**, 2896-2900 (1985).
[36] T. M. Trnka, J. B. Bonanno, B. M. Bridgewater, and G. Parkin, *Organometallics* **20**, 3255-3264 (2001).
[37] S. R. Daly, D. Y. Kim, Y. Yang, J. R. Abelson, and G. S. Girolami, *J. Am. Chem. Soc*. **132**, 2106-2107 (2010).
[38] S. R. Daly and G. S. Girolami, *Chem. Commun*. **46**, 407 (2010).
[39] K. N. Raymond and C. W. Eigenbrot, *Acc. Chem. Res*. **13**, 276-283 (1980).
[40] R. G. Denning, *J. Phys. Chem. A* **111**, 4125-4143 (2007).
[41] S. A. Kozimor, P. Yang, E. R. Batista, K. S. Boland, C. J. Burns, D. L. Clark, S. D. Conradson, R. L. Martin, M. P. Wilkerson, and L. E. Wolfsberg, *J. Am. Chem. Soc*. **131**, 12125-12136 (2009).

# STRUCTURE AND PROPERTIES OF (HYDROXY)ALKYLAMMONIUM SALTS OF FLURBIPROFEN

**C. H. Schwalbe, M. Ramirez, B. R. Conway and C. J. Bache**
***School of Life & Health Sciences, Aston University, Birmingham B4 7ET, UK***

**S. J. Coles**
***School of Chemistry, University of Southampton, Southampton SO17 1BJ, UK***

**P. Timmins**
***Bristol-Myers Squibb, Reeds Lane, Moreton CH46 1QW, UK***

## 1. ABSTRACT

Interactions with hydrogen atoms strongly affect the structure of salts of the anti-inflammatory drug flurbiprofen. With cations of the form $H_3N^+C(CH_3)_{3-n}(CH_2OH)_n$ for n = 0-3 charge-assisted hydrogen bonding is the most obvious feature. In the t-butylammonium (n = 0) salt successive $R_4^3(10)$ rings are formed by $^+$N-H…OCO$^-$ interactions. With n = 1 the additional OH is disordered and has little effect. However, n = 2 changes the pattern: now one $^+$N-H…OCO$^-$ and one O-H…OCO$^-$ hydrogen bond link a cation to a carboxylate anion. When n = 3, this motif persists in one polymorph. However, another polymorph has two independent anions related by pseudo-translation and two independent cations related by a pseudo-glide, while extensive disorder results from application of the "opposite" pseudo-symmetry operation. Enantiomer discrimination at flurbiprofen sites depends on the environment of H and $CH_3$ in the $HCCH_3$ group. Hirshfeld surfaces show normal van der Waals contacts around ordered methyl groups but tight contacts around major sites for disordered ones, which become worse around the minor sites. Similar effects are observed in the vicinity of the fluorine atoms in the fluorophenyl rings. Whereas the major sites for disordered atoms and the sites for ordered atoms are involved in normal or slightly short van der Waals contacts, the minor sites suffer from tighter contacts.

## 2. INTRODUCTION

Flurbiprofen [Fbp, (*RS*)-2-(2-fluorobiphenyl-4-yl)propanoic acid] is a non-steroidal anti-inflammatory drug which is useful in the treatment of chronic conditions such as arthritis. However, because of its low aqueous solubility of only 0.03(1) mg mL$^{-1}$ [1] it does not readily provide rapid pain relief. To enhance the solubility we have prepared a series of salts of Fbp with cations of general formula $H_3N^+C(CH_3)_{3-n}(CH_2OH)_n$ for n = 0-3, starting from t-butylammonium and finishing with Tris. Successively changing methyl to hydroxymethyl groups is expected to increase the affinity of the cation for water, but this affinity may not translate into higher solubility if hydrogen bonding sufficiently augments the stability of the crystal. Making this series of salts has increased the solubility of Fbp compared to its free acid form, and in this case the solubility does increase with the number of hydroxymethyl groups [1]:

2.77 mg $mL^{-1}$ with n = 0, 8.9(14) mg $mL^{-1}$ with n = 1, and 11.6(12) mg $mL^{-1}$ with n = 2. The solubility of the Tris salt with n = 3 will be discussed later.

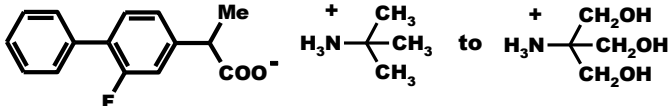


Hydrogen atoms profoundly influence the interactions within the crystal. The numerous possibilities for hydrogen bonding are their most salient feature. In addition, Fbp is a chiral molecule for which the enantiomers can be interchanged by swapping one H atom and a $CH_3$ group. All our samples were prepared from racemic mixtures and crystallized in centrosymmetric space groups. Enantiomer discrimination depends upon a sufficient difference between the environment of the H site and that of the $CH_3$ site. Insufficient discrimination can lead to disorder with minor occupancy of the Fbp site by the "wrong" enantiomer and, of course, an equal population of the opposite enantiomer at the centrosymmetrically related site. An additional opportunity for disorder is 180° rotation of the fluorophenyl ring around the axis linking the two rings, which is possible if the surroundings of H and F are permissive.

## 3. METHODS

Salts were prepared by mixing equimolar quantities of Fbp and base dissolved in acetonitrile. Sample crystals were grown from acetonitrile or methanol. Wherever possible, data were collected at the National Crystallography Service, Southampton, on a diffractometer equipped with a rotating anode generator and focusing optics. Two salts (FAmp with n = 1 and one polymorph of FTris with n = 3) diffracted so weakly that synchrotron data were required, which were collected on station I19 at the Diamond synchrotron.

Hirshfeld surfaces [2,3] encoded with $d_{norm}$ [4] were generated with the program Crystal Explorer [5]. The normalization with respect to van der Waals radii embodied in the definition of $d_{norm}$ enables the closeness of intermolecular contacts involving different elements to be compared, e. g. H and F. Contacts shorter than van der Waals separations are represented as red spots on the surface, normal van der Waals contacts appear white, and longer contacts are blue.

## 4. RESULTS AND DISCUSSION

### 4.1 Crystal data

Unit cell dimensions of the salts, including two polymorphs of the Tris salt, are given below. The space groups are, respectively, $P2_1/n$, $P2_1/c$, and finally P-1 for the last three. Z' is 1 and one cell dimension falls within the range 6.19-6.29 Å except for FTris polymorph I, where Z' = 2 and all axes are longer.

| TABLE 1 |
| --- |
| Unit cell dimensions and n in the stoichiometry $(CH_3)_{3-n}(CH_2OH)_n$ |

| Abbr.,n | a/Å | b/Å | c/Å | α/Å | β/Å | γ/Å |
| --- | --- | --- | --- | --- | --- | --- |
| FTbut,0 | 15.9343(11) | 6.2903(4) | 19.1949(11) | 90 | 114.705(3) | 90 |
| FAmp,1 | 16.133(8) | 6.270(3) | 18.852(3) | 90 | 114.883(5) | 90 |
| FAmp2,2 | 6.1928(2) | 9.5205(4) | 15.135 (6) | 82.627(2) | 87.874(3) | 89.058(2) |
| FTrisII,3 | 6.1930 (1) | 9.9421(2) | 14.6846(3) | 93.937(1) | 90.032(2) | 90.718(2) |
| FTrisI,3 | 10.016(18) | 11.073(21) | 16.652(29) | 84.52(7) | 78.81(4) | 88.15(8) |

Packing diagrams [Figure 1(a-d)] drawn with Mercury [6] in projection down the shortest axis show an almost edge-on view of a pair of Fbp anions with fluorophenyl and phenyl rings juxtaposed but neither parallel nor perpendicular, either in the middle of the cell or straddling one side. Disorder in $CH_3$ groups and F substituents is evident in FTbut and FAmp but not FAmp2 or FTrisII. Disorder in FTrisI [Figure 1(e)] is so pervasive and extreme that this structure needs to be discussed separately.

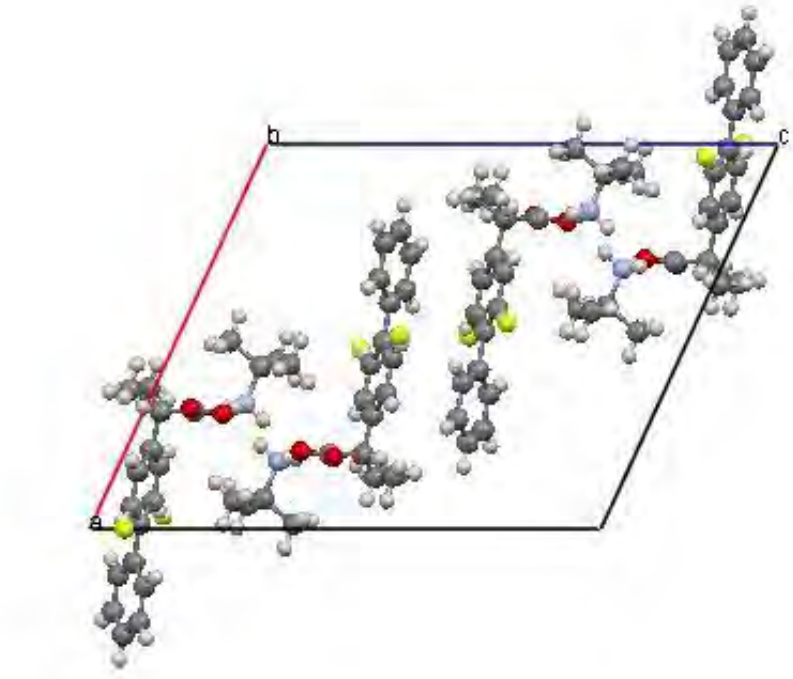


**Figure 1.** (a) Packing of FTbut viewed down the *b* axis.

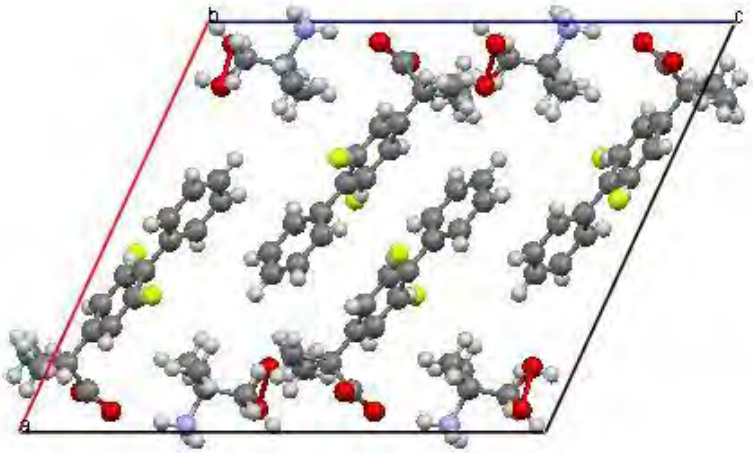

**Figure 1.** (b) FAmp viewed down the *b* axis.

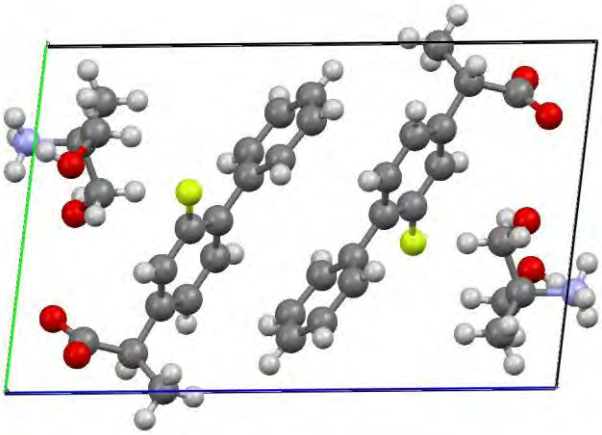

**Figure 1.** (c) FAmp2 viewed down the *a* axis.

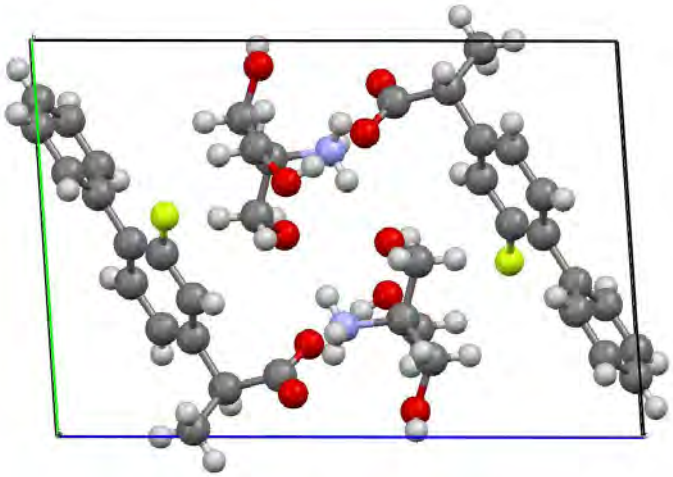

**Figure 1.** (d) FTris polymorph II viewed down the *a* axis.

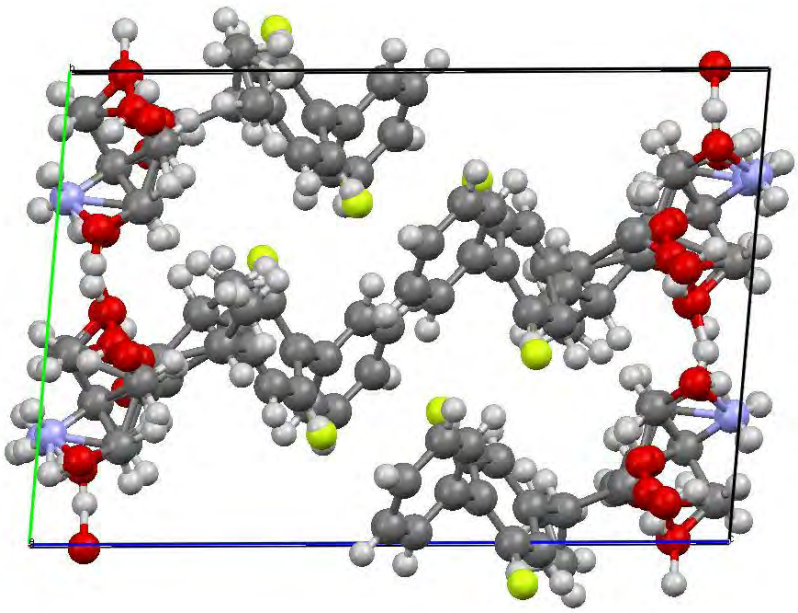

**Figure 1.** (e) FTris polymorph I viewed down the *a* axis.

### 4.2 Flurbiprofen geometry

Rotations about the two oppositely directed exit bonds from the fluorophenyl ring are a major influence on the shape of the flurbiprofen anion. Carbon atoms are numbered according to the following scheme: C1 in $OCO^-$, C2 in CH, C3 in $CH_3$, C4 to C8 in the fluorophenyl ring with F attached at C6, and C9-C14 in the second ring.

TABLE 2

C3-C2-C4-C5 torsion angles (in structures where the $CH_3$ groups are disordered, major C3 then minor) followed by the angle between fluorophenyl and phenyl ring planes

| Abbr. | Major C3-C2-C4-C5 / ° | Minor C3-C2-C4-C5 / ° | C1-C2-C4-C5 / ° | Interplanar angle / ° |
|---|---|---|---|---|
| FTbut | 129.6(5) | 58(2) | -104.1(5) | 44.4(1) |
| FAmp | 122.9(6) | 59(1) | -105.4(6) | 43.8(2) |
| FAmp2 | -81.8(2) | | 42.5(3) | 46.0(1) |
| FTrisII | -81.2(2) | | 43.7(2) | 43.7(1) |
| FTrisI | -51(2) | -110(2) | 79(2) | 54.6(3) |
| | -54(1) | | 82(1) | 61.4(3) |

At the propanoic acid end there is a noteworthy pairwise similarity between FTbut and FAmp, and between FAmp2 and FTrisII. The relevant torsion angles in FTrisI are roughly 180° away from those in the first two structures. A clash of H against F or H against H atoms militates against a coplanar arrangement of rings in *ortho*-fluorobiphenyl derivatives. The *ca.* 45° twist between rings in the first four structures is close to the mean value of 43(2)° for 42 observations shown in Figure 2.

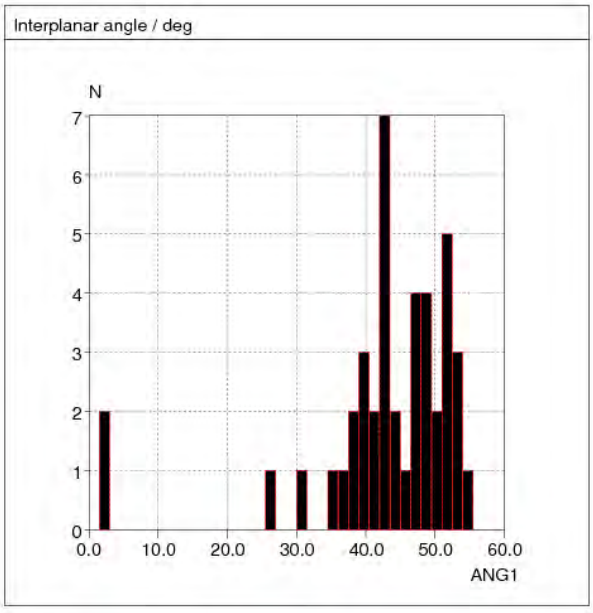


**Figure 2.** Interplanar angles for *ortho*-fluorobiphenyl structures lacking other *ortho* substituents in the Cambridge Structural Database with R < 10%.

### 4.3 Hydrogen bonding

In FTbut donation of hydrogen bonds from $^{+}NH_3$ to $COO^{-}$ forms ladders built out of $R_4^3(10)$ rings along a 2-fold screw axis, Type II in the classification of Lemmerer et al. [7].

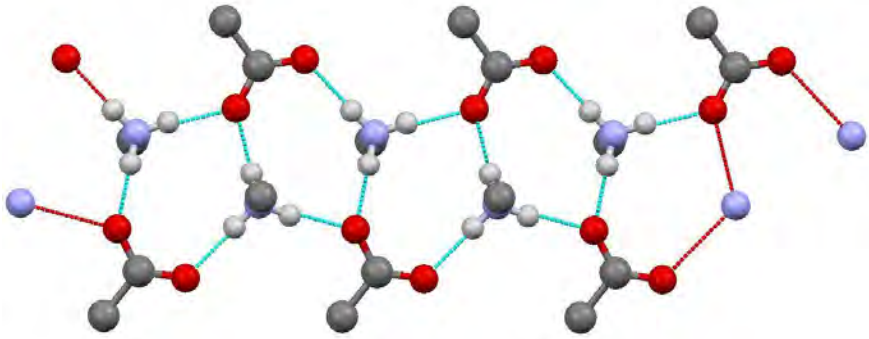

**Figure 3.** $R_4^3(10)$ rings formed by $C(NH_3)^+$ and $C(OCO)^-$ moieties of FTbut.

Substitution with one OH group to make FAmp does not change this pattern: this OH group lacks a credible hydrogen bond acceptor and is disordered. However, when a second OH group is introduced (FAmp2), the pattern changes fundamentally.

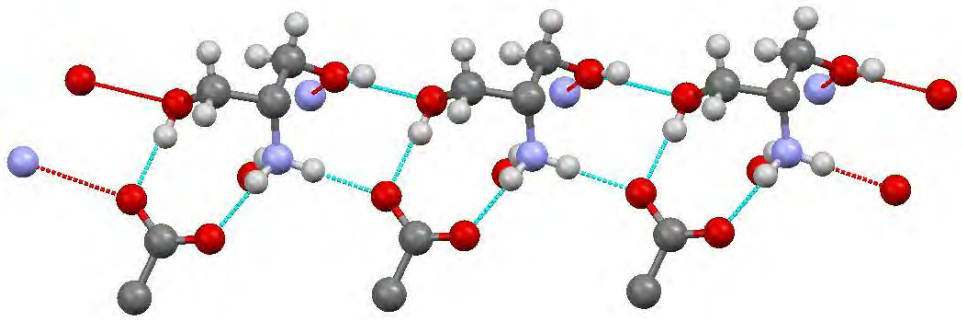

**Figure 4.** Hydrogen bonds formed by $Amp2^+$ cations (methyl groups omitted for clarity) and $C(OCO)^-$ moieties of FAmp2.

Cations deploy one NH and one OH hydrogen atom in hydrogen bonds to one anion. The other OH group links intermolecularly to the first one while NH finds $OCO^-$. The third amino H atom pairs with OH as acceptor to form a centrosymmetric dimer. Thereby $R_2^2(9)$, $R_3^2(9)$, and $R_2^2(10)$ rings are formed. The well ordered cations and anions in FTris form II create similar hydrogen bonds to those in FAmp2, the additional OH of the cation donating a second hydrogen bond to the carboxylate O atom that previously accepted just one. In the disordered crystals of FTris form I each carboxylate O atom accepts only one hydrogen bond. Remarkably, the two independent anions are related by the translation *x*,0.5+*y*,*z* while cations show the pseudo-glide 0.452-*x*, 0.5+*y*,*z* ! The pivot atom of Tris is suitably positioned to satisfy both. Minor sites in the disorder satisfy the "opposite" pseudo-operation.

### 4.4 Hirshfeld surfaces, environment of H and $CH_3$ groups, and disorder

An overview of the interaction with its surroundings of the entire Fbp anion, not just the polar groups involved in hydrogen bonding, is provided by the Hirshfeld surfaces. These surfaces are presented for 4 of the 5 structures reported here, but the extensive disorder present in FTrisI would make such a calculation unreliable [3].

With the Fbp anions presented in a common orientation (Figure 5) having the C-$CH_3$ pointing vertically upwards the similarity between FTbut and FAmp and between FAmp2 and FTrisII is once again evident. Wherever carboxylate oxygen atoms appear on the visible upper surface, bright red patches show that charge-assisted hydrogen bonding has shrunk the H…O contacts involving these atoms to well below normal van der Waals separations. Such shortening is expected and indicates a favorable interaction, but red patches involving less polar H atoms are likely to indicate unfavorable overcrowding.

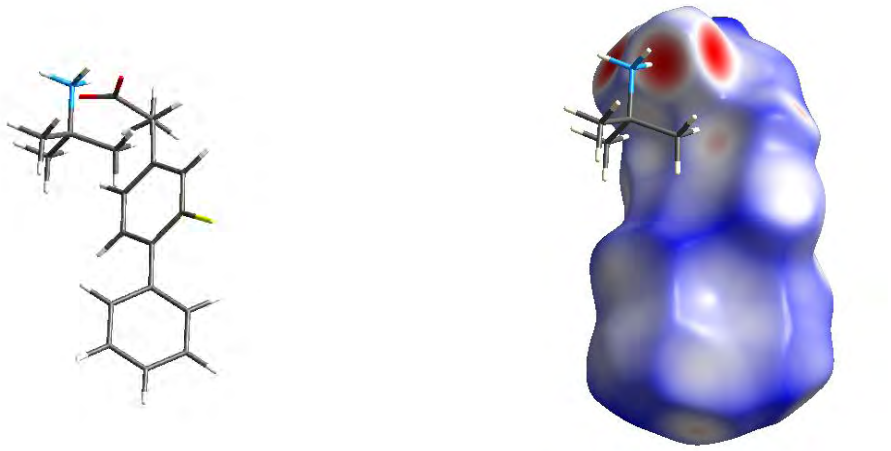

**Figure 5.** (a) Stick drawings and Hirshfeld surfaces encoded with $d_{norm}$ for FTbut with its major $CH_3$ site.

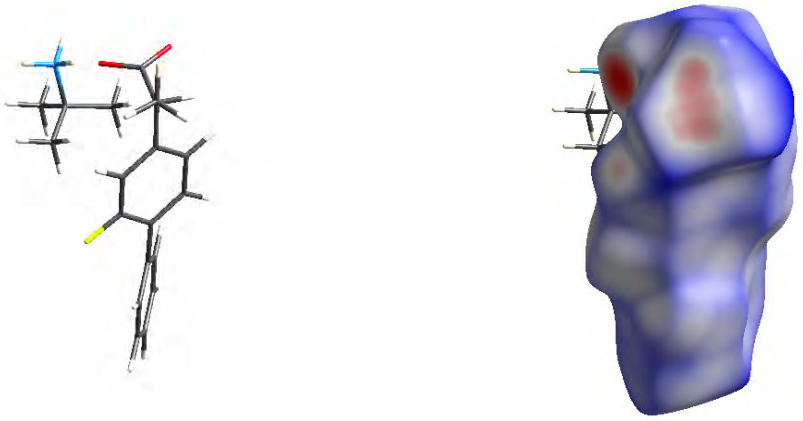

**Figure 5.** (b) FTbut with its minor $CH_3$ site.

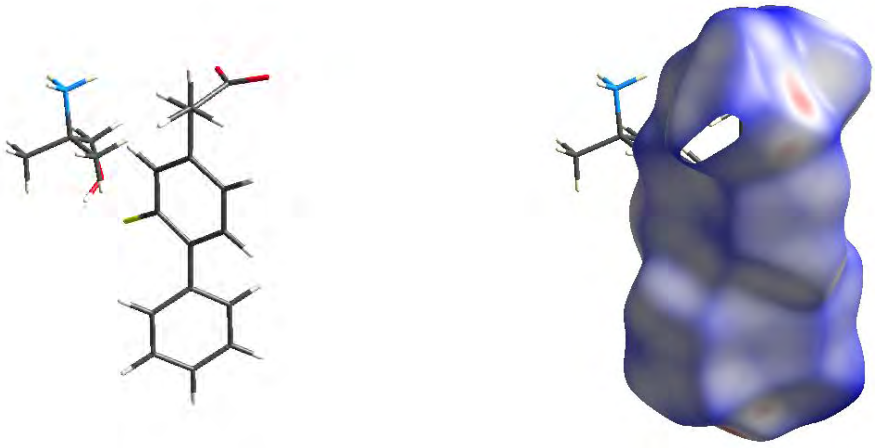

**Figure 5.** (c) FAmp with its major $CH_3$ site.

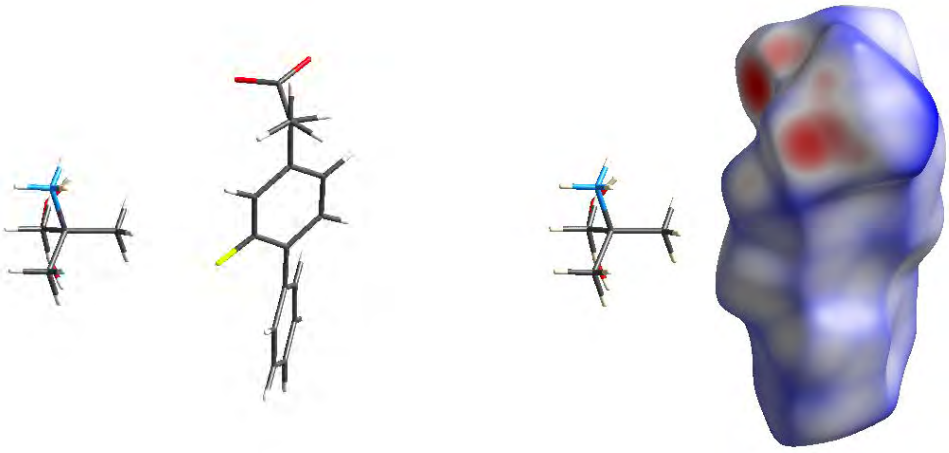

**Figure 5.** (d) FAmp with its minor $CH_3$ site.

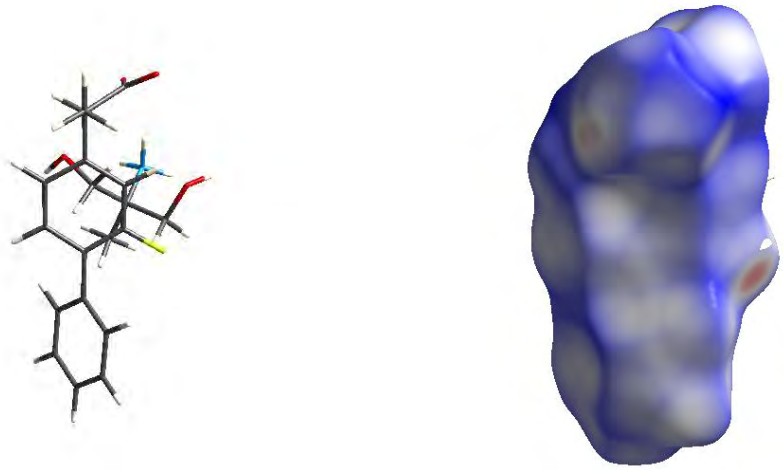

**Figure 5.** (e) FAmp2 with no disorder in the $CH_3$ site.

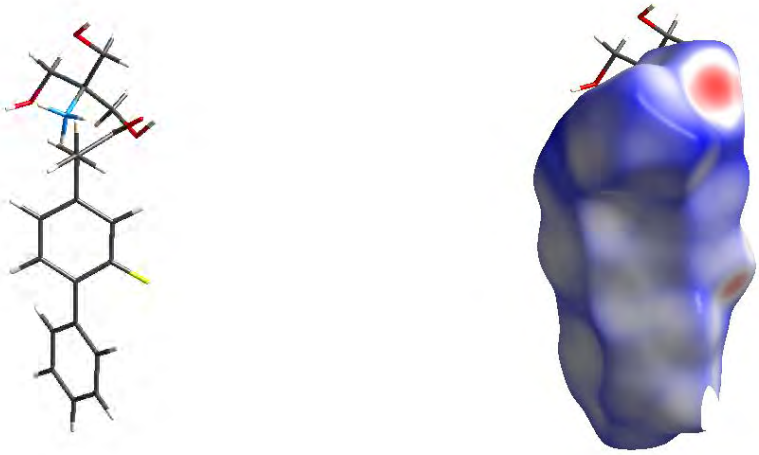

**Figure 5.** (f) FTrisII with no disorder in the $CH_3$ site.

FTbut and FAmp show two alternative positions for their methyl groups with occupancy factors that refined to 0.882:0.118 and 0.759:0.241 respectively. The major sites are positioned uppermost in Figures 5(a) and 5(c); the minor sites, in 5(b) and 5(d). Small dull red patches suggest that the major sites suffer contacts that are slightly too close, but more extensive and brighter red patches around the minor sites suggest worse crowding. The surfaces around the ordered $CH_3$ groups in Figures 5(e) and 5(f) mainly have white patches indicating normal van der Waals contacts.

Figure 6 presents a similar graphical analysis of twofold H/F disorder in the fluorophenyl ring. All drawings are in an orientation that places the fluorophenyl ring plane 10° from the vertical with the C-F bond pointing upwards.

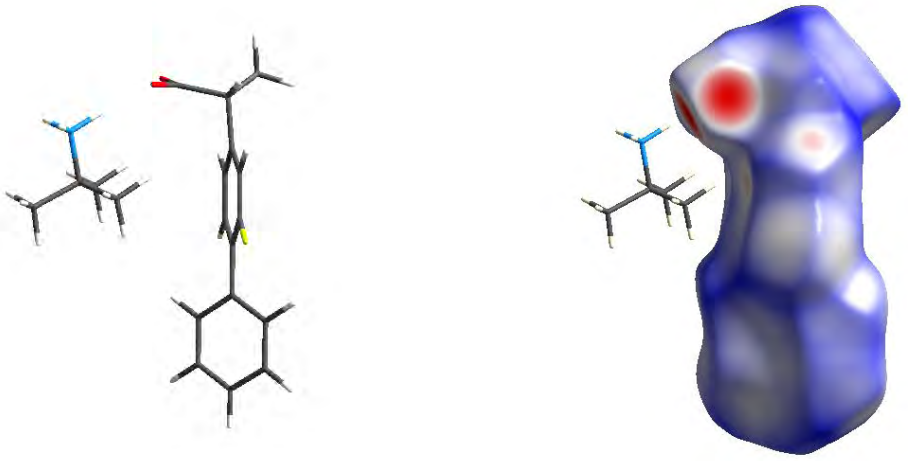

**Figure 6.** (a) Stick drawings and Hirshfeld surfaces encoded with $d_{norm}$ for FTbut with its major F site.

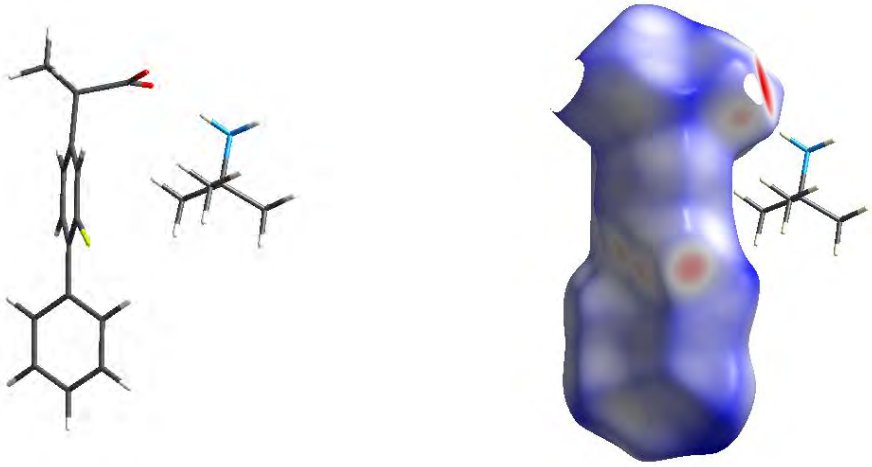

**Figure 6.** (b) FTbut with its minor F site.

**Figure 6.** (c) FAmp with its major F site.

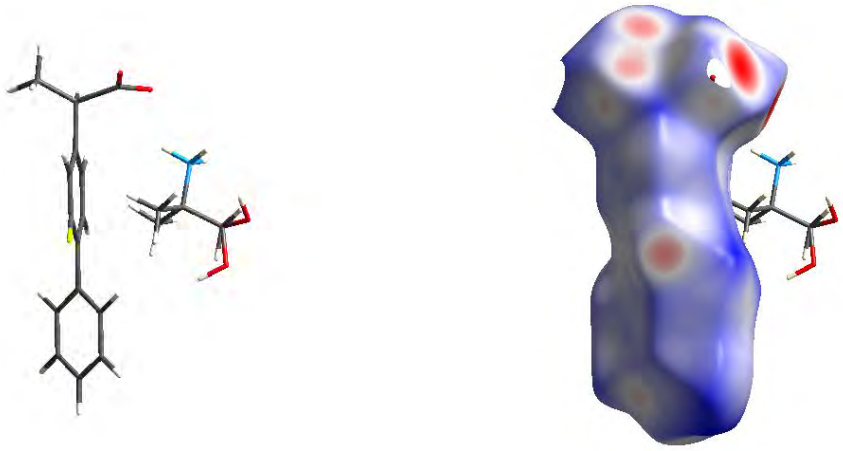

**Figure 6.** (d) FAmp with its minor F site.

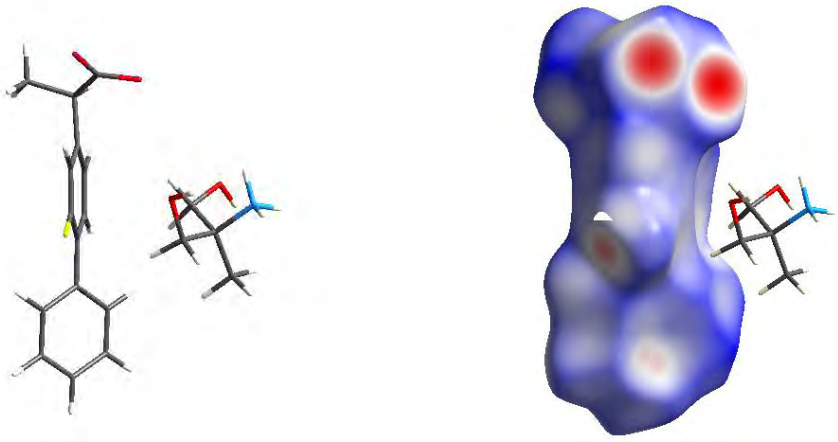

**Figure 6.** (e) FAmp2 with no disorder in the F site.

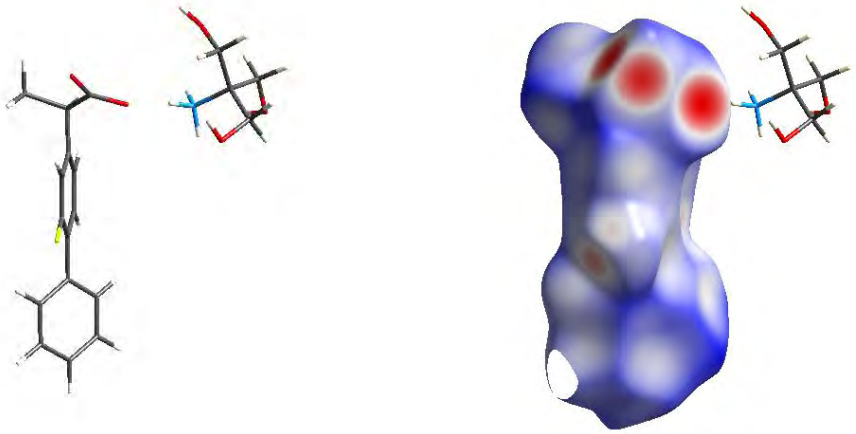

**Figure 6.** (f) FTrisII with no disorder in the F site.

Once again FTbut and FAmp have two alternative sites for a disordered fluorine atom with respective occupancy factors 0.895:0.105 and 0.842:0.158 while Famp2 and FTrisII are ordered. Whereas the Hirshfeld surfaces are white or faint red in the vicinity of ordered and major F sites, stronger red patches indicate close contacts around minor sites of disordered F atoms.

### 4.5 Pharmaceutical implications

Whereas the twist angle between rings in the biphenyl moiety of Fbp is 44-46° in the other structures and averages ca. 43° in *ortho*-fluorobiphenyl structures in the literature, the higher values of 55° and 61° in FTrisI may imply higher energy. The widespread disorder in this form suggests that intermolecular interactions are suboptimal. Thus there are good grounds for the assumption that FTrisI should have higher energy than FTrisII, yet FTrisI melts at a higher temperature. Both forms show similarly improved aqueous solubility [8] of 14.2(7) mg $mL^{-1}$ for I and 13.6(4) mg $mL^{-1}$ for II. The poor crystal quality of FTrisI matches its poor mechanical properties; it produces weak compacts with troublesome elastic recovery. On the other hand, FTrisII forms strong tablets with shiny faces and excellent mechanical properties [8]. Thus the objective of enhancing the solubility while retaining desirable pharmaceutical properties has been achieved, albeit with the necessity for careful control of crystallization conditions.

## 5. ACKNOWLEDGMENTS

We are grateful for use of the Diamond synchrotron to collect data on FAmp and FTrisI, and for the work of Prof. W. Clegg and Drs. R. Harrington, L. Russo and S. Callear on data collection and processing.

## 6. REFERENCES


[1] S.E. David, Ph.D. Thesis (Aston University, 2005)
[2] M.A. Spackman and P.A. Byrom, *Chem. Phys. Lett.* **267** (1997), 215.
[3] M.A. Spackman and D. Jayatilaka, *CrystEngComm* **11** (2009), 19.
[4] J.J. McKinnon, D. Jayatilaka and M.A. Spackman, *Chem. Commun.* (2007), 3814.
[5] S.K. Wolff, D.J. Grimwood, J.J. McKinnon, D. Jayatilaka and M.A. Spackman, Crystal Explorer 2.1 (University of Western Australia, Perth, 2007).
[6] C.F. Macrae, I.J. Bruno, J.A. Chisholm, P.R. Edgington, P. McCabe, E. Pidcock, L. Rodriguez-Monge, R. Taylor, J. van de Streek and P.A. Wood, *J. Appl. Cryst.*, **41** (2008), 466.
[7] A. Lemmerer, S.A. Bourne and M.A. Fernandes, *CrystEngComm*, **10** (2008), 1605.
[8] M. Ramirez, C.H. Schwalbe, B.R. Conway, C.J. Bache, S.J. Coles and P. Timmins, in preparation (2010)

# NEUTRON DIFFRACTION STUDIES OF METAL-HYDRIDES: INVESTIGATIONS OF OXIDATIVE ADDITION OF DIHYRDOGEN TO A METAL CENTER AND HYDRIDES IN METAL CLUSTERS

Muhammed Yousufuddin
*Center for Nanostructured Materials, University of Texas at Arlington, Arlington, TX*

## 1. ABSTRACT

Neutron diffraction is the method of choice when locating chemically interesting hydrogen atoms, particularly in systems containing a heavy metal. In this article, two fascinating complexes containing hydrogen atoms that were unambiguously located with neutron diffraction will be highlighted. The first complex, $OsH_3Cl(PPh_3)_3$, is a Kubas-type complex containing a rare elongated dihydrogen ligand. Results from the neutron diffraction study showed that the dihydrogen ligand demonstrated an H…H distance of 1.48(2) Å. In the second study, a four-coordinate hydrogen atom was located and measured for the first time using neutron diffraction. Results from this study showed that the hydrogen atom occupied the interstitial space of a tetrahedral yttrium ($Y_4$) cluster.

## 2. INTRODUCTION

Unlike x-rays, the scattering factors for neutrons are not proportional to atomic number. This makes neutron diffraction ideal for studying chemically interesting hydrogen atoms. Whereas x-rays are scattered from electrons, the point of diffraction for neutrons is the nucleus of an atom. A second feature to note is that neutrons have the ability to distinguish between some isotopes (notably H from D) since the scattering factor for hydrogen has an opposite sign than deuterium. This makes neutron diffraction invaluable for studies of H/D exchange.

## 3. OXIDATIVE ADDITION TO A H-H BOND

Oxidative addition of $H_2$ to a metal is one process that, to this point has not been well characterized from a structural point of view. Kubas and coworkers [1] made a breakthrough discovery when they first reported that $H_2$ can exist as a ligand in the molecule $W(CO)_3(H_2)(P\text{-}^iPr_3)_3$ [1a]. Further studies using neutron diffraction [1b] demonstrated that the $H_2$ ligand was bound side-on to the metal (structure **I** in Scheme 1). It can be speculated that, if enough complexes could be analyzed, the oxidative addition of $H_2$ to a metal could be isolated structurally in a series of interactions (see Scheme 1 below).

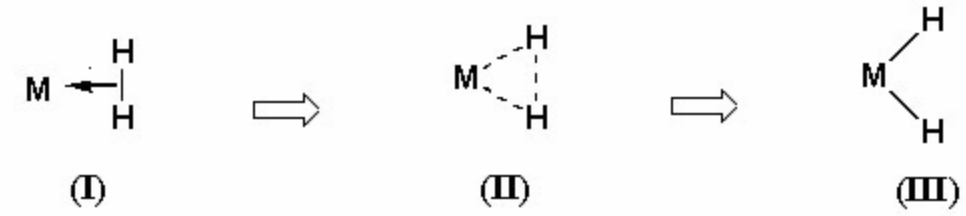


**Scheme 1**

In interaction **I** above, the $H_2$ ligand (often referred to as the dihydrogen ligand [2]) forms a weak interaction with the metal. The metal then activates the H-H bond upon further insertion into the $H_2$ ligand (**II**). Eventually, the H…H interaction is completely broken forming two terminal metal-hydride bonds (**III**). Many examples of type **III** had already been reported [3] before Kubas made his breakthrough discovery, and comparable reaction profiles in organic systems had already been investigated using x-ray diffraction [4a].

Thorough analysis of metal-dihydrogen examples has provided significant information regarding the oxidative addition reaction pathway. The side-on complexes **I**, have an H-H bond length on the order of 0.8-1.0 Å while classical dihydride complexes **III** (with essentially no H···H interactions) generally have H···H distances greater than 1.7 Å.

Interestingly, a later study by Brammer, Koetzle, and coworkers [4] reported an unusual H…H distance of 1.357(7) Å amongst the seven hydrogens in the complex $ReH_7[P(p\text{-tolyl})_3]_2$, which fit neither (**I**) nor (**III**). The authors determined that they had discovered the first example of an intermediate state (**II**) between the non-classical dihydrogen ligand and the classical hydride. It was later established that the intermediate, or stretched dihydrogen complexes (**II**) have H-H distances in the range 1.1-1.5 Å [5].

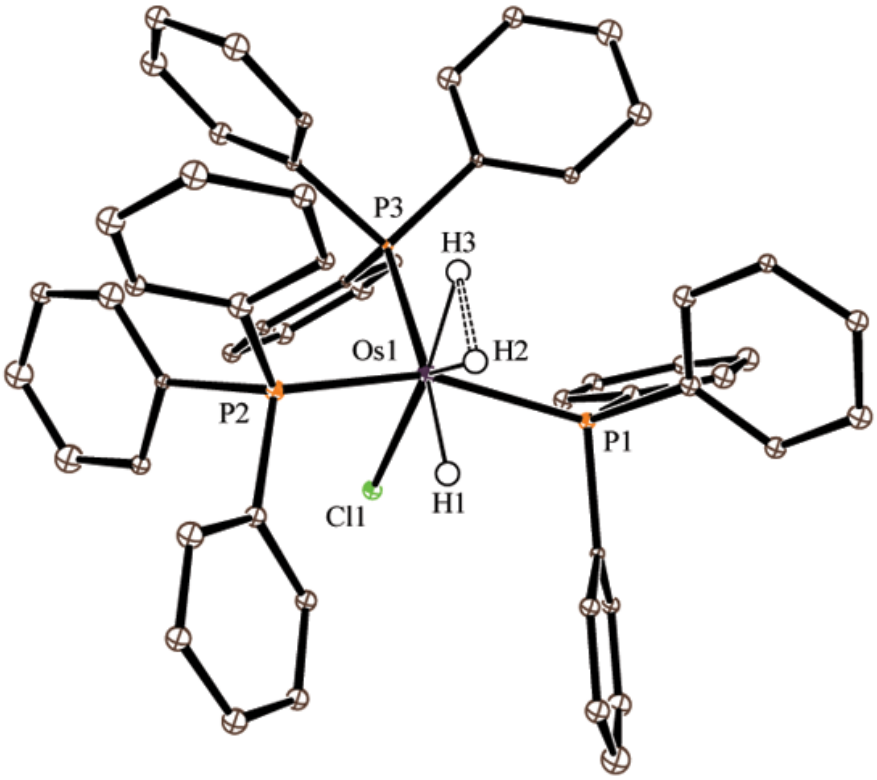


**Figure 1:** ORTEP of $OsH_3Cl(PPh_3)_3$

Since this study, several examples of the intermediate state (**II**) have been structurally characterized by neutron diffraction. In one specific study, a dihydrogen ligand was located in the complex $OsH_3Cl(PPh_3)_3$ [6] (Figure 1). This particular dihydrogen demonstrated a H…H distance of 1.48(2) Å, which placed it on the high end of the generally agreed upon range for known dihydrogen ligands (1.1-1.5 Å). This complex was initially reported much earlier [7] and was erroneously formulated as $OsClH(PPh_3)_3$. A later $^1H$ NMR study by Caulton and coworkers [8] was able to establish the presence of a non-classical dihydrogen ligand. It is suspected that the presence of the electronegative chloride ligand trans to the dihydrogen ligand promotes the closer H…H interaction. An earlier neutron diffraction study of $OsH_4(PMe_2Ph_2)_3$ showed that, with the absence of the electronegative chloride ligand, the complex contains only four classical hydride ligands (with no hint of a dihydrogen ligand). The only obvious difference between these two compounds is the presence of the chloride ligand trans to the dihydrogen ligand.

## 4. HYDROGEN ATOMS IN METAL CLUSTERS

Hydrogen atoms have the ability to occupy interstitial cavities in metal lattices. It is well known that hydrogen can occupy interstitial sites in non-stoichiometric hydrides of metals leading to high coordination [9]. These materials have historically been studied with surface diffraction techniques using x-rays but gave only limited information concerning bulk interstitial H atoms. However, among organometallic cluster complexes, these high coordination numbers are much rarer and in the case of 4 coordinate hydrogen was only recently observed (*vida infra*). Single crystals of organometallic complexes are often obtainable which allows for a more penetrating mode of analysis such as diffraction. And because of the difficulty of locating hydrogen atoms in the vicinity of a metal (let alone metal clusters) the method of choice when studying hydrogen in metal clusters is neutron diffraction.

The tendency for H atoms to occupy interstitial cavities has led to unusually high coordination numbers such as 4, 5, and 6. Some time ago, a 6-coordinate hydrogen ($\mu_6$-H) was discovered in the metal cluster anions $[HCo_6(CO)_{15}]^-$ and $[HRu_6(CO)_{18}]^-$ [10]. The hydrogen atom was located in the interstitial space formed by the metal octahedron. These results were compared with other neutron diffraction studies of cobalt clusters and a careful analysis reveals a relationship between the coordination number of the hydrogen atom and its corresponding metal-hydrogen distance. For the following distances found in a series of cobalt compounds: Co-H (terminal), $Co_2(\mu_2$-H), $Co_3(\mu_3$-H), $Co_6(\mu_6$-H), a noticeable increase in Co-H distance (1.56, 1.64, 1.73, 1.82 Å) is observed. This can be rationalized as a decrease in Co-H bond order as the coordination number for hydrogen increases (Table 1).

**Table 1**. Variation of Co-H Distance with H Coordination Number

| Compound | H coord no | Co-H dist(Å) |
|---|---|---|
| $CoH(CO)_4$ | 1 | 1.558(18) |
| $Co_2(\mu_2\text{-H})_3(\eta^5\text{-Cp*})_2$ | 2 | 1.641(6) |
| $Co_3Fe(\mu_3\text{-H})(CO)_9[P(OMe)_3]_3$ | 3 | 1.734(4) |
| $[Co_6(\mu_6\text{-H})(CO)_{15}]^-$ | 6 | 1.823(13) |

(*footnote: for the original version of this table, complete with literature citations, see ref 10.)

Five-coordinate hydrogen ($\mu_5$-H) has been discovered and studied using neutron diffraction [11]. Two H atoms were located in the interstitial cavity of two square pyramidal positions of $[H_2Rh_{13}(CO)_{24}]^{3-}$. As with Co-H, the Rh-H distance increased as the number of metal atoms around the H atom increased.

The first four-coordinate hydrogen ($\mu_4$-H) studied by single crystal neutron diffraction has been reported recently [12]. The H atom was located in the center of the tetrahedral metal complex $Y_4H_8(Cp")_4(THF)$ [Cp"=$C_5Me_4(SiMe_3)$]. The complex consists of a tetranuclear yttrium cluster forming a pseudo-tetrahedron. The four-coordinate H atom resides in the interstitial space of this tetrahedron and is accompanied by one face bridging hydride and six edge bridging hydride ligands. The four individual Y-H distances to the four-coordinate H atom are 2.184(16), 2.189(16), 2.221(13) and 2.168(12) Å.

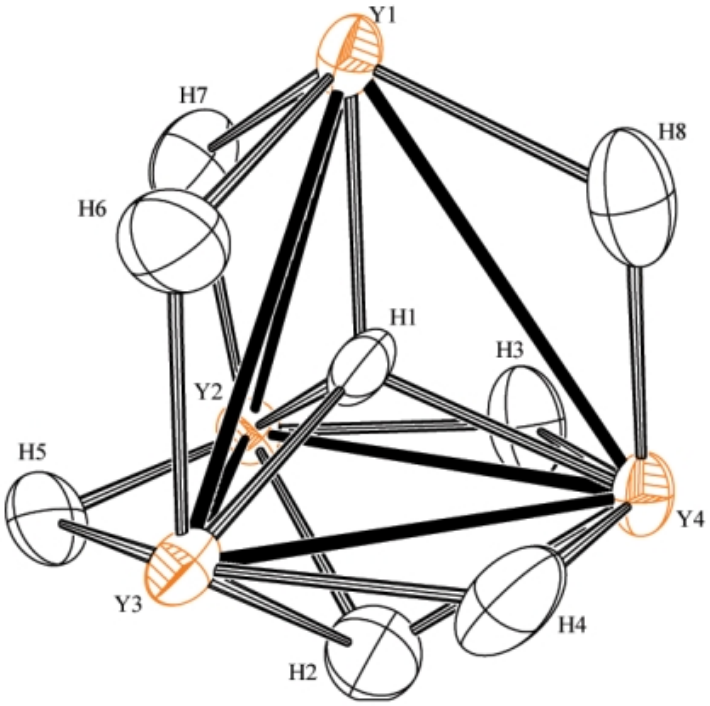


**Figure 2**. ORTEP plot of core of $[Cp"YH_2]_4(THF)$

The more common features in metal clusters include edge-bridging (2-coordinate H) and face-bridging hydride ligands (3-coordinate H) [3,13], however high-connectivity hydride ligands (e.g 4, 5, and 6) were much more rare. This recent finding of the four-coordinate H atom completes the series of high coordination hydride ligands.

The presence of three different types of linkages in the same complex [($\mu_2$-H), ($\mu_3$-H), as well as ($\mu_4$-H) metal-hydrogen bonds] allows for a unique comparison of all three linkages. Interestingly, the trend one observes for Co-H bonds in Table 1 is not apparent in the $Y_4$ complex. One does observe the expected increase from $Y_2(\mu_2$-H) [2.171(11) Å] to $Y_3(\mu_3$-H) [2.350(11)] Å), however, the Y-H distance decreases in the next step from $Y_3(\mu_3$-H) [(2.350(11) Å) to $Y_4(\mu_4$-H) [2.200(10)Å]. One explanation is that the tight interstitial cavity in $Y_4(\mu_4$-H) accounts for the short Y-H bond distances.

Curiously, one does not observe this tightness in the interstitial sites of octahedral cavities. Studies have shown that there is enough space for a hydride to "rattle around" in the octahedral cage. In the complexes $[HCo_6(CO)_{15}]^-$ [10] and $[HRu_6(CO)_{18}]^-$ [14] the H atom is located in the center of the cavity but in $[HNi_{12}(CO)_{21}]^{3-}$ and $[H_2Ni_{12}(CO)_{21}]^{2-}$ [15] the H atom is considerably off-centered. In addition, Inelastic Neutron Scattering [16] and low-temperature vibrational studies [17] show that, in the case of $[HCo_6(CO)_{15}]^-$, there is sufficient room for the hydride to "rattle around" in the interstitial cavity.

## 5. CONCLUSION

Neutron diffraction has been shown to provide essential chemical information in a wide range of systems. It has been invaluable in the studies of oxidative addition of $H_2$ to a metal center and for studying H atoms located in metal clusters.

## 6. ACKNOWLEDGEMENT

This article is dedicated to the memory of Professor Robert Bau who was a pioneer in the use of single crystal neutron diffraction to solve problems related to chemistry.

## 7. REFERENCES

[1] (a) G. J. Kubas, R. R. Ryan, B. I. Swanson, P. J. Vergamini, H. J. Wasserman, *J. Am. Chem. Soc.*, **106**, 451 (1985); (b) L. S. Van der Sluys, J. Eckert, O. Eisenstein, J. H. Hall, J. C. Huffman, S. A. Jackson, T. F. Koetzle, G. J. Kubas, P. J. Vergamini, K. G. Caulton, *J. Am. Chem. Soc.*, **112**, 4831 (1990)

[2] (a) G. Kubas, *Metal Dihydrogen and s-Bond Complexes: Structure, Theory, and Reactivity*, Kluwer Academic/Plenum Publishers, N.Y. (2001); (b) Crabtree, Robert H. *Accts. Chem. Res.*, **23**, 95-101 (1990)

[3] (a) R. Bau, R.G. Teller, S.W. Kirtley, and T.F. Koetzle, *Accts. Chem. Res.*, ***12***, 176 (1979); (b) R.G. Teller and R. Bau, *Structure and Bonding*, ***44***, 1 (1981)

[4] L. Brammer, J. A. K. Howard, O. Johnson, T. F. Koetzle, J. L. Spencer, A. M. Stringer, *Chem. Commun.*, 241, (1991)

[5] (a) H. B. Bürgi, J. D. Dunitz, *Acc. Chem. Res.* 16, 153, (1983); (b) D. R. Lide, (ed.), *CRC Handbook of Chemistry and Physics*, CRC Press, 75th edn. (1994)

[6] M. Yousufuddin, T. B. Wen, S. A. Mason, G. J. McIntyre, G. Jia, R. Bau**,** *Angew. Chem. Inter. Edit.*, **44**, 7227-7230, (2005)

[7] A. Oudeman, F. Van Rantwijk, H. J. Van Bekkum, J. Coord. Chem., 4, 1 (1974)

[8] G. Ferrando, K. G. Caulton, Inorg. Chem., 38, 4168 (1999)

[9] *Metal Hydrides*; Mueller, W. M., Blackledge, J. P., Libowitz, G. G., Eds.; Academic Press: New York (1968)

[10] (a) D. W. Hart, R. G. Teller, C. Y. Wei, R. Bau, G. Longoni, S. Campanella, P. Chini, T. F. Koetzle, *Angew. Chem. Int. Ed.*, 18, 80 (1979); (b) D. W. Hart, R. G. Teller, C. Y. Wei, R. Bau, G. Longoni, S. Campanella, P. Chini, T. F. Koetzle, *J.A.C.S.*, 103, 1458 (1981)

[11] R. Bau, M. H. Drabnis, L. Garlaschelli, W. T. Klooster, Z. Xie, T. F. Koetzle, S. Martinengo, *Science*, 275, 1099 (1997)

[12] (a) M. Yousufuddin, M. J. Gutmann, J. Baldamus, O. Tardif, Z. Hou, S. A. Mason, G. J. McIntyre, and R. Bau, 130, 388 (2008) (b) M. Yousufuddin, J. Baldamus, O. Tardif, Z. Hou, S. A. Mason, G. J. McIntyre, and R. Bau, *Physica B*, 385-386, 231 (2006)

[13] R. Bau and M. Drabnis, *Inorg. Chim. Acta*, **259**, 27 (1997)

[14] P. F. Jackson, B.F.G. Johnson, J. Lewis, P.R. Raithby, M. McPartlin, W.J.H. Nelson, K.D. Rouse, J.Allibon and S.A. Mason, *Chem. Commun.*, 295 (1980)

[15] R. W. Broach, L.F. Dahl, G. Longoni, P. Chini, A.J. Schultz and J.M. Williams, *Adv. Chem. Ser.*, 167, 93 (1979)

[16] (a) D. Graham, J. Howard, T.C. Waddington, and J. Tomkinson, *J. Chem. Soc. (Faraday Trans. 2)*, 79, 1713 (1983); (b) J. Eckert, A. Albinati and G. Longoni, *Inorg. Chem.*, 28, 4055 (1989)

[17] P.L. Stanghellini and G. Longoni, *J.C.S. (Dalton)*, 685 (1987)